The Astrophysical Journal Supplement Series, 192:6 (33pp), 2011 January doi:10.1088/0067-0049/192/1/6

A *GALEX* ULTRAVIOLET IMAGING SURVEY OF GALAXIES IN THE LOCAL VOLUME

Janice C. Lee[1,11], Armando Gil de Paz[2], Robert C. Kennicutt, Jr.[3,4], Matthew Bothwell[3], Julianne Dalcanton[5], José G. Funes, S. J.[6], Benjamin D. Johnson[3], Shoko Sakai[7], Evan Skillman[8], Christy Tremonti[9], and Liese van Zee[10]
[1] Carnegie Observatories, 813 Santa Barbara Street, Pasadena, CA 91101, USA; jlee@obs.carnegiescience.edu
[2] Departamento de Astrofísica, Universidad Complutense de Madrid, Madrid 28040, Spain
[3] Institute of Astronomy, University of Cambridge, Madingley Road, Cambridge, CB3 0HA, UK
[4] Steward Observatory, University of Arizona, Tucson, AZ 85721, USA
[5] Department of Astronomy, University of Washington, P.O. Box 351580, Seattle, WA 98195, USA
[6] Vatican Observatory, Specola Vaticana, V00120 Vatican, Italy
[7] Division of Astronomy and Astrophysics, University of California, Los Angeles, Los Angeles, CA 90095-1562, USA
[8] Department of Astronomy, University of Minnesota, Minneapolis, MN 55455, USA
[9] Department of Astronomy, University of Wisconsin-Madison, Madison, WI 53706, USA
[10] Astronomy Department, Indiana University, Bloomington, IN 47405, USA
Received 2010 July 06; accepted 2010 October 30; published 2010 December 22

ABSTRACT

We present results from a *GALEX* ultraviolet (UV) survey of a complete sample of 390 galaxies within ∼11 Mpc of the Milky Way. The UV data are a key component of the composite Local Volume Legacy, an ultraviolet-to-infrared imaging program designed to provide an inventory of dust and star formation in nearby spiral and irregular galaxies. The ensemble data set is an especially valuable resource for studying star formation in dwarf galaxies, which comprise over 80% of the sample. We describe the *GALEX* survey programs that obtained the data and provide a catalog of far-UV (∼1500 Å) and near-UV (∼2200 Å) integrated photometry. General UV properties of the sample are briefly discussed. We compute two measures of the global star formation efficiency, the star formation rate (SFR) per unit H I gas mass, and the SFR per unit stellar mass, to illustrate the significant differences that can arise in our understanding of dwarf galaxies when the FUV is used to measure the SFR instead of Hα. We find that dwarf galaxies may not be as drastically inefficient in converting gas into stars as suggested by prior Hα studies. In this context, we also examine the UV properties of late-type dwarf galaxies that appear to be devoid of star formation because they were not detected in previous Hα narrowband observations. Nearly all such galaxies in our sample are detected in the FUV and have FUV SFRs that fall below the limit where the Hα flux is robust to Poisson fluctuations in the formation of massive stars. Otherwise, the UV colors and star formation efficiencies of Hα-undetected, UV-bright dwarf irregulars appear to be relatively unremarkable with respect to those exhibited by the general population of star-forming galaxies.

Key words: catalogs – galaxies: dwarf – galaxies: evolution – stars: formation – surveys – ultraviolet: galaxies

Online-only material: color figures, machine-readable tables

1. INTRODUCTION

Since the *Galaxy Evolution Explorer* (*GALEX*; Martin et al. 2005) was successfully launched in 2003, the study of star formation in the ultraviolet (UV) has been broadly enabled and expanded to regimes previously unexplored. In particular, *GALEX* far-UV (FUV; ∼1500 Å) imaging has proved to be an exquisite probe of the recent star formation in relatively dust-free galactic environments that are characterized by low density and low-surface brightness.

A major theme that has emerged from work based on *GALEX* data is that there may be more star formation in low-density environments than previously recognized. For example, an early surprise from the mission was the detection of FUV emission extending to several times the optical disks of the nearby systems M83 (Thilker et al. 2005) and NGC 4625 (Gil de Paz et al. 2005), and it was reported that the amount and extent of the star formation in these "XUV disks" was greater than formerly seen in images of the Hα nebular emission line. Subsequent studies, which have begun to constrain the prevalence of XUV disks in the overall population, have indicated that extended star formation is common and occurs in roughly one-quarter to one-third of disk galaxies (Thilker et al. 2007; Zaritsky & Christlein 2007; Goddard et al. 2010).

Later work investigated the globally integrated UV star formation rates (SFRs) of local dwarf and low-surface brightness galaxies, and several groups showed that, again, the amount of activity inferred from the UV in such systems tends to be greater than would be expected from previous Hα measurements (e.g., Meurer et al. 2009; Lee et al. 2009b; Boselli et al. 2009; Hunter et al. 2010). Our own study—based on the UV data set presented in this paper—was the first to establish this systematic trend with a statistically significant sample of dwarf galaxies with SFRs from 0.1 $M_\odot$ yr^{-1} down to 0.0001 $M_\odot$ yr^{-1} (Lee et al. 2009b). We find that at SFR ∼0.003 $M_\odot$ yr^{-1}, the average Hα-to-FUV flux ratio is lower than expected by about a factor of two, and at the lowest SFRs probed by our sample, the ratio exhibits up to an order-of-magnitude discrepancy. Prior to our work, there was a lack of deep UV observations for a complete, well-defined sample of dwarf galaxies, and this had prevented the trend from being clearly delineated in the past.

Until *GALEX*, a great deal of our knowledge of star formation in local galaxies had been based on Hα observations (e.g., Hodge 1974; Kennicutt 1989; Kennicutt et al. 2008, and references therein). From the recent *GALEX* results just summarized, however, it is now thought that the UV may be a more robust

[11] Carnegie Starr Fellow.

diagnostic of star formation activity in the low SFR intensity regime. UV emission should be less prone to stochastic effects from sparse sampling of the upper end of the stellar initial mass function (IMF) and to possible uncertainties in the fate of ionizing photons in low-density gas; that is, whether the H II regions, or even entire galaxies, can be safely assumed to be ionization-bounded (e.g., Melena et al. 2009). This is because the UV flux is directly emitted from the photospheres of O- through later-type B-stars ($M_* \gtrsim 3\,M_\odot$), whereas the Hα nebular emission arises from the recombination of hydrogen which can only be ionized by the most massive O- and early-type B-stars ($M_* \gtrsim 17\,M_\odot$). However, it is currently debated whether stochasticity or the potential leakage of Lyman continuum photons can fully account for the magnitude of the observed systematic between UV and Hα SFRs. A range of other causes have been considered (e.g., dust attenuation, metallicity, and discontinuous star formation histories), the most debated of which is an IMF deficient in the most massive stars (Pflamm-Altenburg et al. 2009, and references therein; Meurer et al. 2009; Lee et al. 2009b; Boselli et al. 2009; Hunter et al. 2010). Though the explanation for the discrepancies between the two tracers is still uncertain, it is clear that UV observations from *GALEX* have challenged our understanding of star formation in low-density environments and are *essential* for the study of the outer disks of spirals, and of low-surface brightness and dwarf galaxies.

In this paper, we present results from a *GALEX* survey of a complete sample of Local Volume galaxies whose primary defining characteristic is that it is dominated by dwarf galaxies—over 80% of the sample have luminosities and SFRs lower than those of the Large Magellanic Cloud (LMC). This effort was undertaken as part of broader multi-wavelength campaign to provide new insight into the mechanisms that drive, regulate, and extinguish global star formation in galaxies, with special focus on the dwarf and low-surface brightness regime. Our survey has sought to build upon the patchwork of existing observations of nearby galaxies, which suffer from common observational biases toward luminous, high-surface brightness systems (e.g., Blanton et al. 2005). Though a great deal has already been learned about the nature of nearby dwarf star-forming galaxies, as low-metallicity, gas-rich, but not necessarily young systems (e.g., Gallagher & Hunter 1984; van Zee 2001; Gil de Paz et al. 2003; Hunter & Elmegreen 2004), the vast majority of prior studies have relied on observations of representative samples of dwarfs. Our work seeks to enable studies which demand dwarf galaxy samples that are not only representative, but are true to the statistics provided by an approximately volume-limited sample (e.g., characterization of the prevalence of starbursts in low-mass systems; Lee et al. 2009a).

Hα narrowband imaging observations for the sample were previously carried out by Kennicutt et al. (2008). The precursor Hα survey and *GALEX* follow-up program together comprise 11HUGS, the 11 Mpc Hα, and Ultraviolet Galaxy Survey. The data from 11HUGS have further been augmented by *Spitzer* IRAC mid-infrared and MIPS far-infrared observations (Dale et al. 2009) through the composite Local Volume Legacy[12] program, which has provided the ensemble UV, Hα, and IR data set to the community through the NASA/IPAC Infrared Science Archive[13] (IRSA). 11HUGS largely focuses on star-forming systems brighter than a certain limit ($B < 15.5$). To extend the coverage of the galaxy population to dwarf spheroidals, dwarf ellipticals, and the faintest irregular galaxies, such systems from the ACS Nearby Galaxy Survey Treasury (ANGST) program (Dalcanton et al. 2009) were also targeted for both *GALEX* and *Spitzer* observations. ANGST has obtained *Hubble Space Telescope* (*HST*) resolved stellar population imaging for a volume-limited sample outside the Local Group and within ~4 Mpc. Altogether, the *GALEX* data set presented in this paper provides the most complete catalog of integrated UV photometry for Local Volume galaxies currently available.

The remainder of the paper is organized as follows. In Section 2, we describe in detail the resultant Local Volume sample selected for *GALEX* follow-up, summarize the observations, and present a catalog of NUV- and FUV-integrated photometry. In Section 3, basic results from the survey are presented. We give an overview of the UV properties of the sample and discuss the detection rate. We compute two measures of the global star formation efficiency, the SFR per unit H I gas mass and the SFR per unit stellar mass, to illustrate the significant differences that can arise in our understanding of dwarf galaxies when the FUV is used to measure the SFR instead of Hα. In particular, the UV properties of late-type dwarf galaxies that appear to be devoid of star formation because they were not detected in previous Hα narrowband observations are examined. We comment on the selection of "transition" dwarf galaxies (dIrr/dSph) based upon the non-detection of Hα emission in gas-rich dwarfs. We adopt $H_0 = 75$ km s^{-1} Mpc^{-1} for distance-dependent quantities, when distance measurements from standard candles or secondary indicators are not available.

2. DATA

2.1. Sample Selection

The Local Volume galaxies that were targeted for *GALEX* imaging were mainly selected from the sample given in Kennicutt et al. (2008, hereafter Paper I), who have carried out a deep, statistically complete, Hα+[N II] narrowband imaging survey within ~11 Mpc. The ANGST program (Dalcanton et al. 2009), which has obtained *HST* ACS and WFPC2 imaging for a ~4 Mpc volume-limited sample, contains about 20 low-luminosity and/or early-type galaxies that were not already included in Paper I, and *GALEX* data were also obtained for these objects. In this section, we first summarize the Paper I sample and then describe the resultant set of galaxies that were observed by *GALEX* in our survey.

Paper I presents a sample of 436 galaxies from existing catalogs which were compiled in two components. The primary component aims to be as complete as possible in its inclusion of known nearby star-forming galaxies within given limits. It consists of all known spirals and irregulars ($T \geqslant 0$) within 11 Mpc that avoid the Galactic plane ($|b| > 20°$) and are brighter than $B = 15$ mag. These particular limits represent the ranges within which the original surveys that have provided the bulk of our knowledge of the Local Volume galaxy population have been shown to be relatively complete (e.g., Tully 1988; de Vaucouleurs et al. 1991), but still span a large enough volume to probe a diverse cross-section of star formation properties. A secondary component consists of galaxies that are within 11 Mpc for which Hα flux measurements are available, but fall outside one of the limits on brightness, Galactic latitude, and morphological type—these were generally targets either observed by our group as telescope time allowed or had Hα fluxes published in the literature. Subsequent statistical tests, as functions of the compiled B-band apparent magnitudes and

12 http://www.ast.cam.ac.uk/research/lvls/
13 http://ssc.spitzer.caltech.edu/spitzermission/observingprograms/legacy/lvl/

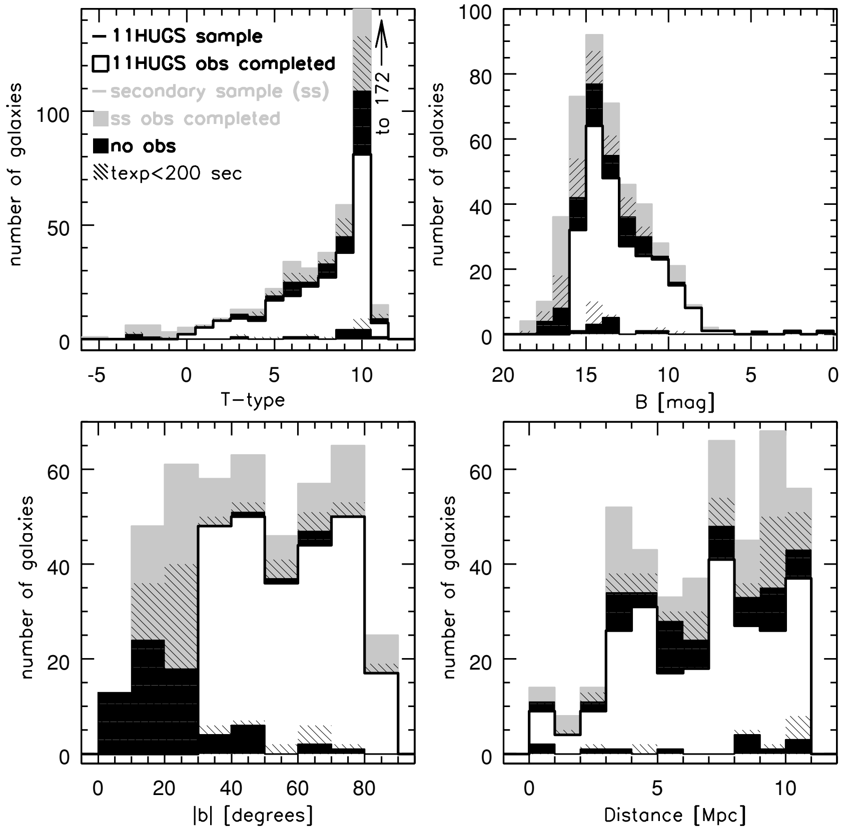

Figure 1. Resultant *GALEX* coverage of the overall 11 Mpc sample as given in Table 1 and described in Section 2.1. Distributions in the properties used to select the sample are shown: RC3 type (top left), apparent B magnitude (top right), Galactic latitude (bottom left), and distance (bottom right). The overall sample is given by the gray histogram, while the subset targeted for *GALEX* observations by 11HUGS ($b > 30^\circ$, $B \leqslant 15.5$) is distinguished in white. The hatched areas of the histograms show the portions of each sample for which only shallow imaging exists ($t_{\rm FUV} < 200$ s), while the black areas show that for which no FUV observations have been carried out. For $b > 30^\circ$ and $B \leqslant 15.5$, there are no strong biases in the available one-orbit-depth *GALEX* imaging in any of these properties.

21 cm (H I) fluxes, show that the overall sample is complete to ~15.5 mag and ~6 Jy km s^{-1}, respectively. This corresponds to limits of $M_B \lesssim -15$ and $M_{\rm H\,I} \gtrsim 2 \times 10^8\, M_\odot$ for $|b| > 20^\circ$ at the edge of the 11 Mpc volume. More details on the parent sample and its properties are given in Paper I (sample construction, Local Volume membership uncertainties, and integrated Hα flux and equivalent width catalog), Lee et al. (2007; overall star formation demographics as traced by the Hα equivalent width), and Lee et al. (2009a; completeness tests and limits, and dwarf galaxy starburst statistics).

Galaxies with $|b| > 30^\circ$ and $B \leqslant 15.5$ from the Paper I sample ($N = 256$) were targeted for UV imaging through the 11HUGS *GALEX* Legacy program (GI1_047, GI4_095). The Galactic latitude limit was imposed to avoid excessive foreground extinction, and fields with bright stars and/or high background levels for which imaging would be prohibited due to the instrument's brightness safety limits. *GALEX* observations for a significant number ($N = 120$) of the remaining lower latitude, fainter galaxies in the parent sample have also been taken by other programs and are publicly available in the *GALEX* archive through MAST.[14] We have performed photometry on these data as well and provide measurements in the tables that follow.

Observations of the 11HUGS galaxies have also been extended into the infrared using the *Spitzer Space Telescope* as part of the Local Volume Legacy survey (Dale et al. 2009). As mentioned above, in addition to galaxies selected from Paper I, Local Volume Legacy also includes targets from ANGST in order to extend coverage of galaxy properties to dwarf spheroidal and ellipticals, and the faintest dwarf irregulars known outside of the Local Group. There are 27 galaxies in the composite Local Volume Legacy sample which are not included in Paper I.[15] *GALEX* observations have also been obtained for all of these galaxies, about half of which were taken through a *GALEX* follow-up program of ANGST galaxies (GI3_06). The photometry for these 27 galaxies is also reported here.

2.2. *GALEX* Observations

GALEX is a NASA Small Explorer launched in 2003 April. It uses a 50 cm aperture telescope with a dichroic beam splitter that enables simultaneous observations in the FUV ($\lambda_{\rm eff} = 1539$ Å, FWHM = 269 Å) and the NUV ($\lambda_{\rm eff} = 2316$ Å, FWHM = 616 Å). The field of view of the camera is circular and has a 1.°2 diameter. The PSF is dependent on the count rate (deteriorates for brighter sources) as well as on the radial

[14] MAST is the Multimission Archive at the Space Telescope Science Institute (http://archive.stsci.edu/index.html). STScI is operated by the Association of Universities for Research in Astronomy, Inc., under NASA contract NAS5-26555. Support for MAST for non-*HST* data is provided by the NASA Office of Space Science via grant NAG5-7584 and by other grants and contracts.

[15] Included in this group of 27 are 4 galaxies for which a revision in the distance estimates placed them outside 11 Mpc after the final sample for Local Volume Legacy *Spitzer* observations had been selected (see Section 2.2).

position on the image (deteriorates at the field edge), but is reasonably well described by a FWHM of 5″± 1″ for the data analyzed here. The images that we use have been uniformly reprocessed by the *GALEX* team with the most recent version of the pipeline (v6) available at the time of the initial preparation of this paper. The v6 pipeline accounts for a drift in the photometric calibration (1.5% and 0.25% dimmer per year for the NUV and FUV bands, respectively), incorporates corrections to the flat-fielding (5% systematic in the FUV and a 2% change in shape in the NUV), and improves the removal of reflected light at the NUV field edge. Full details on the satellite, telescope, instrument and calibration, and data processing pipeline are given in Martin et al. (2005), Morrissey et al. (2005), and Morrissey et al. (2007).

Our primary survey objective is to provide a statistically complete UV data set for a deep Local Volume galaxy sample. To do this, our program leverages upon existing data and homogeneously fills significant gaps in prior *GALEX* coverage of the $D < 11$ Mpc, $b > 30°$, $B < 15.5$ population ($N = 256$). The *GALEX* team's Nearby Galaxy Survey and Medium Imaging Survey has supplied imaging for ∼30% of this sample (Gil de Paz et al. 2007), with cumulative exposure times of ∼1500 s per field (close to the time available in one orbit), while a small fraction (∼10%) were observed to similar depth by other independent guest investigator programs. This exposure time corresponds to surface brightness limits of $m_{AB} \sim 27.5$ mag arcsec^{-2} or an SFR of $\sim 10^{-3}\ M_\odot$ yr^{-1} kpc^{-2} (Martin et al. 2005; Gil de Paz et al. 2007). Our Cycle 1 (GI1-047) and Cycle 4 (GI4-095) programs obtained one-orbit-depth data for an additional ∼50% of the sample. The status of *GALEX* observations for the remaining of ∼10% of this sample is as follows. Observations for 10 galaxies are prohibited due to bright foreground stars and/or high background (LMC, SMC, ISZ399, NGC1313, NGC3077, NGC7713, UGC5076, UGC7490, UGC8508, and UGC8837).[16] Observations for 10 galaxies have not been completed to sufficient depth in the FUV (i.e., less than 1/3 the requested integration time or 500 s), and only shallow imaging from the *GALEX* All-sky Imaging Survey (AIS) is available (IC625, IC2782, IC4316, NGC3675, NGC5608, UGC5451, UGC8091, UGC9128, UGC9211, and UGC9660).[17] No data are available for four galaxies (ESO252-IG001, ESO306-G013, UGC5151, and UGCA103). Overall, observations for the ensemble data set were taken over five years between 2004 and 2009. Intermittent FUV detector failures, or "transient overcurrent events," that have occurred since 2004 (Morrissey 2006), caused the completion of the survey to require more time than initially anticipated.

UV imaging is also available from other *GALEX* programs for another 120 of the remaining 180 galaxies in Paper I which fall outside the limits of the main $b > 30°$ and $B \leqslant 15.5$ sample. Approximately half of these galaxies have shallow AIS imaging ($\lesssim$200 s), while the remainder have deep ($\geqslant$1500 s) exposures.

Figure 1 summarizes the resultant *GALEX* coverage of the overall 11 Mpc sample as described above. Distributions of the morphological type, B magnitude, Galactic latitude, and distance (i.e., the properties used to define our samples) are shown. The overall 11 Mpc parent sample (Table 1) is given by the gray histogram, while the subset selected for *GALEX* observations by 11HUGS ($b > 30°$, $B \leqslant 15.5$) is distinguished in white. The hatched portions of the histograms show the fractions of each sample for which only shallow imaging exists ($t_{FUV} < 200$ s), while the black portions show those for which no FUV observations have been carried out. There are no strong biases in the available one-orbit-depth *GALEX* imaging in any of these properties.

Table 1 lists specific exposure times and information on the original *GALEX* programs that obtained the data, along with general properties of the targets. To facilitate cross-comparison with the Hα data presented in Paper I, basic properties given in the first table of Paper I are repeated in Columns 1–9 with some updates, and all 436 galaxies are listed, whether they have been observed by *GALEX* or not. Galaxies in the composite Local Volume Legacy sample which are not included in Paper I (generally targets drawn from the ANGST sample) are listed separately at the end of the table. The columns in Table 1 are as follows.

Column 1: the running index number.

Column 2: galaxy name.

Columns 3 and 4: J2000 right ascension and declination as reported in NASA/IPAC Extragalactic Database (NED).

Column 5: galactic latitude as reported in NED.

Column 6: adopted distance. Measurements based on standard candles or secondary distance indicators were compiled from the literature when available, otherwise distances computed from recessional velocities corrected to the centroid of the Local Group (following Karachentsev & Makarov 1996, as reported in NED) and adopting $H_0 = 75$ km s^{-1} Mpc^{-1} are listed. Original references for the direct distances are given in Paper I, Table 1, with the exception of galaxies targeted by the ANGST program, for which non-Cepheid distances have been updated to be consistent with the tip of the red giant branch measurements reported in Dalcanton et al. (2009).

Column 7: distance determination method, with the following abbreviations: Cepheid variables (ceph), tip of the red giant branch (trgb), surface brightness fluctuations (sbf), membership in a group with measured distance (mem), brightest blue stars (bs), Tully–Fisher relation (tf), and Local Group corrected recessional velocity distances (flow).

Column 8: apparent B-band magnitude. The photometry was compiled as discussed in Lee et al. (2009a), and references are given in Paper I, Table 1.

Column 9: RC3 morphological type.

Column 10: a flag indicating whether the galaxy is included in the *Spitzer* Local Volume Legacy program (1) or not (0). The same $|b| > 30°$, $B < 15.5$ Local Volume population was targeted for both *GALEX* and *Spitzer* (IRAC 3.6, 4.5, 5.8, and 8.0 μm and MIPS 24, 70, and 160 μm) follow-up. However, changes in the adopted distances for some galaxies which occurred between the selection of the *Spitzer* and final *GALEX*/Paper I samples led to slight differences between the samples. This flag is provided here to help clarify these differences. As described in Dale et al. (2009), four galaxies targeted for *Spitzer* observations have updated distances which place them outside of 11 Mpc. These galaxies appear at the end of the table. The flow model initially applied was also updated to provide consistency with one used by NED. As a result, 30 Paper I galaxies with $|b| > 30°$, $B < 15.5$ do not have *Spitzer* imaging in Dale et al. (2009). The galaxies are generally between 10

[16] Although observations for fields close to NGC1313 and NGC3077 are currently not allowed, some early data were taken by the *GALEX* team for these galaxies. A shallow All-sky Imaging Survey (AIS) 211 s pointing exists for NGC1313. Observations of NGC3077 were attempted by the Nearby Galaxy Survey, but in the effort to shift the offending bright stars off of the *GALEX* FOV, the galaxy was moved too close to the field edge, and only about half of it was captured in the resultant imaging.

[17] Two of these galaxies, IC2782 and UGC9128, have deep (>1500 s) exposures in the NUV, though their FUV data are shallow. This is a consequence of intermittent FUV detector failures, during which observations still proceeded in the NUV channel.

Table 1
GALEX Observations of Local Volume Galaxies

No.	Galaxy Name	R.A. (J2000)	Decl. (J2000)	*b* (deg)	D (Mpc)	Method	*B* (mag)	T	Local Volume Legacy	t_{fuv} (s)	t_{nuv} (s)	Tile Name
(1)	(2)	(3)	(4)	(5)	(6)	(7)	(8)	(9)	(10)	(11)	(12)	(13)
1	UGC12894	000022.5	392944	−22.32	8.2	v(flow)	16.6	10	0	. . .	. . .	. . .
2	WLM	000158.1	−152739	−73.63	0.92	trgb	11.03	10	1	1440	1440	NGA_WLM
3	ESO409-IG015	000531.8	−280553	−79.79	10.4	v(flow)	15.1	6	0	1608	1608	GI1_009016_HPJ0005m28
4	ESO349-G031	000813.3	−343442	−78.12	3.21	trgb	15.6	10	0	1608	1608	GI1_047001_ESO349_G031
5	NGC24	000956.7	−245744	−80.43	8.1	v(flow)	12.2	5	1	1579	1579	NGA_NGC0024
6	NGC45	001404.0	−231055	−80.67	7.1	v(flow)	11.32	8	1	2220	2220	GI4_095001_NGC0045
7	NGC55	001454.0	−391149	−75.74	2.10	trgb	8.42	9	1	1482	1482	NGA_NGC0055
8	NGC59	001525.4	−212642	−80.02	5.3	sbf	13.1	−3	1	2393	2393	GI4_095002_NGC0059
9	MCG-04-02-003	001911.4	−224006	−81.44	9.8	v(flow)	15.6	9	0	1655	3429	GI1_047003_MCG_04_02_003
10	IC10	002023.1	591735	−3.34	0.66	ceph	11.8	10	0	. . .	. . .	. . .
11	ESO473-G024	003122.5	−224557	−83.70	8.0	v(flow)	16.04	10	0	1600	1600	GI1_009007_HPJ0031m22
12	AndIV	004230.1	403433	−22.27	6.11	trgb	16.60	10	0	3562	3562	NGA_M31_MOS12
13	NGC224	004244.3	411609	−21.57	0.79	ceph	4.36	3	0	. . .	. . .	. . .
14	IC1574	004303.8	−221449	−84.76	4.92	trgb	14.50	10	1	1626	1627	GI4_095043_IC1574
15	NGC247	004708.3	−204538	−83.56	3.52	trgb	9.67	7	1	2507	2507	NGA_NGC0247
16	NGC253	004733.1	−251718	−87.96	3.44	trgb	8.04	5	1	3272	3272	NGA_NGC0253
17	UGCA15	004949.2	−210054	−83.88	3.31	trgb	15.4	10	1	1513	1513	GI1_009002_UGCA015
18	SMC	005244.8	−724943	−44.33	0.06	ceph	2.70	9	1	. . .	. . .	. . .
19	NGC300	005453.5	−374100	−79.42	2.00	ceph	8.72	7	1	1628	1628	NGA_NGC0300
20	LGS3	010355.0	215306	−40.89	0.62	trgb	16.18	99	0	1700	1700	NGA_LGS3
21	UGC668	010447.8	020704	−60.56	0.65	ceph	9.88	10	1	1696	1696	NGA_IC1613
22	UGC685	010722.4	164102	−46.02	4.70	trgb	14.20	9	1	1609	1609	GI1_047004_UGC00685
23	UGC695	010746.4	010349	−61.53	10.2	v(flow)	15.3	6	1	1635	1635	GI1_047005_UGC00695
24	UGC891	012118.9	122443	−49.80	10.8	v(flow)	14.72	9	1	2685	4333	GI1_047006_UGC00891
25	UGC1056	012847.3	164119	−45.26	10.3	v(flow)	14.9	10	1	2620	2620	GI4_095003_UGC01056
26	UGC1104	013242.5	181902	−43.47	7.5	bs	14.41	9	1	1168	2864	GI1_036006_UGC01104
27	NGC598	013350.9	303937	−31.33	0.84	ceph	6.27	6	1	3361	3361	NGA_M33_MOS0
28	NGC625	013504.2	−412615	−73.12	4.07	trgb	11.7	9	1	4530	4530	GI1_047007_NGC0625
29	NGC628	013641.7	154659	−45.71	7.3	bs	9.95	5	1	1636	1636	NGA_NGC0628
30	UGC1176	014009.9	155417	−45.37	9.0	bs	14.4	10	1	1696	3200	GI1_047008_UGC01176
31	UGCA20	014314.7	195832	−41.25	9.0	v(flow)	15.78	10	0	3382	5078	GI1_047010_UGCA020
32	ESO245-G005	014503.7	−433553	−70.29	4.43	trgb	12.7	10	1	2424	2424	GI1_047011_ESO245_G005
33	UGC1249	014730.6	271952	−33.90	7.2	bs	12.1	9	1	1526	3097	GI1_047012_IC1727
34	NGC672	014754.3	272559	−33.78	7.2	bs	11.47	6	1	1526	3097	GI1_047012_IC1727
35	UGC1281	014931.4	323519	−28.71	5.13	trgb	13.61	8	0	137	137	AISCHV4_058_06877
36	ESO245-G007	015106.3	−442641	−68.95	0.44	trgb	13.3	10	1	1702	1702	NGA_Phoenix
37	NGC784	020117.0	285015	−31.59	5.19	trgb	12.23	8	1	2267	2267	GI4_095004_NGC0784
38	UGC1561	020405.1	241230	−35.75	10.5	v(flow)	16.2	10	0	1693	1693	GI1_047013_UGC01561
39	NGC855	021403.6	275238	−31.53	9.7	sbf	13.3	−4	1	1500	1500	NGA_NGC0855
40	UGC1807	022113.4	424546	−17.12	9.2	mem	16.50	10	0	7355	7667	GI2_019004_3C66B
41	NGC891	022233.4	422057	−17.41	9.2	mem	10.8	3	0	1696	1696	NGA_NGC0891
42	UGC1865	022500.2	360216	−23.10	9.2	mem	14.4	9	0	169	169	AISCHV4_059_06618
43	NGC925	022716.9	333445	−25.17	9.16	ceph	10.7	7	0	1671	1671	NGA_NGC0925
44	UGC1924	022749.8	314336	−26.82	10.4	v(flow)	15.23	6	0	144	144	AISCHV3_064_07003
45	NGC949	023048.6	370814	−21.63	9.2	mem	12.4	4	0	181	181	AISCHV4_059_06618
46	NGC959	023224.0	352942	−23.00	9.2	mem	12.9	8	0	1694	1694	NGA_NGC0959
47	UGC2014	023254.0	384050	−20.05	9.2	mem	15.7	10	0	170	170	AISCHV4_059_06618
48	UGC2023	023318.2	332928	−24.74	9.2	mem	13.9	10	0	108	108	AISCHV4_064_06804
49	UGC2034	023342.9	403141	−18.29	9.2	mem	13.7	10	0	. . .	. . .	. . .
50	ESO115-G021	023748.1	−612018	−51.43	4.99	trgb	13.34	8	1	2220	2220	GI4_095005_ESO115_G021
51	NGC1003	023916.6	405221	−17.54	9.2	mem	12.00	6	0	114	114	AISCHV4_059_06440
52	Maffei2	024154.9	593615	−0.33	3.3	tf	14.8	4	0	. . .	. . .	. . .
53	NGC1058	024329.9	372027	−20.37	9.2	mem	11.8	5	0	2778	2778	GI3_067002_SN2007gr_p
54	UGC2259	024755.4	373218	−19.80	9.2	mem	15.2	8	0	. . .	. . .	. . .
55	ESO154-G023	025650.4	−543417	−54.31	5.76	trgb	12.69	8	1	1573	1573	GI4_095006_ESO154_G023
56	NGC1156	025942.6	251417	−29.20	7.8	bs	12.75	10	0	1423	1423	NGA_NGC1156
57	ESO300-G014	030937.8	−410150	−58.46	11.0	v(flow)	13.0	9	0	1640	1640	GI1_047015_ESO300_G014
58	ESO300-G016	031010.5	−400011	−58.62	7.8	v(flow)	15.6	10	0	1646	1646	GI1_009006_NGC1249
59	NGC1291	031718.3	−410628	−57.05	9.4	v(flow)	9.39	0	1	1705	1705	NGA_NGC1291
60	NGC1313	031815.8	−662953	−44.64	4.15	trgb	9.2	7	1	211	211	AISCHV4_393_39112
61	NGC1311	032007.4	−521107	−52.66	5.45	trgb	13.18	9	1	1855	1855	MIS2DFR_38632_0859
62	UGC2684	032023.7	171745	−32.75	6.5	bs	16.30	10	0	4065	6692	GI1_047018_UGC02684
63	UGC2689	032127.7	404806	−13.68	5.9	v(flow)	14.95	−2	0	. . .	. . .	. . .

Table 1
(Continued)

No. (1)	Galaxy Name (2)	R.A. (J2000) (3)	Decl. (J2000) (4)	b (deg) (5)	D (Mpc) (6)	Method (7)	B (mag) (8)	T (9)	Local Volume Legacy (10)	t_{fuv} (s) (11)	t_{nuv} (s) (12)	Tile Name (13)
64	UGC2716	032407.2	174512	−31.82	6.2	v(flow)	14.64	8	1	4065	6692	GI1_047018_UGC02684
65	IC1959	033311.8	−502438	−51.54	6.06	trgb	13.26	9	1	1504	1504	GI1_047019_IC1959
66	UGC2847	034648.9	680546	10.58	3.03	ceph	9.37	6	0	4466	5747	LGAL_IC342
67	IC2000	034907.3	−485131	−49.60	10.7	v(flow)	13	6	0	544	544	MIS2DFR_38660_0817
68	ESO302-G014	035140.9	−382708	−50.88	9.6	v(flow)	16	10	0	1696	1696	GI1_047021_ESO302_G014
69	NGC1487	035546.1	−422205	−49.76	9.1	v(flow)	12.34	7	1	1696	1696	GI1_047022_NGC1487
70	ESO249-G036	035915.6	−455221	−48.61	9.6	v(flow)	15.8	10	0	1501	3095	GI1_047023_HorDwarf
71	UGCA86	035950.1	670837	10.65	2.96	trgb	13.50	10	0	155	155	AISCHV4_052_05261
72	NGC1510	040332.6	−432400	−48.23	9.8	v(flow)	13.5	−2	1	2370	2370	NGA_NGC1512
73	NGC1512	040354.3	−432057	−48.16	9.6	v(flow)	11.13	1	1	2370	2370	NGA_NGC1512
74	NGC1522	040607.7	−524009	−45.97	9.3	v(flow)	13.9	11	1	1434	3059	GI1_009026_NGC1518
75	NGC1518	040649.6	−211029	−45.31	10.8	v(flow)	12.3	8	0	1652	1737	GI1_047024_NGC1518
76	ESO483-G013	041241.3	−230936	−44.58	10.4	v(flow)	14.2	−3	1	2307	2307	GI4_095007_ESO483_G013
77	NGC1556	041744.5	−500952	−44.78	10.5	v(flow)	13.5	2	0	1504	3101	GI1_009038_NGC1556
78	UGCA90	042113.5	−215044	−42.31	10.4	v(flow)	12.7	7	0	1690	1690	GI1_047026_UGCA090
79	NGC1592	042940.8	−272431	−41.91	10.6	v(flow)	14.6	10	0	1552	3248	GI1_009020_HPJ0429m27
80	NGC1569	043049.0	645053	11.24	3.36	trgb	11.86	10	0	7148	7148	NGA_NGC1569
81	UGCA92	043204.9	633649	10.52	1.8	bs	15.22	10	0	221	221	AISCHV4_050_07132
82	NGC1560	043247.7	715246	16.02	3.45	trgb	12.2	7	0	209	209	AISCHV4_050_04972
83	ESO158-G003	044616.7	−572035	−39.30	10.0	v(flow)	14.01	9	1	2654	2654	GI4_095038_ESO158_G003
84	UGC3174	044834.5	001430	−26.91	8.1	v(flow)	15.02	10	0	192	192	AISCHV4_188_26696
85	ESO119-G016	045129.2	−613903	−37.77	9.8	v(flow)	14.8	10	1	3638	3638	GI4_095008_ESO119_G016
86	NGC1705	045413.7	−532141	−38.74	5.10	trgb	12.8	11	1	1436	3673	NGA_NGC1705
87	ESO252-IG001	045658.7	−424814	−38.50	6.0	v(flow)	14.4	99	0	...	...	...
88	NGC1744	045957.6	−260119	−35.02	7.7	v(flow)	11.6	6	1	1883	3874	GI1_047027_NGC1744
89	NGC1796	050242.8	−610823	−36.55	10.3	v(flow)	12.9	5	1	2587	2587	GI4_095009_NGC1796
90	ESO486-G021	050319.7	−252523	−34.13	8.9	v(flow)	14.5	2	1	1687	1687	GI4_095010_ESO486_G021
91	MCG-05-13-004	050624.1	−315711	−35.12	6.6	v(flow)	13.2	9	1	1695	4598	NGA_NGC1800
92	NGC1800	050625.4	−315715	−35.12	8.2	v(flow)	13.07	9	1	1695	4598	NGA_NGC1800
93	NGC1808	050742.3	−373046	−35.90	10.6	v(flow)	10.76	1	0	2155	2155	GI2_121004_LGG127_POS2
94	ESO305-G009	050807.6	−381833	−35.94	10.9	v(flow)	13	8	0	2829	2829	GI1_009064_HPJ0508m38
95	UGCA103	051047.0	−313550	−34.14	10.4	v(flow)	13.1	9	0	...	...	...
96	UGCA106	051159.3	−325821	−34.20	9.8	v(flow)	13.1	9	1	1616	4439	GI1_047029_UGCA106
97	UGCA105	051415.0	623431	13.66	3.15	trgb	14.5	10	0	216	216	AISCHV4_095_02872
98	LMC	052334.5	−694522	−32.89	0.05	ceph	0.91	9	1	...	...	...
99	UGC3303	052459.5	043018	−16.92	7.2	bs	13.95	10	0	...	...	...
100	ESO553-G046	052705.7	−204041	−27.42	5.0	v(flow)	14.5	1	0	225	225	AISCHV4_299_27736
101	ESO306-G013	053858.3	−414414	−30.67	10.8	v(flow)	14.2	3	0	...	...	...
102	UGCA114	055054.3	−144645	−19.94	9.8	v(flow)	12.97	7	0	110	110	AISCHV4_296_27462
103	UGCA116	055542.6	032330	−10.77	9.1	v(flow)	15.5	11	0	2465	2465	GI3_089007_IIZw40
104	KKH34	055941.2	732539	22.35	4.61	trgb	17.10	10	0	214	214	AISCHV3_094_02649
105	ESO364-G?029	060545.2	−330451	−23.37	7.4	v(flow)	14.0	10	0	...	...	...
106	AM0605-341	060719.3	−341217	−23.40	7.0	v(flow)	15.5	10	0	...	...	...
107	NGC2188	061009.5	−340622	−22.81	6.8	v(flow)	12.1	9	0	...	...	...
108	UGCA120	061116.3	−213557	−18.19	8.7	v(flow)	14.1	10	0	...	...	...
109	UGCA127	062055.5	−82942	−10.61	7.5	v(flow)	14.16	6	0	...	...	...
110	UGC3475	063028.8	393014	13.14	7.0	v(flow)	15.0	9	0	...	...	...
111	ESO255-G019	064548.2	−473152	−20.56	10.4	v(flow)	14	9	0	...	...	...
112	KKH37	064745.8	800726	26.54	3.26	trgb	16.40	10	1	1672	1672	GI3_061011_kkh037
113	ESO207-G007	065039.9	−520825	−21.21	10.7	v(flow)	14.2	9	0	116	116	AISCHV4_410_40316
114	UGC3600	065540.0	390543	17.48	7.3	bs	16.19	10	0	221	221	AISCHV4_082_04070
115	AM0704-582	070518.8	−583113	−21.15	4.90	trgb	14.95	9	0	...	...	...
116	NGC2337	071013.5	442726	21.80	7.9	bs	13.48	10	0	220	220	AISCHV4_078_03629
117	UGC3817	072244.5	450631	24.11	8.6	bs	15.96	10	0	87	87	AISCHV4_078_03729
118	UGC3860	072817.2	404612	23.93	7.81	trgb	15.1	10	0	1688	1688	GI4_016002_DDO43
119	NGC2366	072854.6	691257	28.53	3.21	trgb	11.43	10	1	2935	2935	NGA_NGC2366
120	UGC3876	072917.5	275358	20.04	10.8	v(flow)	14.1	6	0	...	...	...
121	ESO059-G001	073118.2	−681117	−21.48	4.57	trgb	13.98	10	0	...	...	...
122	NGC2427	073627.9	−473805	−12.70	9.0	v(flow)	12.33	8	0	...	...	...
123	NGC2403	073651.4	653609	29.18	3.22	ceph	8.93	6	1	3317	3317	NGA_NGC2403
124	UGC3966	074126.0	400644	26.17	6.8	bs	13.9	10	0	2857	2857	GI4_016003_DDO46
125	UGC3974	074155.4	164809	18.54	8.04	trgb	13.6	10	0	2493	2493	GI4_016004_DDO47
126	CGCG262-028	074732.1	511129	29.37	6.9	v(flow)	14.9	5	0	140	140	AISCHV3_079_03433
127	UGC4115	075701.8	142327	20.90	7.72	trgb	15.23	10	0	1315	1315	GI4_042006_AOHI075702p142337

Table 1
(Continued)

No. (1)	Galaxy Name (2)	R.A. (J2000) (3)	Decl. (J2000) (4)	b (deg) (5)	D (Mpc) (6)	Method (7)	B (mag) (8)	T (9)	Local Volume Legacy (10)	$t_{\rm fuv}$ (s) (11)	$t_{\rm nuv}$ (s) (12)	Tile Name (13)
128	NGC2500	080153.3	504415	31.56	7.6	v(flow)	12.2	7	1	2979	2979	NGA_NGC2500
129	NGC2537	081314.7	455926	32.96	6.9	bs	12.82	8	1	3204	3204	NGA_NGC2537
130	UGC4278	081358.9	454434	33.06	7.6	v(flow)	13.1	7	1	3204	3204	NGA_NGC2537
131	UGC4305	081904.0	704309	32.69	3.38	trgb	11.1	10	1	1677	1677	NGA_HolmbergII
132	NGC2552	081920.1	500025	34.29	7.7	v(flow)	12.6	9	1	1696	3386	MISDR1_03473_0440
133	M81dwA	082356.0	710145	33.01	3.44	trgb	18.69	10	1	1677	1677	NGA_HolmbergII
134	SDSSJ0825+3532	082555.5	353232	33.73	9.3	v(flow)	18.05	11	0	1120	2493	NGA_HS0822p3542
135	UGC4426	082828.4	415124	35.21	10.28	trgb	15.0	10	1	1696	1696	GI1_047032_UGC04426
136	UGC4459	083407.2	661054	34.95	3.61	trgb	14.78	10	1	1693	1693	NGA_DDO053
137	ESO495-G021	083615.4	−262434	8.58	7.8	v(flow)	12.46	11	0	...	...	...
138	UGC4483	083703.0	694631	34.38	3.41	trgb	15.27	10	1	1393	1393	NGA_UGC4483
139	NGC2683	085241.4	332514	38.76	7.7	sbf	10.64	3	1	1597	1597	GI4_095011_NGC2683
140	UGC4704	085900.3	391236	40.74	7.8	v(flow)	15.3	8	1	1247	2287	NGA_IRAS08572
141	LSBCD564-08	090253.8	200432	37.60	8.67	trgb	16.90	10	0	1582	1582	GI4_016008_F564mV3
142	UGC4787	090734.9	331636	41.81	6.5	v(flow)	15.4	8	1	1595	1595	GI4_095012_UGC04787
143	LSBCD634-03	090853.5	143455	36.94	9.46	trgb	17.50	10	0	149	149	AISCHV3_194_23888
144	UGCA148	090946.5	−230033	16.66	9.8	mem	15.3	10	0	...	...	...
145	NGC2784	091219.5	−241021	16.35	9.8	sbf	11.3	−2	0	5861	7250	NGA_NGC2784
146	UGCA153	091312.1	−192431	19.59	6.5	v(flow)	15.40	10	0	116	116	AISCHV4_210_25319
147	NGC2835	091752.9	−222118	18.51	8.0	v(flow)	11.0	5	0	106	106	AISCHV4_322_25486
148	LSBCD565-06	091930.0	213612	41.76	9.08	trgb	16.95	10	0	112	112	AISCHV3_193_16500
149	UGCA162	092128.1	−223007	19.03	7.5	v(flow)	15.2	9	0	117	117	AISCHV4_322_25486
150	UGC4998	092512.1	682259	38.89	10.5	sbf	14.72	10	1	1948	1948	NGA_Arp300
151	NGC2915	092611.5	−763736	−18.36	3.78	trgb	13.20	0	0	4728	4728	NGA_NGC2915
152	NGC2903	093210.1	213004	44.54	8.9	bs	9.68	4	1	1915	1915	NGA_NGC2903
153	UGC5076	093236.4	515219	45.57	8.3	v(flow)	15.2	10	1	...	...	...
154	CGCG035-007	093444.9	062532	38.99	5.2	v(flow)	15.5	5	1	1869	3472	GI1_047033_CGCG035_007
155	LeoT	093453.4	170305	43.66	0.42	trgb	16.40	10	0	1549	1550	NGA_LeoT
156	UGC5151	094027.1	482015	47.60	10.7	v(flow)	13.8	10	0	...	...	...
157	UGC5139	094032.3	711056	38.66	3.90	trgb	14.17	10	1	1704	1704	NGA_HolmbergI
158	IC559	094443.9	093655	42.70	4.9	v(flow)	14.8	5	1	1470	2704	GI1_047034_IC0559
159	UGC5209	094504.2	321418	49.51	6.4	v(flow)	16.06	10	0	208	208	AISCHV4_214_02210
160	NGC2976	094715.3	675500	40.90	3.56	trgb	11.24	5	1	1693	1693	GI3_061016_KK77
161	UGC5272b	095019.4	312721	50.55	7.1	mem	17.76	10	0	1542	1543	GI4_095013_UGC05272
162	UGC5272	095022.4	312916	50.56	7.1	bs	15.41	10	1	1542	1543	GI4_095013_UGC05272
163	UGC5288	095117.0	074939	43.25	6.8	bs	14.32	8	1	1676	1676	GI1_047035_UGC05288
164	NGC3037	095123.5	−270036	20.70	7.9	v(flow)	13.7	9	0	218	218	AISCHV4_322_25658
165	BK3N	095348.5	685809	40.83	3.86	trgb	18.78	10	1	3075	3075	NGA_M81andM82
166	NGC3031	095533.2	690355	40.90	3.63	ceph	7.89	2	1	3075	3075	NGA_M81andM82
167	NGC3034	095552.2	694047	40.57	3.37	trgb	9.30	7	1	3075	3075	NGA_M81andM82
168	UGC5340	095645.7	284935	51.62	5.9	bs	14.8	10	1	1439	1439	GI1_047036_UGC05340
169	KDG61	095703.1	683531	41.28	3.49	trgb	15.17	−6	1	16218	16218	GI2_024001_NGC3077_Stream
170	UGC5336	095732.0	690245	41.06	3.61	trgb	14.3	10	1	3075	3075	NGA_M81andM82
171	ESO435-G016	095846.2	−283719	20.57	9.1	v(flow)	13.6	3	0	4228	5882	NGA_Tol2
172	ESO435-IG020	095920.7	−280754	21.03	9.0	v(flow)	14.4	10	0	4228	5882	NGA_Tol2
173	UGC5364	095926.4	304447	52.42	0.69	trgb	12.9	10	1	1536	1536	GI4_016005_DDO69
174	UGC5373	100000.1	051956	43.78	1.39	trgb	11.8	10	1	1085	1085	NGA_SextansB
175	UGCA193	100236.0	−60049	37.43	9.7	mem	14.84	7	1	2169	2169	GI4_095015_UGCA193
176	NGC3109	100306.6	−260932	23.07	1.28	trgb	10.39	9	1	10338	13636	NGA_NGC3109
177	NGC3077	100320.6	684404	41.66	3.83	trgb	10.6	6	1	...	...	...
178	UGCA196	100341.8	−270140	22.49	8.8	v(flow)	13.4	6	0	11735	15032	NGA_Antlia_Dw
179	NGC3113	100426.1	−282639	21.51	10.5	v(flow)	13.3	7	0	...	...	...
180	UGC5427	100441.0	292155	53.40	7.1	bs	15.9	8	0	1594	1594	GI1_047038_UGC05427
181	UGC5428	100506.4	663332	43.09	3.53	trgb	15.95	10	1	1704	1704	GI3_061017_UGC05428
182	NGC3115	100514.0	−74307	36.78	9.7	sbf	9.87	−3	0	1304	1304	NGA_NGC3115
183	UGC5423	100530.6	702152	40.81	5.3	bs	15.20	10	1	1698	1698	NGA_M81DwB
184	NGC3125	100633.6	−295609	20.64	10.8	v(flow)	13.5	11	0	3024	5927	NGA_NGC3125
185	UGC5453	100707.3	155904	50.40	9.3	v(flow)	15.8	10	0	...	...	...
186	UGC5451	100719.0	470022	52.31	8.7	v(flow)	14.4	10	0	122	122	AISCHV3_081_01122
187	UGC5456	100719.6	102146	47.94	3.80	trgb	13.7	5	1	1552	1552	GI4_095016_UGC05456
188	KUG1004+392	100723.0	385810	53.99	7.8	v(flow)	16.0	10	0	119	119	AISCHV3_086_01586
189	NGC3137	100907.5	−290352	21.67	10.8	v(flow)	12.1	6	0	...	...	...
190	SextansA	101100.8	−44134	39.88	1.32	ceph	11.86	10	1	1689	1689	NGA_SextansA
191	NGC3175	101442.1	−285219	22.58	10.7	v(flow)	12.13	2	0	225	225	AISCHV4_328_25973

Table 1
(Continued)

No. (1)	Galaxy Name (2)	R.A. (J2000) (3)	Decl. (J2000) (4)	b (deg) (5)	D (Mpc) (6)	Method (7)	B (mag) (8)	T (9)	Local Volume Legacy (10)	$t_{\rm fuv}$ (s) (11)	$t_{\rm nuv}$ (s) (12)	Tile Name (13)
192	NGC3239	102505.6	170937	54.82	8.3	v(flow)	11.7	9	1	1766	1766	GI1_047039_NGC3239
193	UGC5672	102820.9	223417	57.33	6.3	bs	15.1	5	1	1772	1772	GI1_047040_UGC05672
194	UGC5666	102821.2	682443	43.61	3.81	trgb	10.8	9	1	1848	3520	NGA_IC2574
195	UGC5692	103035.0	703707	42.18	3.80	trgb	13.71	9	1	1821	3505	GI1_047041_UGC05692
196	NGC3274	103217.1	274007	59.21	6.5	bs	13.2	7	1	1661	1661	GI1_047042_NGC3274
197	UGC5740	103445.8	504606	54.98	9.3	v(flow)	15.6	9	0	100	100	AISCHV4_092_01025
198	UGCA212	103523.2	−244515	28.62	10.1	v(flow)	13.2	8	0	175	175	AISCHV4_324_25706
199	NGC3299	103623.8	124227	55.29	10.4	mem	14.1	8	1	1076	2253	GI4_095017_NGC3299
200	UGC5764	103643.3	313248	60.43	7.1	v(flow)	15.2	10	1	1614	1614	GI1_047043_UGC05764
201	UGC5797	103925.2	014305	49.44	6.8	v(flow)	15.0	10	1	1660	1660	GI1_047044_UGC05797
202	IC625	104238.0	−235608	30.22	10.1	v(flow)	13.8	5	0	214	214	AISCHV4_324_25582
203	UGC5829	104242.2	342656	61.53	7.9	v(flow)	13.7	10	1	2189	2189	GI1_047045_UGC05829
204	NGC3344	104330.9	245522	61.26	6.6	v(flow)	10.4	4	1	1414	1718	NGA_NGC3344
205	NGC3351	104357.8	114214	56.37	10.00	ceph	10.53	3	1	1701	1701	NGA_NGC3351
206	NGC3365	104612.6	014848	50.75	10.5	v(flow)	13.2	6	0	2987	2987	GI1_047046_NGC3365
207	NGC3368	104645.7	114912	57.01	10.52	ceph	10.1	2	1	1698	1698	NGA_NGC3368
208	UGC5889	104722.3	140410	58.29	9.3	bs	14.2	9	1	1639	1639	GI3_084014_J104728p135322
209	UGC5917	104853.9	464314	58.98	10.3	v(flow)	16.1	10	0	106	106	AISCHV4_091_01363
210	UGC5923	104907.6	065502	54.64	7.2	v(flow)	14.0	0	1	3259	3259	GI3_046013_UGC5923
211	UGC5918	104936.5	653150	47.12	7.4	bs	15.22	10	1	1530	1530	GI4_016006_DDO87
212	NGC3412	105053.3	132444	58.70	10.4	mem	11.4	−2	0	1641	1641	GI3_084016_J104952p130942
213	ESO376-G022	105121.0	−342550	22.20	9.0	v(flow)	14.2	10	0	...	...	...
214	NGC3432	105231.3	363711	63.16	7.9	v(flow)	11.7	9	1	1717	1717	GI4_095018_NGC3432
215	KDG73	105257.1	693258	44.23	4.03	trgb	17.28	10	1	1703	1703	GI1_047048_KDG073
216	NGC3489	110018.6	135404	60.91	10.4	mem	11.1	−1	0	1642	1642	GI3_087007_NGC3489
217	NGC3486	110023.9	285830	65.49	8.2	v(flow)	11.05	5	1	1488	3069	GI4_095046_NGC3486
218	UGC6102	110148.4	284121	65.78	8.5	v(flow)	15.5	10	0	541	1989	NGA_NGC3486
219	NGC3510	110343.4	285313	66.21	8.6	v(flow)	14	8	1	1565	1565	GI1_047049_NGC3510
220	ESO377-G003	110355.2	−342130	23.45	9.2	v(flow)	14.9	4	0	110	110	AISCHV4_455_37081
221	MRK36	110458.5	290822	66.49	7.8	v(flow)	15.7	11	0	1565	1565	GI1_047049_NGC3510
222	NGC3521	110548.6	−00209	52.83	8.0	v(flow)	9.83	4	1	1809	1809	NGA_NGC3521
223	UGC6161	110649.2	434324	63.19	10.3	v(flow)	15	8	0	1460	1460	GI3_121012_J110638p432344
224	MESSIER108	111131.0	554027	56.25	10.4	v(flow)	10.69	6	0	1623	1623	GI4_034001_M108
225	NGC3593	111437.0	124904	63.21	6.5	v(flow)	11.86	0	1	1596	1596	GI4_095041_NGC3593
226	NGC3599	111527.0	180637	66.14	9.6	v(flow)	12.8	−2	0	2468	2468	GI3_079016_NGC3608
227	NGC3600	111552.1	413532	65.68	9.7	v(flow)	14.0	1	0	1583	1583	GI1_047050_NGC3600
228	NGC3621	111816.0	−324842	26.10	6.64	ceph	10.2	7	0	10926	10926	NGA_NGC3621
229	NGC3623	111855.9	130537	64.22	8.9	v(flow)	10.25	1	1	1650	1650	GI3_041004_NGC3623
230	NGC3627	112015.0	125930	64.42	10.05	ceph	9.7	3	1	1680	3072	NGA_NGC3627
231	NGC3628	112016.9	133520	64.78	9.4	v(flow)	10.28	3	1	7511	7512	NGA_NGC3628_cen
232	IC2782	112255.3	132629	65.21	9.7	v(flow)	14.9	8	0	102	1625	AISCHV4_232_12480, GI5_002014_HI1123377p125353_0001
233	IC2787	112319.1	133747	65.40	7.7	v(flow)	16.1	6	0	...	...	...
234	NGC3675	112608.6	433509	66.19	10.6	v(flow)	11.0	3	0	105	105	AISCHV4_102_01355
235	UGC6457	112712.2	−05941	55.34	10.2	v(flow)	15	10	1	2241	3353	GI4_095019_UGC06457
236	UGC6456	112759.9	785939	37.33	4.34	trgb	15.9	10	0	1642	1642	NGA_VIIZw403
237	UGC6541	113328.9	491414	63.28	3.89	trgb	14.40	11	1	1648	1648	GI4_016011_MRK178
238	NGC3738	113548.8	543126	59.31	4.90	trgb	11.97	10	1	1620	1620	GI4_016009_NGC3738
239	NGC3741	113606.2	451701	66.45	3.24	trgb	14.49	10	1	1663	3231	GI1_047051_NGC3741
240	LEDA166115	114711.2	434019	68.98	4.51	trgb	18.62	10	0	122	122	AISCHV3_102_01354
241	UGC6817	115053.0	385249	72.74	2.59	trgb	13.56	10	1	2373	2373	GI1_047053_UGC06817
242	UGC6900	115539.4	313110	77.08	7.5	v(flow)	14.8	10	1	1677	1677	GI1_047054_UGC06900
243	BTS76	115844.1	273506	78.29	6.0	v(flow)	16.50	10	0	1417	1417	GI1_026016_Arp305
244	NGC4020	115856.6	302444	78.05	9.7	v(flow)	13.8	7	1	1680	1680	GI1_047055_NGC4020
245	UGC7007	120133.1	332029	77.58	10.1	v(flow)	16.30	9	0	136	136	AISCHV4_112_12396
246	NGC4068	120400.8	523518	63.04	4.31	trgb	13.02	10	1	2569	2569	GI4_095022_NGC4068
247	NGC4080	120451.8	265933	79.63	6.9	v(flow)	14.3	10	1	1688	1688	GI1_047056_NGC4080
248	NGC4096	120601.0	472840	67.79	8.3	v(flow)	11.48	5	1	1660	1660	GI1_047058_NGC4096
249	KUG1207+367	120956.4	362607	77.20	4.5	v(flow)	15.50	10	0	7205	10324	GI4_015004_NGC4163
250	NGC4144	120958.4	462727	69.01	9.8	bs	12.1	6	1	1664	4541	GI1_047059_NGC4144
251	NGC4163	121209.1	361009	77.70	2.87	trgb	13.75	10	1	1677	1677	GI3_061001_NGC4163
252	NGC4190	121344.7	363803	77.59	3.5	bs	13.9	10	1	1677	1677	GI3_061001_NGC4163
253	UGC7242	121408.4	660541	50.60	5.42	trgb	14.7	6	1	1697	1697	MISDR1_00419_0493
254	UGCA276	121457.9	361308	78.06	2.95	trgb	15.70	10	1	1677	1677	GI3_061001_NGC4163

Table 1
(Continued)

No.	Galaxy Name	R.A. (J2000)	Decl. (J2000)	b (deg)	D (Mpc)	Method	B (mag)	T	Local Volume Legacy	t_{fuv} (s)	t_{nuv} (s)	Tile Name
(1)	(2)	(3)	(4)	(5)	(6)	(7)	(8)	(9)	(10)	(11)	(12)	(13)
255	NGC4204	121514.5	203931	79.50	10.4	v(flow)	14.0	8	0	1546	1693	GI1_047061_NGC4204
256	UGC7267	121523.6	512058	64.84	7.3	v(flow)	15.3	8	1	1658	1658	GI1_047062_UGC07267
257	UGC7271	121533.3	432606	72.15	7.8	v(flow)	15.53	7	0	1669	2568	GI1_047063_UGC07271
258	NGC4214	121538.9	361940	78.07	3.04	trgb	10.2	10	1	2003	2003	GI4_095023_NGC4214
259	CGCG269-049	121546.7	522315	63.87	3.2	v(flow)	15.30	10	1	1652	1652	GI3_061013_CGCG269_049
260	UGC7298	121630.1	521339	64.06	4.21	trgb	16.06	10	0	1674	1674	GI3_061013_CGCG269_049
261	NGC4236	121642.1	692746	47.36	4.45	trgb	10.1	8	1	1690	1690	NGA_NGC4236
262	NGC4244	121729.9	374829	77.16	4.49	trgb	10.9	6	1	1607	3087	GI1_047064_NGC4244
263	NGC4242	121730.1	453708	70.32	7.4	v(flow)	11.4	8	1	559	2250	NGA_NGC4242
264	NGC4248	121750.3	472431	68.68	7.2	v(flow)	13.21	3	1	1642	1642	GI4_095048_NGC4258
265	IC3104	121846.0	−794334	−16.95	2.27	trgb	13.5	10	0	...	...	...
266	NGC4258	121857.5	471814	68.84	7.98	ceph	9.10	4	1	1642	1642	GI4_095048_NGC4258
267	UGC7356	121909.1	470523	69.05	6.7	sbf	15.58	10	0	...	1674	...
268	ISZ399	121959.5	−172331	44.83	9.0	v(flow)	14.7	11	1	...	...	...
269	NGC4288	122038.1	461733	69.89	7.7	v(flow)	13.3	7	1	1510	2756	GI1_047066_NGC4288
270	UGC7408	122115.0	454841	70.38	6.9	v(flow)	13.3	9	1	1510	2756	GI1_047066_NGC4288
271	UGC7490	122425.3	702001	46.62	8.4	v(flow)	13.1	9	1	...	...	...
272	LEDA166137	122527.9	282857	84.10	6.0	v(flow)	16.50	10	0	95	95	AISCHV4_113_12847
273	NGC4395	122548.9	333248	81.53	4.61	trgb	10.6	9	1	1696	1696	NGA_NGC4395
274	UGCA281	122616.0	482937	68.08	5.7	bs	15.4	11	1	1672	1672	GI1_047067_UGCA281
275	UGC7559	122705.1	370833	78.74	4.87	trgb	14.2	10	1	1680	1680	GI1_047068_UGC07559
276	UGC7577	122740.9	432944	72.94	2.58	trgb	12.8	10	1	1687	1687	GI1_047069_UGC07577
277	UGC7584	122802.9	223522	83.02	7.3	v(flow)	16.20	9	0	2462	2462	GI1_047071_NGC4455
278	LSBCF573-01	122805.4	221727	82.82	7.2	v(flow)	17.00	10	0	2462	2462	GI1_047071_NGC4455
279	NGC4449	122811.2	440536	72.40	4.21	trgb	10.0	10	1	845	845	NGA_NGC4449
280	UGC7599	122828.5	371401	78.79	6.9	bs	14.88	8	1	1680	1680	GI1_047068_UGC07559
281	UGC7605	122838.7	354303	80.14	4.43	trgb	14.8	10	1	1680	1680	GI1_047070_UGC07605
282	NGC4455	122844.1	224921	83.29	7.8	v(flow)	14	7	1	2462	2462	GI1_047071_NGC4455
283	UGC7608	122845.3	431335	73.26	7.8	v(flow)	13.7	10	1	1687	1687	GI1_047069_UGC07577
284	NGC4460	122845.5	445151	71.69	9.6	sbf	12.8	−1	1	845	845	NGA_NGC4449
285	MCG+07-26-011	122852.2	421041	74.26	6.0	v(flow)	16.33	8	0	1587	2810	NGA_NGC4490
286	UGC7639	122953.4	473152	69.17	8.0	bs	13.99	10	1	3249	5883	GI1_047072_UGC07639
287	MCG+07-26-012	123023.8	425406	73.66	6.4	v(flow)	16.47	6	0	1671	1671	GI4_095025_UGC7690
288	NGC4485	123031.1	414201	74.81	7.1	v(flow)	12.32	10	1	1587	2810	NGA_NGC4490
289	NGC4490	123036.1	413834	74.87	8.0	v(flow)	10.22	7	1	1587	2810	NGA_NGC4490
290	UGC7678	123200.7	394959	76.67	9.3	v(flow)	16	6	0	103	103	AISCHV3_107_01912
291	UGC7690	123226.8	424218	73.95	7.7	v(flow)	13.1	10	1	1671	1671	GI4_095025_UGC7690
292	UGC7699	123248.0	373718	78.80	6.8	v(flow)	13.6	6	1	1654	1654	GI1_047074_UGC07699
293	UGC7698	123254.4	313228	84.02	6.1	bs	13.0	10	1	1671	1671	GI1_047075_UGC07698
294	UGC7719	123400.6	390110	77.57	9.4	v(flow)	15.3	8	1	1677	3287	GI1_047076_UGC07719
295	NGC4534	123405.4	353108	80.83	10.8	v(flow)	13.0	8	0	1677	1677	GI1_047077_NGC4534
296	UGC7774	123622.5	400019	76.75	7.4	v(flow)	15.02	7	1	1661	1661	GI4_095042_UGC7774
297	UGCA290	123721.8	384438	78.02	6.70	trgb	15.74	11	0	121	121	AISCHV4_107_01563
298	UGCA292	123840.0	324601	83.72	3.62	trgb	16.10	10	1	1728	3301	GI4_016001_CVNIDWA
299	M104	123959.4	−113723	51.15	9.3	sbf	8.98	1	1	1911	1911	NGA_NGC4594
300	NGC4605	124000.3	613629	55.47	5.47	trgb	10.89	5	1	1654	1654	GI1_047078_NGC4605
301	NGC4618	124132.7	410904	75.83	7.8	v(flow)	11.22	8	1	3242	3242	NGA_NGC4625
302	NGC4625	124152.6	411626	75.72	8.7	v(flow)	12.92	9	1	3242	3242	NGA_NGC4625
303	NGC4631	124208.0	323226	84.22	8.1	v(flow)	9.8	7	1	1465	1465	NGA_NGC4631
304	UGC7866	124215.1	383012	78.46	4.57	trgb	13.7	10	1	1680	1680	GI1_047079_IC3687
305	NGC4656	124357.7	321005	84.70	8.6	v(flow)	10.96	9	1	1672	3376	GI1_047080_NGC4656
306	UGC7916	124425.1	342312	82.59	8.2	v(flow)	15	10	1	1349	1349	GI1_047081_UGC07916
307	ESO381-G020	124600.4	−335017	29.02	5.44	trgb	14.7	10	0	94	94	AISCHV4_432_45330
308	UGCA298	124655.4	263351	88.85	10.3	v(flow)	15.6	−3	0	116	116	AISCHV4_113_12985
309	UGC7950	124656.4	513646	65.50	7.9	v(flow)	15.1	10	1	1664	1664	GI1_047082_UGC07950
310	UGC7949	124659.8	362835	80.60	9.9	bs	15.12	10	1	1950	2846	GI1_047083_UGC07949
311	NGC4707	124822.9	510953	65.96	7.4	v(flow)	13.4	9	1	1664	1664	GI1_047082_UGC07950
312	NGC4736	125053.0	410714	76.01	4.66	trgb	9.0	2	1	3994	3994	NGA_NGC4736
313	UGC8024	125405.2	270855	89.41	4.3	bs	13.9	10	1	1442	1442	NGA_DDO154
314	UGC8055	125604.3	034843	66.66	6.6	v(flow)	17.00	10	0	110	110	AISCHV4_228_13578
315	NGC4826	125643.7	214052	84.42	7.5	sbf	9.36	2	1	1330	5813	WDST_GD_153
316	UGC8091	125840.4	141303	76.98	2.08	trgb	14.68	10	1	110	110	AISCHV4_223_13511
317	UGC8146	130208.1	584205	58.37	10.6	v(flow)	14.4	6	0	6599	6599	GI2_025004_PG1259p593
318	UGCA319	130214.4	−171415	45.56	7.4	v(flow)	15.0	9	1	1456	7086	GI1_047084_UGCA319

Table 1
(Continued)

No.	Galaxy Name	R.A. (J2000)	Decl. (J2000)	b (deg)	D (Mpc)	Method	B (mag)	T	Local Volume Legacy	$t_{\rm fuv}$ (s)	$t_{\rm nuv}$ (s)	Tile Name
(1)	(2)	(3)	(4)	(5)	(6)	(7)	(8)	(9)	(10)	(11)	(12)	(13)
319	UGCA320	130316.8	−172523	45.36	7.2	v(flow)	13.5	9	1	1456	7086	GI1_047084_UGCA319
320	NGC4945	130527.5	−492806	13.34	3.6	mem	9.3	6	0	...	...	...
321	UGC8188	130549.5	373618	79.09	4.49	ceph	12	9	1	1666	1666	GI1_047085_IC4182
322	UGC8201	130624.8	674225	49.36	4.57	trgb	12.8	10	1	1701	1701	NGA_DDO165
323	MCG-03-34-002	130756.6	−164121	46.00	10.2	v(flow)	14.8	4	1	1658	1658	GI4_095039_MCG_03_34_002
324	UGC8215	130803.6	464941	70.03	4.55	trgb	16.08	10	0	1584	3105	GI1_047086_UGC08215
325	UGC8245	130834.2	785613	38.16	3.6	v(flow)	15.2	10	1	1549	1549	GI4_095026_UGC08245
326	NGC5023	131212.1	440220	72.58	5.4	bs	12.8	6	1	1586	4723	GI1_047087_NGC5023
327	CGCG217-018	131251.8	403235	75.87	8.2	v(flow)	15.1	10	1	1321	2901	GI4_095027_CGCG217_018
328	UGC8308	131322.7	461913	70.32	4.19	trgb	15.54	10	0	1576	3105	GI1_047088_UGC08308
329	UGC8313	131354.1	421236	74.24	8.7	v(flow)	14.78	5	1	1655	1655	NGA_NGC5055
330	UGC8320	131427.9	455509	70.66	4.33	trgb	13.11	10	1	1576	3105	GI1_047088_UGC08308
331	UGC8331	131530.3	472956	69.09	8.2	bs	14.31	10	1	1628	2503	GI1_047090_UGC08331
332	NGC5055	131549.2	420149	74.29	7.5	v(flow)	9.31	4	1	1655	1655	NGA_NGC5055
333	NGC5068	131854.6	−210220	41.38	6.2	v(flow)	10.7	6	1	1601	4783	GI1_047091_NGC5068
334	NGC5102	132157.6	−363749	25.84	3.40	trgb	10.35	−3	0	...	...	...
335	NGC5128	132527.6	−430109	19.42	3.66	trgb	7.84	−2	0	20073	30429	NGA_Cen_A_Jet
336	IC4247	132644.4	−302145	31.89	4.97	trgb	14.6	2	1	1663	1663	GI4_095028_IC4247
337	ESO324-G024	132737.3	−412850	20.88	3.73	trgb	12.9	10	0	121	121	AISCHV4_471_45528
338	NGC5204	132936.2	582506	58.00	4.65	trgb	11.7	9	1	1488	1488	GI4_095029_NGC5204
339	NGC5194	132952.7	471143	68.56	8.0	mem	8.96	4	1	2520	2520	NGA_M51
340	NGC5195	132958.7	471605	68.49	8.0	sbf	10.45	2	1	2520	2520	NGA_M51
341	UGC8508	133044.4	545436	61.31	2.58	trgb	13.94	10	1	...	...	...
342	SBS1331+493	133322.9	490606	66.58	9.3	v(flow)	16.5	11	0	...	...	...
343	NGC5206	133343.8	−480904	14.12	3.6	mem	12	−3	0	...	...	...
344	NGC5229	133402.7	475455	67.61	5.1	bs	14.18	7	1	2757	2757	GI1_047092_NGC5229
345	NGC5238	133442.7	513651	64.19	5.2	bs	13.60	8	1	1618	1618	GI1_047093_NGC5238
346	ESO270-G017	133447.3	−453251	16.66	8.9	tf	12	4	0	...	...	...
347	[KK98]208	133635.5	−293417	32.28	4.68	trgb	14.30	−1	1	13361	13366	GI3_050007_NGC5236
348	NGC5236	133700.8	−295159	31.97	4.47	ceph	8.20	5	1	13361	13366	GI3_050007_NGC5236
349	ESO444-G084	133720.1	−280246	33.74	4.61	trgb	15.5	10	1	1571	6357	GI1_047094_ESO444_G084
350	UGC8638	133919.4	244632	78.98	4.27	trgb	15	10	1	1604	1604	GI1_047095_UGC08638
351	UGC8651	133953.8	404421	73.12	3.14	trgb	14.45	10	1	1690	1690	GI1_047096_UGC08651
352	NGC5253	133955.9	−313824	30.10	3.15	ceph	10.9	11	1	1657	1657	GI4_095049_NGC5253
353	IC4316	134018.4	−285332	32.77	4.40	trgb	14.6	10	0	217	217	AISCHV4_491_35380
354	NGC5264	134136.9	−295450	31.71	4.53	trgb	12.6	9	1	1878	1878	GI4_095030_NGC5264
355	UGC8683	134232.4	393930	73.58	9.6	v(flow)	15.6	10	0	2400	5044	GI1_047097_UGC08683
356	ESO325-G011	134500.5	−415140	19.91	3.40	trgb	14.0	10	0	...	...	...
357	ESO383-G087	134917.8	−360342	25.36	3.45	trgb	11.7	8	0	...	...	...
358	ESO383-G091	135032.3	−371720	24.10	3.6	mem	14.43	7	0	136	136	AISCHV4_466_45755
359	UGC8760	135050.6	380109	73.45	3.22	trgb	14.45	10	1	2425	2425	GI1_047098_UGC08760
360	UGC8837	135445.7	535403	60.80	8.3	bs	13.71	10	1	...	...	...
361	UGC8833	135448.7	355015	73.96	3.08	trgb	15.15	10	1	1234	2706	GI1_047099_UGC08833
362	ESO384-G016	135701.5	−352002	25.65	4.53	trgb	15.0	10	0	111	111	AISCHV4_351_45685
363	NGC5457	140312.5	542055	59.77	6.70	ceph	8.31	6	1	1040	1040	NGA_M101
364	NGC5408	140321.0	−412244	19.50	4.81	trgb	12.2	10	0	...	...	...
365	NGC5474	140501.5	533945	60.19	7.2	bs	11.82	6	1	1604	1604	NGA_NGC5474
366	NGC5477	140533.1	542739	59.49	7.7	bs	14.24	9	1	1040	1040	NGA_M101
367	KKR03	140710.7	350337	71.99	1.97	trgb	17.84	10	1	2090	2090	GI3_061004_KKR03
368	Circinus	141309.3	−652021	−3.81	2.8	tf	12.1	3	0	...	...	...
369	KUG1413+573	141509.4	570515	56.56	7.4	mem	16.10	10	0	108	108	AISCHV4_101_11865
370	UGC9128	141556.5	230319	70.46	2.21	trgb	14.46	10	1	1986	5293	GI4_016007_DDO187
371	SBS1415+437	141701.4	433005	66.20	9.5	v(flow)	18	11	0	112	112	AISCHV3_109_01380
372	NGC5585	141948.2	564346	56.48	5.7	bs	11.2	7	1	2936	2936	GI4_095032_NGC5585
373	UGC9211	142232.2	452302	64.28	10.7	v(flow)	14.80	10	0	96	96	AISCHV4_105_10645
374	NGC5608	142317.9	414633	66.19	10.2	v(flow)	14.1	10	0	121	121	AISCHV3_109_01380
375	UGC9240	142443.4	443133	64.48	2.79	trgb	13.31	10	1	2737	4209	GI1_047101_UGC09240
376	UKS1424-460	142803.7	−461806	13.38	3.58	trgb	16.50	10	0	...	...	...
377	ESO222-G010	143502.6	−492514	10.05	5.4	v(flow)	16.33	10	0	...	...	...
378	UGC9405	143524.4	571519	54.71	8.0	bs	14.57	10	1	1523	1523	GI4_095033_UGC09405
379	MRK475	143905.4	364821	65.31	9.0	v(flow)	15.5	11	1	1932	3618	GI1_047102_MRK0475
380	ESO272-G025	144325.5	−444219	13.75	5.6	v(flow)	14.93	8	0	...	...	...
381	UGC9497	144412.8	423744	62.37	10.0	v(flow)	15.9	6	0	192	192	AISCHV4_110_10896
382	NGC5832	145745.7	714056	42.16	8.8	v(flow)	12.9	3	1	1432	1432	GI1_047103_NGC5832

Table 1
(Continued)

No. (1)	Galaxy Name (2)	R.A. (J2000) (3)	Decl. (J2000) (4)	b (deg) (5)	D (Mpc) (6)	Method (7)	B (mag) (8)	T (9)	Local Volume Legacy (10)	t_{fuv} (s) (11)	t_{nuv} (s) (12)	Tile Name (13)
383	ESO223-G009	150108.7	−481726	9.17	6.49	trgb	13	10	0	...	...	...
384	UGC9660	150109.3	444153	58.73	10.2	v(flow)	14.2	4	0	198	198	AISCHV4_105_10892
385	ESO274-G001	151413.6	−464836	9.34	3.09	trgb	11.7	7	0	...	...	...
386	NGC5949	152800.7	644547	44.97	8.5	v(flow)	13.4	4	1	1578	3822	GI1_047104_NGC5949
387	UGC9893	153257.3	462710	52.90	10.9	v(flow)	15	7	0	8379	8379	GI4_015005_IZW115
388	UGC9992	154147.8	671515	42.37	8.6	v(flow)	14.86	10	1	2239	3447	GI1_047105_UGC09992
389	LEDA100404	160858.9	173025	43.60	6.8	v(flow)	17.4	9	0	...	...	...
390	ESO137-G018	162059.2	−602916	−7.43	6.40	trgb	12.2	5	0	...	...	...
391	ESO179-IG013	164720.0	−572628	−7.90	9.0	v(flow)	15	9	0	...	...	...
392	UGC10669	170025.3	701724	34.68	9.2	v(flow)	16.3	10	0	181	181	AISCHV4_002_09801
393	UGC10736	170805.0	692750	34.27	9.8	v(flow)	15.1	8	0	1561	1561	GI1_047106_UGC10736
394	IC4662	174706.4	−643825	−17.85	2.44	trgb	11.7	10	0	158	158	AISCHV4_476_43915
395	NGC6503	174927.1	700840	30.64	5.27	trgb	10.91	6	1	1597	4303	GI1_097010_NGC6503
396	ESO140-G019	182246.4	−621613	−20.61	10.8	v(flow)	16.8	10	0	...	...	...
397	IC4710	182838.1	−665854	−22.65	7.7	v(flow)	12.5	9	0	...	...	...
398	NGC6689	183450.1	703127	26.83	9.8	v(flow)	13.1	6	0	...	...	...
399	ESO104-G022	185541.2	−644839	−24.81	8.7	v(flow)	15.5	10	0	...	...	...
400	NGC6744	190946.2	−635125	−26.14	9.4	v(flow)	9.1	4	0	1290	1290	LGAL_NGC6744n
401	ESO104-G044	191123.1	−641309	−26.38	8.4	v(flow)	14.9	9	0	1290	1290	LGAL_NGC6744n
402	NGC6789	191641.9	635818	21.52	3.60	trgb	14	10	0	1403	1403	NGA_NGC6789
403	ESO594-G004	192959.0	−174041	−16.29	1.04	trgb	13.99	10	0	2898	2898	GI4_016010_SAGDIG
404	IC4870	193737.6	−654843	−29.27	9.9	v(flow)	14.4	10	0	216	216	AISCHV4_373_44415
405	NGC6822	194456.6	−144721	−18.40	0.50	ceph	9.31	10	0	4590	6132	NGA_NGC6822
406	IC4951	200931.2	−615047	−32.84	9.3	v(flow)	13.9	8	1	2401	2401	GI4_095050_IC4951
407	UGC11583	203015.3	602625	12.31	5.9	bs	15.70	10	0	...	...	...
408	LEDA166192	203032.9	602117	12.23	5.9	bs	16.50	8	0	...	...	...
409	LEDA166193	203132.0	604844	12.39	5.9	bs	16.70	10	0	...	...	...
410	NGC6946	203452.3	600914	11.67	5.9	bs	9.61	6	0	885	885	UVX_NGC6946
411	KKR55	204520.8	602440	10.78	5.9	bs	18	10	0	...	...	...
412	DDO210	204651.8	−125053	−31.34	0.94	trgb	14.1	10	1	1695	1695	GI1_047107_DDO210
413	KKR56	204824.1	583706	9.37	5.9	bs	17.60	10	0	...	...	...
414	CEPHEUS1	205110.6	565325	8.01	5.9	mem	15.40	10	0	...	...	...
415	IC5052	205206.3	−691213	−35.81	5.9	v(flow)	11.8	7	1	2666	2666	GI4_095045_IC5052
416	KKR59	210324.2	571714	6.99	5.9	bs	15.70	10	0	...	...	...
417	KKR60	210551.3	571232	6.69	5.9	mem	18.00	10	0	...	...	...
418	NGC7064	212903.0	−524603	−44.82	9.9	v(flow)	13.1	5	1	1971	1971	GI1_047108_NGC7064
419	NGC7090	213628.6	−543324	−45.38	10.4	v(flow)	11.3	5	1	3010	3091	GI1_047109_NGC7090
420	IC5152	220241.9	−511744	−50.19	1.97	trgb	10.7	10	1	4076	4077	GI4_095034_IC5152
421	UGC11891	220333.9	434457	−9.36	10.8	v(flow)	15.3	10	0	...	...	...
422	ESO238-G005	222230.0	−482418	−54.24	8.9	v(flow)	15.60	10	0	2418	2418	GI1_047110_ESO238_G005
423	IC5256	224945.8	−684126	−44.73	10.8	v(flow)	14.6	8	1	1856	1856	GI4_095040_IC5256
424	NGC7640	232206.6	405043	−18.94	8.9	v(flow)	11.9	5	0	...	...	...
425	UGC12588	232442.4	412048	−18.64	9.5	v(flow)	14.4	8	0	...	...	...
426	UGCA438	232627.5	−322320	−70.86	2.18	trgb	14.7	10	1	1693	1693	NGA_UGCA438
427	ESO347-G017	232656.0	−372049	−69.49	9.4	v(flow)	14.41	9	1	2252	2252	GI4_095035_ESO347_G017
428	UGC12613	232836.2	144435	−43.55	0.76	trgb	12.5	10	1	1576	2932	MISDR2_28664_0746
429	UGC12632	232958.7	405925	−19.31	9.6	v(flow)	12.8	9	0	196	196	AISCHV3_037_08795
430	IC5332	233427.4	−360605	−71.37	9.5	v(flow)	11.2	7	1	2646	2646	GI4_095036_IC5332
431	NGC7713	233615.4	−375619	−70.88	9.3	v(flow)	11.5	7	1	...	...	...
432	UGC12713	233814.4	304229	−29.58	7.7	v(flow)	14.91	0	0	2896	2896	GI3_089016_MRK328
433	UGCA442	234345.5	−315722	−74.53	4.27	trgb	13.6	9	1	871	871	GI4_095037_UGCA442
434	ESO348-G009	234923.5	−374619	−73.17	8.6	v(flow)	17	10	0	2534	4032	GI1_047111_ESO348_G009
435	ESO149-G003	235202.8	−523440	−62.24	6.4	tf	15.0	10	1	1563	1622	GI1_047112_ESO149_G003
436	NGC7793	235749.7	−323530	−77.17	3.91	trgb	9.63	7	1	1552	1552	NGA_NGC7793
1	ESO410-G005	001531.4	321047	−80.71	2.01	trgb	14.95	−1	1	1501	1501	GI3_061005_ESO410_G005
2	SCULPTOR-DE1	002351.7	−244218	−83.34	4.19	trgb	17.8	−3	1	1584	1584	GI3_061022_SculptordE1
3	ESO294-G010	002633.4	−415119	−74.42	1.94	trgb	15.52	−3	1	2703	2703	GI3_061006_ESO294_G010
4	ESO540-G030	004920.9	−180432	−80.93	3.33	trgb	16.46	−1	1	1656	1656	GI3_061012_ESO540_G030
5	ESO540-G032	005024.3	−195424	−82.77	3.54	trgb	16.6	−3	1	1247	1247	GI3_061014_ESO540_G032
6	UGC521	005112.2	120131	−50.85	11.3	v(flow)	15.31	10	1	1613	1613	GI1_078003_UGC00521
7	NGC0404	010927.0	354304	−27.01	3.05	trgb	11.51	−1	1	2472	2472	NGA_NGC0404_CEN
8	IC2049	041204.3	−583325	−43.35	16.7	v(flow)	15.19	7	1	2602	2603	GI1_047025_IC2049
9	UGCA133	073411.4	665310	28.96	3.10	trgb	15.80	−3	1	1696	1696	GI3_061009_UGCA133

Table 1
(Continued)

No. (1)	Galaxy Name (2)	R.A. (J2000) (3)	Decl. (J2000) (4)	b (deg) (5)	D (Mpc) (6)	Method (7)	B (mag) (8)	T (9)	Local Volume Legacy (10)	t_{fuv} (s) (11)	t_{nuv} (s) (12)	Tile Name (13)
10	F8D1	094447.1	672619	40.95	3.66	trgb	16.14	−3	1	1693	1693	GI3_061016_KK77
11	FM2000_1	094510.0	684554	40.29	3.53	trgb	17.80	−3	1	17206	18110	GI2_024002_NGC2976_stream
12	LEDA166101	095010.5	673024	41.36	3.55	trgb	16.94	−3	1	1693	1693	GI3_061016_KK77
13	ARPSLOOP	095732.6	691660	40.92	3.78	trgb	16.8	10	1	3075	3075	NGA_M81andM82
14	KKH057	100015.9	631106	44.55	3.90	trgb	17.95	−3	1	1694	1694	MISDR1_00432_0487
15	AM1001-270	100403.9	−271955	22.31	1.29	trgb	16.51	10	1	11735	15032	NGA_Antlia_Dw
16	BK05N	100441.1	681522	42.05	3.49	trgb	17.77	−3	1	3391	3391	GI3_061018_UGC05442
17	UGC05442	100701.9	674939	42.48	3.72	trgb	15.78	−3	1	3391	3391	GI3_061018_UGC05442
18	IKN	100805.9	682357	42.21	3.61	trgb	17.31	−3	1	1699	1699	NGA_NGC3077
19	HS98_117	102125.2	710651	41.30	3.82	trgb	17.01	10	1	101	101	AISCHV4_118_00227
20	DDO078	102627.4	673916	43.00	3.66	trgb	15.8	−3	1	138	138	AISCHV4_118_00227
21	BK06N	103429.8	660030	45.70	3.80	trgb	16.85	−3	1	1508	1508	GI3_061020_BK06N
22	UGC6782	114857.2	235016	75.53	14.0	bs	15.07	9	1	2304	4756	GI1_047052_UGC06782
23	ESO321-G014	121349.6	−381353	24.05	3.18	trgb	15.6	10	1	1485	1485	GI3_061010_ESO321_G014
24	UGC7321	121733.8	223226	81.05	20.0	tf	14.15	7	1	1670	2802	GI4_095024_UGC07321
25	KKH086	135433.5	041435	62.60	2.59	trgb	16.99	10	1	1675	1675	GI3_061008_kkh086
26	KKR25	161347.9	542216	44.41	1.93	trgb	16.5	−1	1	1548	1548	MISDR1_10449_0621
27	KKH098	234534.0	384304	−22.37	2.54	trgb	17.22	10	1	2493	2493	GI3_061007_kkh098

(This table is also available in a machine-readable form in the online journal.)

and 11 Mpc, where flow distance uncertainties (±15%) may scatter objects in and out of the volume. Such uncertainties, however, should not be significant for studies seeking to use the sample to statistically characterize the physical properties of local galaxies. As we previously commented in Paper I and in Dale et al. (2009), an inherent difficulty with efforts to construct a local volume-limited sample is that its membership will necessarily be fluid until accurate distance and photometric measurements are available for all of the galaxies that are within the volume and around its periphery.

Both the archival and newly obtained *Spitzer* imaging for the Local Volume Legacy sample have been uniformly processed (Dale et al. 2009). The full set of IRAC, MIPS, and available Hα and *GALEX* UV imaging for the Local Volume Legacy galaxies are all provided online (see footnote 13). UV photometry measured in apertures identical to those used for the *Spitzer* photometry and spectral energy distributions published in Dale et al. (2009) is provided in Table 3.

Column 13: *GALEX* "tile" name(s) giving information on the original program that requested observations for the galaxy.

2.3. GALEX Photometry

The procedures used to perform photometry closely follow those used by Gil de Paz & Madore (2005), for ground-based optical imaging, and Gil de Paz et al. (2007) for the *GALEX* Atlas of Nearby Galaxies. Both total (asymptotic) magnitudes based on curve-of-growth analyses and aperture magnitudes are measured and reported in Tables 2 and 3. Details on the contents of the tables are given at the end of this section.

To prepare the images for photometry, foreground stars and background galaxies are masked in a two-step procedure. The IRAF task STARFIND is used to identify all point sources down to 4σ significance (i.e., at the *GALEX* resolution, $\sim 5''$), and those with FUV–NUV > 1 are flagged as foreground Galactic stars. These initial masks are then inspected by eye. The nuclei of a few early-type dwarf galaxies that were flagged by STARFIND are unmasked. Blue foreground stars are also identified during this inspection and added to the mask. We note that such stars are rare at the Galactic latitudes targeted by 11HUGS ($|b| > 30^\circ$) and are readily differentiated from stellar clusters or associations in the target galaxy. Background galaxies were also identified by visual inspection, based upon the morphology in available optical imaging and/or anomalous UV color. The masked pixels are replaced by values interpolated from the surrounding pixels.

To perform surface photometry and obtain total (asymptotic) magnitudes, knowledge of the sky background level is required. We measure the background using pixels in equal-area regions distributed in azimuth around the galaxy in two concentric annuli and compute the average sky background, local background standard deviation, and standard deviation of the mean across the field. The annuli are chosen to lie well beyond the RC3 (Third Reference Catalog of Bright Galaxies; de Vaucouleurs et al. 1991) B-band 25 mag arcsec^{-2} isophote (typically 2–4 times D_{25}), where no emission from the galaxy is detected. The image used in this calculation is completely masked of all objects, including the target galaxy itself. The masks for this sky calculation are created from objects detected in the *GALEX* pipeline and extracted from the *GALEX* merged catalog file, MCAT.

The surface photometry is carried out on the masked, locally interpolated image using the IRAF task ELLIPSE, with fixed central coordinates, ellipticity, and position angle. The central coordinates are given in Table 1. The position angles, and the semimajor and semiminor axis sizes on which the ellipticities are based, are given in Table 2. Values for these parameters are drawn from NED and are generally based on B-band measurements published in the RC3. The resulting elliptical apertures were individually checked by eye to ensure that they adequately described the galaxy on optical DSS images and were correctly centered on the *GALEX* images. Manual adjustments to the values taken from NED were made as necessary.

Surface brightness profiles are computed by ELLIPSE, where errors in the azimuthally averaged surface brightnesses are taken into account, and include contributions from the photon noise and both high- and low-frequency errors in the background error budget (see Gil de Paz et al. 2007 and Gil de Paz & Madore 2005 for more details). To determine the asymptotic magnitudes, the

Table 2
GALEX Aperture and Asymptotic Magnitudes

No.	Galaxy Name	$E(B-V)$	a	b	P.A.	FUV_{ap}		NUV_{ap}		$(FUV-NUV)_{ap}$		FUV_{asym}		NUV_{asym}	
			($''$)	($''$)	(deg)	(mag)		(mag)		(mag)		(mag)		(mag)	
(1)	(2)	(3)	(4)	(5)	(6)	(7)	(8)	(9)	(10)	(11)	(12)	(13)	(14)	(15)	(16)
1	UGC12894	0.11	...	...	...	...	...	...	...	...	...	...	...	...	...
2	WLM	0.04	516	180	4	12.48	0.05	12.35	0.03	0.13	0.06	12.49	0.05	12.38	0.03
3	ESO409-IG015	0.02	90	40	−40	15.94	0.05	15.82	0.04	0.12	0.06	15.94	0.05	15.81	0.04
4	ESO349-G031	0.01	72	72	0	17.05	0.05	16.91	0.04	0.14	0.06	17.04	0.05	16.88	0.04
5	NGC24	0.02	258	58	46	14.04	0.05	13.77	0.03	0.27	0.06	14.01	0.05	13.75	0.03
6	NGC45	0.02	378	262	−38	12.55	0.05	12.36	0.03	0.19	0.06	12.52	0.06	12.32	0.05
7	NGC55	0.01	1452	251	−72	10.17	0.05	9.87	0.03	0.30	0.06	10.17	0.05	9.88	0.04
8	NGC59	0.02	150	75	−53	16.06	0.06	15.31	0.03	0.75	0.07	16.08	0.06	15.31	0.03
9	MCG-04-02-003	0.02	36	36	0	17.46	0.05	17.18	0.03	0.28	0.06	17.19	0.41	17.00	0.17
10	IC10	1.56	...	...	...	...	...	...	...	...	...	...	...	...	...
11	ESO473-G024	0.02	108	65	29	16.75	0.06	16.71	0.07	0.04	0.09	16.77	0.06	16.75	0.07
12	AndIV	0.09	54	42	−40	17.65	0.06	17.15	0.04	0.50	0.07	17.37	0.14	16.48	0.18
13	NGC224	0.68	...	...	...	...	...	...	...	...	...	...	...	...	...
14	IC1574	0.02	120	46	−5	16.56	0.05	16.07	0.03	0.49	0.06	16.55	0.05	16.05	0.03
15	NGC247	0.02	954	307	−6	11.37	0.05	11.15	0.03	0.22	0.06	11.38	0.05	11.16	0.03
16	NGC253	0.02	1236	305	52	11.16	0.05	10.63	0.03	0.53	0.06	11.16	0.05	10.64	0.03
17	UGCA15	0.02	72	30	42	16.81	0.05	16.64	0.03	0.17	0.06	16.77	0.06	16.58	0.04
18	SMC	0.04	...	...	...	...	...	...	...	...	...	...	...	...	...
19	NGC300	0.01	984	697	−69	10.21	0.05	10.08	0.04	0.13	0.06	10.22	0.06	10.10	0.05
20	LGS3	0.04	48	48	0	19.16	0.11	18.36	0.05	0.80	0.12	19.11	0.19	17.54	0.39
21	UGC668	0.02	726	650	50	11.42	0.05	11.31	0.06	0.11	0.08	11.43	0.05	11.35	0.07
22	UGC685	0.06	60	45	−60	16.04	0.05	15.66	0.03	0.38	0.06	16.03	0.05	15.61	0.03
23	UGC695	0.03	78	64	−45	16.61	0.05	16.24	0.04	0.37	0.06	16.62	0.05	16.25	0.04
24	UGC891	0.03	102	44	47	16.31	0.05	16.08	0.03	0.23	0.06	16.31	0.05	16.07	0.03
25	UGC1056	0.07	78	52	45	16.63	0.05	16.25	0.03	0.38	0.06	16.64	0.05	16.25	0.03
26	UGC1104	0.06	78	47	5	15.60	0.05	15.41	0.03	0.19	0.06	15.60	0.05	15.40	0.03
27	NGC598	0.04	2070	1219	23	8.00	0.05	7.71	0.03	0.29	0.06	7.86	0.05	7.59	0.04
28	NGC625	0.02	342	112	−88	13.72	0.05	13.34	0.03	0.38	0.06	13.76	0.05	13.39	0.03
29	NGC628	0.07	780	706	25	11.62	0.05	11.34	0.04	0.28	0.07	11.66	0.05	11.40	0.04
30	UGC1176	0.06	204	160	25	15.43	0.09	15.26	0.10	0.17	0.14	15.43	0.12	15.22	0.13
31	UGCA20	0.06	228	59	−27	16.33	0.09	16.24	0.09	0.09	0.13	16.33	0.11	16.18	0.10
32	ESO245-G005	0.02	318	283	−58	13.62	0.05	13.55	0.04	0.07	0.06	13.63	0.05	13.58	0.04
33	UGC1249	0.08	306	137	−30	13.44	0.05	13.27	0.03	0.17	0.06	13.44	0.05	13.27	0.03
34	NGC672	0.08	318	115	65	13.19	0.05	12.84	0.03	0.35	0.06	13.20	0.05	12.85	0.03
35	UGC1281	0.05	330	59	38	15.04	0.09	14.73	0.07	0.31	0.12	15.08	0.09	14.74	0.07
36	ESO245-G007	0.02	216	181	90	16.18	0.20	15.34	0.05	0.84	0.20	16.23	0.20	15.29	0.07
37	NGC784	0.06	294	67	0	13.93	0.05	13.49	0.03	0.44	0.06	13.92	0.05	13.48	0.03
38	UGC1561	0.08	72	65	−80	16.34	0.09	16.07	0.04	0.27	0.10	16.36	0.09	16.06	0.05
39	NGC855	0.07	114	44	60	15.91	0.08	15.25	0.04	0.66	0.09	15.92	0.08	15.19	0.05
40	UGC1807	0.08	72	72	0	16.14	0.13	15.85	0.08	0.29	0.15	16.11	0.13	15.82	0.08
41	NGC891	0.06	600	111	22	14.61	0.19	13.80	0.06	0.81	0.20	14.61	0.19	13.82	0.06
42	UGC1865	0.07	114	86	80	16.08	0.08	15.69	0.05	0.39	0.09	16.04	0.11	15.66	0.06
43	NGC925	0.08	456	256	−78	12.09	0.05	11.88	0.03	0.21	0.06	12.08	0.05	11.87	0.03
44	UGC1924	0.08	84	15	3	16.96	0.09	16.62	0.05	0.34	0.10	16.96	0.09	16.59	0.05
45	NGC949	0.06	102	55	−35	14.98	0.08	14.38	0.04	0.60	0.09	14.98	0.08	14.37	0.04
46	NGC959	0.07	126	77	65	14.70	0.06	14.29	0.03	0.41	0.07	14.70	0.06	14.29	0.03
47	UGC2014	0.05	54	16	−4	17.94	0.11	17.85	0.08	0.09	0.14	17.89	0.14	17.81	0.20
48	UGC2023	0.09	108	108	0	15.14	0.11	14.94	0.06	0.20	0.13	15.11	0.12	14.91	0.06
49	UGC2034	0.06	...	...	...	...	...	...	...	...	...	...	...	...	...
50	ESO115-G021	0.03	366	37	44	14.63	0.05	14.36	0.04	0.27	0.06	14.62	0.05	14.35	0.04
51	NGC1003	0.07	390	135	−83	13.68	0.05	13.05	0.07	0.63	0.09	13.67	0.05	13.07	0.07
52	Maffei2	2.42	...	...	...	...	...	...	...	...	...	...	...	...	...
53	NGC1058	0.06	222	207	−85	13.69	0.05	13.24	0.03	0.45	0.06	13.58	0.06	13.25	0.06
54	UGC2259	0.07	...	...	...	...	...	...	...	...	...	...	...	...	...
55	ESO154-G023	0.02	378	80	39	13.78	0.05	13.52	0.04	0.26	0.06	13.79	0.05	13.52	0.04
56	NGC1156	0.22	246	186	25	12.58	0.09	12.38	0.05	0.20	0.10	12.63	0.09	12.40	0.05
57	ESO300-G014	0.02	264	132	−14	14.88	0.06	14.65	0.03	0.23	0.07	14.89	0.06	14.65	0.03
58	ESO300-G016	0.02	63	63	0	...	...	17.06	0.04	...	...	17.29	0.05	17.06	0.05
59	NGC1291	0.01	438	362	−15	14.23	0.10	13.39	0.05	0.84	0.11	14.19	0.10	13.34	0.05
60	NGC1313	0.11	516	391	40	10.59	0.08	10.43	0.04	0.16	0.09	10.58	0.08	10.42	0.05
61	NGC1311	0.02	216	58	40	14.84	0.05	14.41	0.03	0.43	0.06	14.85	0.05	14.42	0.03
62	UGC2684	0.14	144	72	−60	16.45	0.19	16.66	0.07	−0.21	0.20	16.67	0.22	16.70	0.07
63	UGC2689	0.15	...	...	...	...	...	...	...	...	...	...	...	...	...

Table 2
(Continued)

No.	Galaxy Name	$E(B-V)$	a	b	P.A.	FUV_{ap}		NUV_{ap}		$(FUV-NUV)_{ap}$		FUV_{asym}		NUV_{asym}	
			($''$)	($''$)	(deg)	(mag)		(mag)		(mag)		(mag)		(mag)	
(1)	(2)	(3)	(4)	(5)	(6)	(7)	(8)	(9)	(10)	(11)	(12)	(13)	(14)	(15)	(16)
64	UGC2716	0.14	96	54	88	15.92	0.06	15.43	0.06	0.49	0.08	15.93	0.06	15.42	0.07
65	IC1959	0.01	204	51	−33	14.37	0.05	14.24	0.03	0.13	0.06	14.37	0.05	14.25	0.03
66	UGC2847	0.56	996	973	−28	8.48	0.13	8.31	0.27	0.17	0.30	8.16	0.13	8.15	0.27
67	IC2000	0.01	270	53	83	15.22	0.06	14.72	0.03	0.50	0.07	15.23	0.06	14.73	0.03
68	ESO302-G014	0.01	126	111	−59	15.75	0.06	15.77	0.05	−0.02	0.08	15.76	0.06	15.78	0.05
69	NGC1487	0.01	294	187	55	13.41	0.05	13.23	0.03	0.18	0.06	13.46	0.05	13.26	0.03
70	ESO249-G036	0.01	150	136	−22	16.13	0.06	16.04	0.03	0.09	0.07	16.13	0.06	16.03	0.03
71	UGCA86	0.94	…	…	…	(14.30)	…	(14.39)	…	…	…	…	…	…	…
72	NGC1510	0.01	96	52	90	15.09	0.05	14.87	0.03	0.22	0.06	15.09	0.05	14.87	0.03
73	NGC1512	0.01	798	502	90	13.36	0.05	13.12	0.07	0.24	0.08	13.27	0.05	13.19	0.12
74	NGC1522	0.01	102	68	42	15.15	0.05	15.02	0.03	0.13	0.06	15.16	0.05	15.02	0.03
75	NGC1518	0.05	222	74	35	13.42	0.05	13.17	0.03	0.25	0.06	13.43	0.05	13.18	0.03
76	ESO483-G013	0.05	138	69	−44	15.75	0.05	15.41	0.03	0.34	0.06	15.79	0.06	15.41	0.03
77	NGC1556	0.02	174	51	−13	14.83	0.05	14.62	0.03	0.21	0.06	14.85	0.05	14.64	0.03
78	UGCA90	0.02	402	151	−48	14.12	0.06	13.94	0.05	0.18	0.08	14.13	0.06	13.95	0.05
79	NGC1592	0.04	102	51	−84	14.06	0.05	14.10	0.03	−0.04	0.06	14.07	0.05	14.10	0.03
80	NGC1569	0.69	264	132	−60	9.65	0.05	9.02	0.04	0.63	0.07	9.77	0.06	9.17	0.05
81	UGCA92	0.78	…	…	…	(15.69)	…	(15.88)	…	…	…	…	…	…	…
82	NGC1560	0.19	396	68	23	13.30	0.05	12.89	0.03	0.41	0.06	13.17	0.06	12.77	0.04
83	ESO158-G003	0.01	114	107	−10	15.47	0.05	15.20	0.03	0.27	0.06	15.48	0.05	15.20	0.03
84	UGC3174	0.09	78	50	85	16.12	0.18	15.76	0.05	0.36	0.18	16.01	0.38	15.56	0.12
85	ESO119-G016	0.02	102	44	25	16.05	0.05	15.77	0.03	0.28	0.06	16.01	0.07	15.73	0.04
86	NGC1705	0.01	138	102	50	13.33	0.05	13.41	0.03	−0.08	0.06	13.34	0.05	13.41	0.03
87	ESO252-IG001	0.01	…	…	…	…	…	…	…	…	…	…	…	…	…
88	NGC1744	0.04	480	261	−12	13.01	0.05	12.83	0.03	0.18	0.06	12.99	0.05	12.81	0.03
89	NGC1796	0.02	108	57	−78	14.94	0.05	14.43	0.03	0.51	0.06	14.93	0.05	14.43	0.03
90	ESO486-G021	0.03	84	56	−73	15.28	0.05	15.07	0.03	0.21	0.06	15.28	0.05	15.07	0.03
91	MCG-05-13-004	0.01	…	…	…	…	…	…	…	…	…	…	…	…	…
92	NGC1800	0.01	144	79	−67	14.59	0.05	14.43	0.03	0.16	0.06	14.61	0.05	14.43	0.03
93	NGC1808	0.03	396	238	−47	14.20	0.10	13.51	0.06	0.69	0.12	14.03	0.12	13.43	0.07
94	ESO305-G009	0.03	240	192	63	14.31	0.07	14.15	0.04	0.16	0.08	14.30	0.07	14.15	0.04
95	UGCA103	0.01	…	…	…	…	…	…	…	…	…	…	…	…	…
96	UGCA106	0.02	258	221	10	13.98	0.05	13.83	0.09	0.15	0.11	13.99	0.05	13.87	0.10
97	UGCA105	0.31	378	240	55	12.55	0.06	12.20	0.35	0.35	0.36	12.51	0.07	12.08	0.35
98	LMC	0.07	…	…	…	…	…	…	…	…	…	…	…	…	…
99	UGC3303	0.13	…	…	…	…	…	…	…	…	…	…	…	…	…
100	ESO553-G046	0.05	78	52	−13	15.11	0.05	15.00	0.05	0.11	0.07	15.11	0.05	15.01	0.05
101	ESO306-G013	0.04	…	…	…	…	…	…	…	…	…	…	…	…	…
102	UGCA114	0.16	126	92	−10	13.75	0.07	13.40	0.08	0.35	0.10	13.72	0.08	13.36	0.08
103	UGCA116	0.82	42	14	−25	12.72	0.10	12.17	0.05	0.55	0.11	12.49	0.12	12.02	0.15
104	KKH34	0.24	…	…	…	(20.06)	…	(20.32)	…	…	…	…	…	…	…
105	ESO364-G?029	0.05	…	…	…	…	…	…	…	…	…	…	…	…	…
106	AM0605-341	0.04	…	…	…	…	…	…	…	…	…	…	…	…	…
107	NGC2188	0.03	…	…	…	…	…	…	…	…	…	…	…	…	…
108	UGCA120	0.08	…	…	…	…	…	…	…	…	…	…	…	…	…
109	UGCA127	0.83	…	…	…	…	…	…	…	…	…	…	…	…	…
110	UGC3475	0.18	…	…	…	…	…	…	…	…	…	…	…	…	…
111	ESO255-G019	0.08	…	…	…	…	…	…	…	…	…	…	…	…	…
112	KKH37	0.07	42	32	50	18.32	0.07	17.81	0.04	0.51	0.08	18.35	0.07	17.70	0.05
113	ESO207-G007	0.08	96	66	6	15.31	0.11	15.10	0.08	0.21	0.14	15.09	0.13	14.97	0.10
114	UGC3600	0.09	36	16	35	17.44	0.09	17.07	0.05	0.37	0.10	16.88	0.23	16.78	0.05
115	AM0704-582	0.12	…	…	…	…	…	…	…	…	…	…	…	…	…
116	NGC2337	0.09	90	70	−60	14.48	0.06	14.14	0.03	0.34	0.07	14.45	0.06	14.10	0.03
117	UGC3817	0.10	102	51	50	16.88	0.25	16.46	0.09	0.42	0.26	17.04	0.26	16.41	0.11
118	UGC3860	0.06	78	54	20	16.33	0.07	15.97	0.04	0.36	0.08	16.32	0.08	15.96	0.04
119	NGC2366	0.04	654	269	25	12.42	0.05	12.34	0.03	0.08	0.06	12.43	0.05	12.35	0.03
120	UGC3876	0.05	…	…	…	…	…	…	…	…	…	…	…	…	…
121	ESO059-G001	0.15	…	…	…	…	…	…	…	…	…	…	…	…	…
122	NGC2427	0.21	…	…	…	…	…	…	…	…	…	…	…	…	…
123	NGC2403	0.04	960	540	−53	10.31	0.05	10.12	0.04	0.19	0.06	10.31	0.05	10.12	0.04
124	UGC3966	0.05	114	114	0	15.83	0.06	15.60	0.05	0.23	0.08	15.82	0.06	15.60	0.05
125	UGC3974	0.03	228	221	0	14.77	0.05	14.46	0.03	0.31	0.06	14.77	0.05	14.45	0.03

Table 2
(Continued)

No.	Galaxy Name	$E(B-V)$	a	b	P.A.	FUV_{ap}		NUV_{ap}		$(FUV-NUV)_{ap}$		FUV_{asym}		NUV_{asym}	
			(″)	(″)	(deg)	(mag)		(mag)		(mag)		(mag)		(mag)	
(1)	(2)	(3)	(4)	(5)	(6)	(7)	(8)	(9)	(10)	(11)	(12)	(13)	(14)	(15)	(16)
126	CGCG262-028	0.07	48	21	−60	15.46	0.06	15.39	0.04	0.07	0.07	15.45	0.07	15.37	0.05
127	UGC4115	0.03	90	50	−35	15.60	0.05	15.37	0.04	0.23	0.07	15.59	0.05	15.37	0.05
128	NGC2500	0.04	210	188	0	13.46	0.06	13.32	0.03	0.14	0.07	13.47	0.06	13.33	0.03
129	NGC2537	0.05	126	111	0	13.88	0.05	13.69	0.03	0.19	0.06	13.88	0.05	13.70	0.03
130	UGC4278	0.05	342	36	−8	14.43	0.05	14.20	0.04	0.23	0.07	14.43	0.05	14.21	0.04
131	UGC4305	0.03	354	282	15	12.32	0.05	12.22	0.03	0.10	0.06	12.28	0.06	12.17	0.04
132	NGC2552	0.05	156	102	45	14.27	0.05	14.09	0.03	0.18	0.06	14.26	0.05	14.08	0.03
133	M81dwA	0.02	72	39	35	17.30	0.05	17.29	0.03	0.01	0.06	17.28	0.05	17.25	0.03
134	SDSSJ0825+3532	0.05	12	6	−40	18.35	0.06	18.32	0.03	0.03	0.07	…	…	18.21	0.03
135	UGC4426	0.04	144	72	10	16.72	0.06	16.48	0.03	0.24	0.07	16.70	0.06	16.44	0.04
136	UGC4459	0.04	108	94	−60	15.27	0.05	15.30	0.04	−0.03	0.06	15.27	0.05	15.29	0.04
137	ESO495-G021	0.11	…	…	…	…	…	…	…	…	…	…	…	…	…
138	UGC4483	0.03	78	57	−18	15.71	0.05	15.75	0.03	−0.04	0.06	15.71	0.05	15.76	0.03
139	NGC2683	0.03	414	98	44	14.14	0.05	13.52	0.05	0.62	0.07	14.13	0.05	13.50	0.06
140	UGC4704	0.03	306	30	−65	15.85	0.07	15.62	0.04	0.23	0.08	15.86	0.07	15.62	0.04
141	LSBCD564-08	0.03	42	30	0	18.99	0.07	18.57	0.05	0.42	0.09	18.76	0.13	18.38	0.05
142	UGC4787	0.02	144	41	6	15.99	0.05	15.57	0.04	0.42	0.06	16.00	0.05	15.58	0.04
143	LSBCD634-03	0.04	…	…	…	(21.85)	…	(21.71)	…	…	…	…	…	…	…
144	UGCA148	0.17	…	…	…	…	…	…	…	…	…	…	…	…	…
145	NGC2784	0.21	246	98	73	15.49	0.37	14.56	0.04	0.93	0.38	14.94	0.66	14.38	0.05
146	UGCA153	0.09	126	82	−40	16.33	0.13	16.01	0.07	0.32	0.15	16.34	0.16	15.92	0.09
147	NGC2835	0.10	264	176	8	12.35	0.05	11.97	0.04	0.38	0.06	12.35	0.05	11.96	0.04
148	LSBCD565-06	0.04	36	31	0	(21.77)	…	19.23	0.24	…	…	…	…	19.19	0.43
149	UGCA162	0.07	147	35	27	…	…	15.76	0.09	…	…	16.12	0.06	15.55	0.29
150	UGC4998	0.06	54	27	80	17.99	0.06	17.35	0.04	0.64	0.07	17.96	0.06	17.24	0.05
151	NGC2915	0.27	138	73	−51	13.31	0.15	13.28	0.03	0.03	0.15	13.35	0.15	13.27	0.03
152	NGC2903	0.03	564	268	17	12.29	0.05	11.74	0.03	0.55	0.06	12.36	0.05	11.76	0.03
153	UGC5076	0.02	…	…	…	…	…	…	…	…	…	…	…	…	…
154	CGCG035-007	0.04	48	36	80	17.14	0.05	16.74	0.03	0.40	0.06	17.14	0.05	16.72	0.03
155	LeoT	0.03	102	102	0	18.85	0.88	18.61	3.45	0.24	3.56	19.28	0.96	18.24	3.48
156	UGC5151	0.02	…	…	…	…	…	…	…	…	…	…	…	…	…
157	UGC5139	0.05	246	205	0	14.60	0.09	14.50	0.05	0.10	0.10	14.59	0.09	14.50	0.05
158	IC559	0.03	66	50	90	16.45	0.05	16.08	0.03	0.37	0.06	16.45	0.05	16.04	0.03
159	UGC5209	0.02	30	30	0	18.10	0.09	17.68	0.05	0.42	0.10	18.08	0.10	17.61	0.05
160	NGC2976	0.07	264	121	−37	13.17	0.05	12.69	0.03	0.48	0.06	13.19	0.05	12.71	0.03
161	UGC5272b	0.02	30	15	−65	18.40	0.06	18.35	0.04	0.05	0.07	18.41	0.07	18.35	0.04
162	UGC5272	0.02	144	55	−65	14.94	0.05	14.87	0.03	0.07	0.06	14.94	0.05	14.87	0.03
163	UGC5288	0.03	96	59	−25	15.73	0.05	15.52	0.03	0.21	0.06	15.70	0.05	15.48	0.03
164	NGC3037	0.09	48	44	44	15.16	0.05	14.57	0.03	0.59	0.06	15.15	0.06	14.55	0.03
165	BK3N	0.08	18	14	0	18.92	0.06	18.88	0.04	0.04	0.07	18.77	0.09	18.72	0.05
166	NGC3031	0.08	1104	578	−23	10.75	0.05	10.44	0.03	0.31	0.06	10.76	0.05	10.42	0.03
167	NGC3034	0.16	834	320	65	12.50	0.19	11.44	0.03	1.06	0.19	12.58	0.19	11.47	0.03
168	UGC5340	0.02	192	71	0	15.07	0.05	15.10	0.03	−0.03	0.06	15.07	0.05	15.10	0.03
169	KDG61	0.07	30	25	40	22.23	0.33	19.65	0.04	2.58	0.34	21.81	0.58	19.09	0.21
170	UGC5336	0.08	168	134	40	14.95	0.08	14.80	0.09	0.15	0.12	14.95	0.08	14.80	0.09
171	ESO435-G016	0.10	126	82	−61	15.45	0.09	14.76	0.03	0.69	0.09	15.54	0.10	14.74	0.03
172	ESO435-IG020	0.09	90	68	−80	14.89	0.05	14.51	0.04	0.38	0.06	14.90	0.05	14.52	0.04
173	UGC5364	0.02	228	139	−70	14.55	0.05	14.24	0.03	0.31	0.06	14.53	0.06	14.21	0.04
174	UGC5373	0.03	228	156	−70	13.68	0.05	13.46	0.05	0.22	0.07	13.65	0.06	13.44	0.05
175	UGCA193	0.04	162	12	17	16.36	0.05	16.05	0.03	0.31	0.06	16.28	0.05	15.96	0.03
176	NGC3109	0.07	1074	208	−87	11.37	0.19	11.09	0.10	0.28	0.21	11.42	0.19	11.14	0.10
177	NGC3077	0.07	…	…	…	…	…	…	…	…	…	…	…	…	…
178	UGCA196	0.08	204	83	53	14.52	0.09	14.15	0.08	0.37	0.11	14.51	0.09	14.13	0.08
179	NGC3113	0.10	…	…	…	…	…	…	…	…	…	…	…	…	…
180	UGC5427	0.02	84	56	−60	16.20	0.05	15.96	0.03	0.24	0.06	16.21	0.05	15.96	0.03
181	UGC5428	0.10	108	108	0	(22.67)	…	17.82	0.09	…	…	…	…	17.66	0.16
182	NGC3115	0.05	510	177	40	15.75	0.21	14.11	0.09	1.64	0.23	15.70	0.21	14.15	0.10
183	UGC5423	0.08	66	44	−40	16.58	0.07	16.38	0.04	0.20	0.08	16.57	0.07	16.35	0.05
184	NGC3125	0.08	126	80	−66	14.37	0.08	13.99	0.04	0.38	0.09	14.40	0.08	14.02	0.04
185	UGC5453	0.03	…	…	…	…	…	…	…	…	…	…	…	…	…
186	UGC5451	0.01	78	36	−77	16.04	0.06	15.66	0.04	0.38	0.07	16.05	0.06	15.64	0.04
187	UGC5456	0.04	90	45	−32	14.96	0.05	14.62	0.03	0.34	0.06	14.96	0.05	14.62	0.03

Table 2
(Continued)

No.	Galaxy Name	$E(B-V)$	a	b	P.A.	FUV_{ap}		NUV_{ap}		$(FUV - NUV)_{ap}$		FUV_{asym}		NUV_{asym}	
			(″)	(″)	(deg)	(mag)		(mag)		(mag)		(mag)		(mag)	
(1)	(2)	(3)	(4)	(5)	(6)	(7)	(8)	(9)	(10)	(11)	(12)	(13)	(14)	(15)	(16)
188	KUG1004+392	0.01	54	27	−5	16.37	0.06	16.27	0.04	0.10	0.07	16.31	0.06	16.24	0.04
189	NGC3137	0.07	...	...	...	...	...	...	...	...	...	...	...	...	...
190	SextansA	0.04	264	219	0	12.55	0.05	12.52	0.03	0.03	0.06	12.54	0.05	12.51	0.03
191	NGC3175	0.07	168	44	56	16.06	0.07	15.02	0.04	1.04	0.08	16.06	0.08	14.98	0.04
192	NGC3239	0.03	222	146	80	12.80	0.05	12.58	0.03	0.22	0.06	12.80	0.05	12.58	0.03
193	UGC5672	0.02	78	22	−22	17.20	0.05	16.60	0.03	0.60	0.06	17.19	0.05	16.47	0.04
194	UGC5666	0.04	588	240	50	12.13	0.06	12.09	0.04	0.04	0.07	12.13	0.06	12.09	0.04
195	UGC5692	0.04	114	64	0	16.42	0.05	15.76	0.03	0.66	0.06	16.42	0.05	15.60	0.03
196	NGC3274	0.02	246	117	−80	14.23	0.06	14.02	0.03	0.21	0.07	14.28	0.06	14.06	0.03
197	UGC5740	0.02	108	76	−40	15.77	0.06	15.60	0.04	0.17	0.07	15.93	0.07	15.73	0.09
198	UGCA212	0.06	162	130	14	14.25	0.06	13.96	0.04	0.29	0.07	14.20	0.09	13.93	0.07
199	NGC3299	0.02	72	56	3	16.27	0.05	15.72	0.04	0.55	0.06	16.26	0.06	15.66	0.04
200	UGC5764	0.02	84	46	60	16.24	0.05	16.15	0.04	0.09	0.06	16.24	0.05	16.15	0.04
201	UGC5797	0.03	78	70	−45	16.85	0.05	16.42	0.03	0.43	0.06	16.85	0.05	16.40	0.03
202	IC625	0.07	126	27	−75	15.13	0.06	14.70	0.04	0.43	0.07	15.10	0.06	14.67	0.04
203	UGC5829	0.02	210	188	55	13.96	0.05	13.89	0.03	0.07	0.06	13.98	0.06	13.89	0.04
204	NGC3344	0.03	504	461	0	12.36	0.05	12.06	0.03	0.30	0.06	12.36	0.05	12.06	0.03
205	NGC3351	0.03	330	223	13	13.27	0.05	12.72	0.03	0.55	0.06	13.26	0.05	12.71	0.03
206	NGC3365	0.05	336	60	−21	15.30	0.10	14.84	0.03	0.46	0.11	15.32	0.10	14.86	0.03
207	NGC3368	0.03	336	230	5	14.00	0.07	13.36	0.04	0.64	0.08	13.99	0.07	13.34	0.04
208	UGC5889	0.03	96	92	30	16.30	0.05	15.87	0.05	0.43	0.07	16.30	0.05	15.87	0.05
209	UGC5917	0.02	54	29	−17	16.55	0.06	16.14	0.04	0.41	0.07	16.54	0.08	16.13	0.04
210	UGC5923	0.03	48	21	−7	17.27	0.05	16.74	0.03	0.53	0.06	17.26	0.05	16.70	0.03
211	UGC5918	0.01	120	120	0	16.41	0.31	16.16	0.09	0.25	0.33	16.38	0.31	16.13	0.09
212	NGC3412	0.03	90	50	−25	18.21	0.16	15.85	0.04	2.36	0.16	18.21	0.16	15.70	0.04
213	ESO376-G022	0.09	...	...	...	...	...	...	...	...	...	...	...	...	...
214	NGC3432	0.01	300	66	38	13.27	0.05	12.84	0.03	0.43	0.06	13.26	0.05	12.84	0.03
215	KDG73	0.02	30	20	−60	18.93	0.06	18.71	0.04	0.22	0.08	18.81	0.08	18.51	0.06
216	NGC3489	0.02	258	147	70	16.54	0.08	14.81	0.03	1.73	0.08	16.60	0.08	14.81	0.03
217	NGC3486	0.02	318	233	80	12.54	0.05	12.30	0.03	0.24	0.06	12.52	0.05	12.27	0.04
218	UGC6102	0.03	66	53	−40	16.53	0.06	16.41	0.04	0.12	0.07	16.51	0.06	16.41	0.04
219	NGC3510	0.03	174	35	−17	14.63	0.05	14.35	0.03	0.28	0.06	14.63	0.05	14.34	0.03
220	ESO377-G003	0.06	48	19	48	15.94	0.06	15.69	0.04	0.25	0.07	15.90	0.07	15.67	0.04
221	MRK36	0.03	60	40	−45	15.64	0.05	15.62	0.03	0.02	0.06	15.64	0.05	15.61	0.03
222	NGC3521	0.06	492	228	−17	13.02	0.06	12.26	0.04	0.76	0.07	13.05	0.07	12.27	0.04
223	UGC6161	0.01	156	72	40	15.37	0.05	15.18	0.03	0.19	0.06	15.36	0.05	15.18	0.03
224	MESSIER108	0.02	390	99	80	13.34	0.05	12.85	0.03	0.49	0.06	13.35	0.05	12.86	0.03
225	NGC3593	0.02	126	92	−88	16.79	0.16	15.31	0.05	1.48	0.17	16.86	0.17	15.21	0.07
226	NGC3599	0.02	96	75	−75	18.19	0.06	16.64	0.04	1.55	0.07	18.14	0.07	16.55	0.04
227	NGC3600	0.02	306	67	3	15.16	0.05	14.77	0.07	0.39	0.09	15.15	0.05	14.79	0.07
228	NGC3621	0.08	696	402	−21	11.62	0.05	11.18	0.05	0.44	0.07	11.60	0.05	11.03	0.08
229	NGC3623	0.02	438	130	−6	14.98	0.08	13.93	0.07	1.05	0.10	15.01	0.08	13.96	0.07
230	NGC3627	0.03	408	188	−7	12.65	0.05	11.98	0.03	0.67	0.06	12.67	0.05	12.00	0.03
231	NGC3628	0.03	660	134	−76	14.36	0.06	13.32	0.03	1.04	0.07	14.33	0.06	13.26	0.03
232	IC2782	0.02	78	64	40	(21.93)	...	17.89	0.08	...	...	...	...	18.31	0.18
233	IC2787	0.03	...	...	...	...	...	...	...	...	...	...	...	...	...
234	NGC3675	0.02	240	126	−2	15.02	0.06	14.18	0.07	0.84	0.09	14.99	0.06	14.19	0.07
235	UGC6457	0.03	90	70	−30	16.33	0.06	15.95	0.03	0.38	0.07	16.32	0.06	15.95	0.03
236	UGC6456	0.04	102	58	−10	15.00	0.05	14.98	0.04	0.02	0.06	15.00	0.05	14.98	0.04
237	UGC6541	0.02	84	42	−47	15.36	0.05	15.17	0.03	0.19	0.06	15.35	0.05	15.15	0.03
238	NGC3738	0.01	108	82	−25	13.77	0.05	13.45	0.03	0.32	0.06	13.77	0.05	13.45	0.03
239	NGC3741	0.02	168	92	5	15.13	0.05	15.00	0.03	0.13	0.06	15.14	0.05	15.00	0.03
240	LEDA166115	0.02	24	16	0	(22.03)	...	19.61	0.17	...	...	...	...	19.41	0.18
241	UGC6817	0.03	306	112	65	14.78	0.05	14.57	0.06	0.21	0.08	14.78	0.05	14.58	0.06
242	UGC6900	0.02	90	56	−65	17.42	0.05	16.91	0.04	0.51	0.07	...	...	16.86	0.05
243	BTS76	0.02	12	8	45	20.39	0.09	19.86	0.05	0.53	0.10	20.37	0.12	19.86	0.06
244	NGC4020	0.02	156	67	15	15.20	0.05	14.82	0.03	0.38	0.06	15.20	0.05	14.83	0.03
245	UGC7007	0.02	60	56	−30	16.98	0.08	16.77	0.05	0.21	0.09	16.91	0.09	16.51	0.07
246	NGC4068	0.02	144	74	30	14.30	0.05	14.08	0.03	0.22	0.06	14.29	0.05	14.07	0.03
247	NGC4080	0.03	114	48	−55	16.08	0.05	15.68	0.03	0.40	0.06	16.08	0.05	15.68	0.03
248	NGC4096	0.02	492	119	20	14.08	0.05	13.59	0.03	0.49	0.06	14.10	0.05	13.61	0.03
249	KUG1207+367	0.03	54	20	−10	17.16	0.05	16.71	0.03	0.45	0.06	17.15	0.05	16.67	0.03

Table 2
(Continued)

No.	Galaxy Name	$E(B-V)$	a	b	P.A.	FUV_{ap}		NUV_{ap}		$(FUV-NUV)_{ap}$		FUV_{asym}		NUV_{asym}	
			($''$)	($''$)	(deg)	(mag)		(mag)		(mag)		(mag)		(mag)	
(1)	(2)	(3)	(4)	(5)	(6)	(7)	(8)	(9)	(10)	(11)	(12)	(13)	(14)	(15)	(16)
250	NGC4144	0.01	444	96	−76	13.95	0.05	13.56	0.04	0.39	0.06	13.96	0.05	13.58	0.04
251	NGC4163	0.02	114	101	10	15.34	0.05	14.95	0.03	0.39	0.06	15.34	0.05	14.95	0.03
252	NGC4190	0.03	120	92	30	14.77	0.05	14.32	0.03	0.45	0.06	14.77	0.05	14.32	0.03
253	UGC7242	0.02	132	53	−8	16.05	0.05	15.51	0.06	0.54	0.08	16.05	0.05	15.52	0.06
254	UGCA276	0.02	66	66	0	(23.55)	…	18.62	0.06	…	…	…	…	18.47	0.16
255	NGC4204	0.03	264	213	−60	14.31	0.08	14.06	0.03	0.25	0.08	14.33	0.08	14.07	0.03
256	UGC7267	0.02	90	34	53	16.30	0.05	15.96	0.03	0.34	0.06	16.29	0.05	15.94	0.03
257	UGC7271	0.01	144	43	−20	16.46	0.05	16.14	0.04	0.32	0.06	16.47	0.05	16.16	0.04
258	NGC4214	0.02	504	391	−40	11.47	0.05	11.27	0.03	0.20	0.06	11.51	0.05	11.29	0.04
259	CGCG269-049	0.02	72	42	−54	16.60	0.05	16.35	0.03	0.25	0.06	16.59	0.05	16.34	0.03
260	UGC7298	0.02	90	42	−40	17.26	0.05	16.95	0.06	0.31	0.08	17.26	0.05	16.93	0.06
261	NGC4236	0.01	936	308	−18	11.76	0.05	11.57	0.03	0.19	0.06	11.79	0.06	11.60	0.04
262	NGC4244	0.02	990	126	48	12.67	0.05	12.20	0.03	0.47	0.06	12.68	0.05	12.20	0.03
263	NGC4242	0.01	222	169	25	13.88	0.05	13.53	0.03	0.35	0.06	13.89	0.05	13.54	0.03
264	NGC4248	0.02	144	53	−72	16.84	0.05	15.87	0.04	0.97	0.06	16.84	0.05	15.83	0.04
265	IC3104	0.41	…	…	…	…	…	…	…	…	…	…	…	…	…
266	NGC4258	0.02	834	323	−30	11.82	0.05	11.40	0.03	0.42	0.06	11.82	0.05	11.39	0.03
267	UGC7356	0.02	48	48	0	…	…	18.69	0.05	…	…	…	…	18.59	0.06
268	ISZ399	0.06	…	…	…	…	…	…	…	…	…	…	…	…	…
269	NGC4288	0.01	186	133	−50	14.57	0.05	14.35	0.03	0.22	0.06	14.57	0.05	14.37	0.03
270	UGC7408	0.01	180	83	−80	16.10	0.05	15.48	0.04	0.62	0.06	16.10	0.05	15.47	0.04
271	UGC7490	0.02	…	…	…	…	…	…	…	…	…	…	…	…	…
272	LEDA166137	0.02	60	20	80	17.24	0.08	16.97	0.05	0.27	0.09	17.08	0.20	16.84	0.05
273	NGC4395	0.02	588	490	−33	11.63	0.05	11.51	0.03	0.12	0.06	11.62	0.05	11.50	0.03
274	UGCA281	0.01	66	50	−85	15.17	0.05	15.16	0.03	0.01	0.06	15.17	0.05	15.16	0.03
275	UGC7559	0.01	222	139	−20	15.09	0.06	15.00	0.03	0.09	0.07	15.06	0.06	14.98	0.03
276	UGC7577	0.02	192	107	−50	14.82	0.05	14.49	0.03	0.33	0.06	14.82	0.05	14.48	0.03
277	UGC7584	0.02	72	40	−60	17.01	0.05	16.70	0.03	0.31	0.06	17.01	0.05	16.68	0.03
278	LSBCF573-01	0.02	42	30	80	18.12	0.06	17.75	0.03	0.37	0.07	18.10	0.07	17.66	0.03
279	NGC4449	0.02	462	328	45	10.83	0.05	10.80	0.03	0.03	0.06	10.84	0.05	10.82	0.03
280	UGC7599	0.02	144	72	−45	16.04	0.05	15.96	0.04	0.08	0.07	16.05	0.05	15.96	0.04
281	UGC7605	0.01	108	78	30	15.78	0.05	15.62	0.03	0.16	0.06	15.78	0.05	15.62	0.03
282	NGC4455	0.02	204	58	16	14.43	0.05	14.16	0.03	0.27	0.06	14.43	0.05	14.17	0.03
283	UGC7608	0.02	150	146	60	14.74	0.06	14.70	0.03	0.04	0.07	14.74	0.06	14.68	0.03
284	NGC4460	0.02	174	52	40	15.53	0.05	14.77	0.03	0.76	0.06	15.53	0.05	14.76	0.03
285	MCG+07-26-011	0.02	48	27	−30	17.26	0.05	16.77	0.03	0.49	0.06	17.26	0.05	16.74	0.03
286	UGC7639	0.01	102	71	−27	16.13	0.05	15.72	0.03	0.41	0.06	16.15	0.05	15.69	0.03
287	MCG+07-26-012	0.02	66	22	−68	17.16	0.05	16.76	0.03	0.40	0.06	17.15	0.05	16.73	0.04
288	NGC4485	0.02	204	142	15	13.47	0.05	13.28	0.03	0.19	0.06	13.51	0.05	13.34	0.03
289	NGC4490	0.02	468	230	−55	11.98	0.05	11.53	0.03	0.45	0.06	12.02	0.05	11.55	0.03
290	UGC7678	0.02	66	47	80	15.42	0.06	15.12	0.03	0.30	0.07	15.39	0.06	15.11	0.03
291	UGC7690	0.03	126	96	20	14.66	0.05	14.29	0.03	0.37	0.06	14.67	0.05	14.30	0.03
292	UGC7699	0.01	282	74	32	14.72	0.05	14.43	0.04	0.29	0.06	14.73	0.05	14.45	0.04
293	UGC7698	0.02	276	190	−10	14.70	0.06	14.54	0.03	0.16	0.07	14.71	0.06	14.55	0.03
294	UGC7719	0.02	138	87	−17	15.93	0.05	15.73	0.04	0.20	0.06	15.95	0.05	15.75	0.04
295	NGC4534	0.01	192	155	−55	13.92	0.05	13.82	0.03	0.10	0.06	13.91	0.05	13.81	0.03
296	UGC7774	0.02	156	22	−78	16.33	0.05	15.76	0.03	0.57	0.06	16.32	0.05	15.74	0.03
297	UGCA290	0.01	48	24	42	15.88	0.06	15.92	0.04	−0.04	0.07	15.84	0.09	15.89	0.05
298	UGCA292	0.02	114	80	35	16.20	0.05	16.21	0.03	−0.01	0.06	16.21	0.05	16.21	0.03
299	M104	0.05	390	157	90	14.54	0.06	13.39	0.05	1.15	0.08	14.56	0.07	13.37	0.05
300	NGC4605	0.01	588	223	−55	12.97	0.06	12.56	0.04	0.41	0.08	13.01	0.06	12.59	0.04
301	NGC4618	0.02	312	253	25	12.80	0.05	12.54	0.03	0.26	0.06	12.83	0.05	12.56	0.03
302	NGC4625	0.02	240	207	−30	14.49	0.05	14.20	0.04	0.29	0.06	14.41	0.07	14.15	0.05
303	NGC4631	0.02	1158	202	86	11.29	0.05	11.07	0.03	0.22	0.06	11.31	0.05	11.09	0.03
304	UGC7866	0.02	150	132	0	14.62	0.05	14.54	0.03	0.08	0.06	14.62	0.05	14.54	0.03
305	NGC4656	0.01	1128	224	33	11.47	0.05	11.48	0.03	−0.01	0.06	11.48	0.05	11.48	0.03
306	UGC7916	0.02	186	126	0	15.73	0.05	15.56	0.06	0.17	0.08	15.75	0.05	15.54	0.06
307	ESO381-G020	0.07	126	50	−42	15.12	0.09	14.84	0.04	0.28	0.10	15.06	0.12	14.82	0.04
308	UGCA298	0.01	36	22	45	17.70	0.09	17.00	0.04	0.70	0.10	17.73	0.11	17.00	0.06
309	UGC7950	0.02	78	60	5	15.23	0.05	15.01	0.03	0.22	0.06	15.23	0.05	15.02	0.03
310	UGC7949	0.02	144	115	60	15.95	0.06	15.81	0.03	0.14	0.07	15.94	0.06	15.80	0.03
311	NGC4707	0.01	162	155	25	15.05	0.05	14.92	0.04	0.13	0.06	15.06	0.05	14.93	0.04

Table 2
(Continued)

No.	Galaxy Name	$E(B-V)$	a	b	P.A.	FUV_{ap}		NUV_{ap}		$(FUV-NUV)_{ap}$		FUV_{asym}		NUV_{asym}	
			($''$)	($''$)	(deg)	(mag)		(mag)		(mag)		(mag)		(mag)	
(1)	(2)	(3)	(4)	(5)	(6)	(7)	(8)	(9)	(10)	(11)	(12)	(13)	(14)	(15)	(16)
312	NGC4736	0.02	834	677	−75	11.75	0.05	11.35	0.04	0.40	0.06	11.74	0.05	11.42	0.05
313	UGC8024	0.01	204	150	35	14.79	0.05	14.82	0.06	−0.03	0.08	14.80	0.05	14.82	0.06
314	UGC8055	0.03	66	51	40	16.70	0.07	16.57	0.05	0.13	0.09	16.61	0.16	16.48	0.14
315	NGC4826	0.04	396	214	−65	13.51	0.08	12.55	0.03	0.96	0.08	13.57	0.08	12.55	0.03
316	UGC8091	0.03	72	65	30	15.21	0.05	15.16	0.04	0.05	0.06	15.20	0.05	15.15	0.04
317	UGC8146	0.01	258	29	30	15.71	0.05	15.34	0.03	0.37	0.06	15.72	0.05	15.36	0.03
318	UGCA319	0.08	60	41	35	16.58	0.05	16.10	0.03	0.48	0.06	16.57	0.05	16.03	0.04
319	UGCA320	0.08	414	52	−60	13.93	0.09	13.71	0.04	0.22	0.09	13.91	0.09	13.69	0.04
320	NGC4945	0.18	…	…	…	…	…	…	…	…	…	…	…	…	…
321	UGC8188	0.01	264	242	−50	13.35	0.05	13.14	0.04	0.21	0.06	13.35	0.05	13.16	0.04
322	UGC8201	0.02	246	134	90	14.49	0.05	14.16	0.03	0.33	0.06	14.51	0.05	14.16	0.03
323	MCG-03-34-002	0.08	60	34	−40	16.10	0.05	15.75	0.03	0.35	0.06	16.09	0.05	15.69	0.04
324	UGC8215	0.01	48	34	60	17.64	0.05	17.34	0.03	0.30	0.06	17.62	0.05	17.29	0.03
325	UGC8245	0.03	90	37	75	16.49	0.05	16.01	0.03	0.48	0.06	16.48	0.05	15.97	0.03
326	NGC5023	0.02	444	44	28	14.65	0.05	14.25	0.03	0.40	0.06	14.66	0.05	14.25	0.03
327	CGCG217-018	0.01	48	34	50	16.60	0.05	16.15	0.03	0.45	0.06	16.59	0.05	16.11	0.03
328	UGC8308	0.01	114	62	−25	16.31	0.05	16.24	0.03	0.07	0.06	16.31	0.05	16.24	0.03
329	UGC8313	0.01	120	35	35	16.32	0.05	16.00	0.03	0.32	0.06	16.32	0.05	15.99	0.03
330	UGC8320	0.02	264	103	−30	14.53	0.05	14.18	0.05	0.35	0.07	14.52	0.05	14.20	0.05
331	UGC8331	0.01	318	106	−40	15.70	0.05	15.47	0.10	0.23	0.12	15.71	0.06	15.56	0.16
332	NGC5055	0.02	942	538	−75	12.30	0.05	11.74	0.04	0.56	0.06	12.32	0.05	11.82	0.04
333	NGC5068	0.10	306	268	−70	11.94	0.09	11.55	0.04	0.39	0.10	11.93	0.09	11.53	0.04
334	NGC5102	0.05	…	…	…	…	…	…	…	…	…	…	…	…	…
335	NGC5128	0.11	396	308	35	11.95	0.05	11.04	0.03	0.91	0.06	11.89	0.05	10.87	0.03
336	IC4247	0.06	90	35	−22	15.96	0.05	15.54	0.03	0.42	0.06	15.96	0.05	15.52	0.03
337	ESO324-G024	0.11	138	99	50	14.45	0.06	14.00	0.06	0.45	0.09	14.41	0.09	13.93	0.06
338	NGC5204	0.01	222	133	5	12.92	0.05	12.70	0.03	0.22	0.06	12.92	0.05	12.68	0.03
339	NGC5194	0.04	498	307	−17	11.03	0.05	10.55	0.03	0.48	0.06	11.05	0.05	10.57	0.03
340	NGC5195	0.04	258	205	79	14.64	0.06	13.81	0.03	0.83	0.07	14.10	0.16	13.46	0.09
341	UGC8508	0.02	…	…	…	…	…	…	…	…	…	…	…	…	…
342	SBS1331+493	0.01	…	…	…	…	…	…	…	…	…	…	…	…	…
343	NGC5206	0.12	…	…	…	…	…	…	…	…	…	…	…	…	…
344	NGC5229	0.02	246	30	−13	15.71	0.06	15.36	0.03	0.35	0.07	15.73	0.06	15.36	0.03
345	NGC5238	0.01	126	74	−20	15.19	0.05	14.97	0.03	0.22	0.06	15.20	0.05	14.98	0.03
346	ESO270-G017	0.11	…	…	…	…	…	…	…	…	…	…	…	…	…
347	[KK98]208	0.04	…	…	…	(23.75)	…	(23.90)	…	…	…	…	…	…	…
348	NGC5236	0.07	1158	1032	0	10.07	0.05	9.51	0.04	0.56	0.06	10.11	0.05	9.57	0.04
349	ESO444-G084	0.07	72	55	−75	16.02	0.06	15.77	0.03	0.25	0.07	15.98	0.07	15.73	0.03
350	UGC8638	0.01	84	56	70	15.76	0.05	15.58	0.03	0.18	0.06	15.77	0.05	15.58	0.03
351	UGC8651	0.01	168	95	80	15.57	0.05	15.45	0.03	0.12	0.06	15.59	0.05	15.45	0.03
352	NGC5253	0.06	372	141	45	12.32	0.05	11.91	0.03	0.41	0.06	12.36	0.05	11.94	0.03
353	IC4316	0.05	60	39	50	16.10	0.06	15.96	0.04	0.14	0.07	16.10	0.06	15.93	0.04
354	NGC5264	0.05	186	112	65	14.90	0.05	14.28	0.08	0.62	0.09	14.92	0.05	14.35	0.08
355	UGC8683	0.01	156	104	−43	16.04	0.06	15.81	0.03	0.23	0.07	15.99	0.08	15.74	0.04
356	ESO325-G011	0.09	…	…	…	…	…	…	…	…	…	…	…	…	…
357	ESO383-G087	0.07	…	…	…	…	…	…	…	…	…	…	…	…	…
358	ESO383-G091	0.08	100	100	−78	17.25	0.12	…	…	…	…	17.18	0.23	16.39	0.04
359	UGC8760	0.02	162	52	33	15.83	0.05	15.60	0.04	0.23	0.06	15.84	0.05	15.60	0.04
360	UGC8837	0.01	…	…	…	…	…	…	…	…	…	…	…	…	…
361	UGC8833	0.01	60	53	−40	16.64	0.05	16.42	0.04	0.22	0.06	16.63	0.05	16.41	0.04
362	ESO384-G016	0.07	24	17	67	18.53	0.23	17.50	0.08	1.03	0.24	18.60	0.24	17.31	0.10
363	NGC5457	0.01	1290	1205	90	9.96	0.05	9.80	0.03	0.16	0.06	9.96	0.05	9.81	0.03
364	NGC5408	0.07	…	…	…	…	…	…	…	…	…	…	…	…	…
365	NGC5474	0.01	342	306	0	12.89	0.05	12.79	0.04	0.10	0.07	12.90	0.05	12.81	0.04
366	NGC5477	0.01	102	78	−85	14.87	0.06	14.88	0.04	−0.01	0.07	14.87	0.06	14.88	0.04
367	KKR03	0.01	36	30	−20	18.38	0.06	18.17	0.04	0.21	0.07	18.12	0.08	18.04	0.04
368	Circinus	1.46	…	…	…	…	…	…	…	…	…	…	…	…	…
369	KUG1413+573	0.01	48	18	0	17.27	0.08	17.10	0.05	0.17	0.09	17.28	0.11	17.07	0.06
370	UGC9128	0.02	120	92	45	16.21	0.05	15.83	0.03	0.38	0.06	16.21	0.05	15.83	0.03
371	SBS1415+437	0.01	72	18	25	15.93	0.06	15.77	0.04	0.16	0.07	15.92	0.06	15.75	0.04
372	NGC5585	0.02	432	276	30	13.03	0.05	12.72	0.03	0.31	0.06	13.03	0.05	12.72	0.03
373	UGC9211	0.01	72	59	−65	16.08	0.06	15.89	0.04	0.19	0.08	15.90	0.16	15.76	0.05

Table 2
(Continued)

No.	Galaxy Name	$E(B-V)$	a	b	P.A.	FUV_{ap}		NUV_{ap}		$(FUV-NUV)_{ap}$		FUV_{asym}		NUV_{asym}	
			(″)	(″)	(deg)	(mag)		(mag)		(mag)		(mag)		(mag)	
(1)	(2)	(3)	(4)	(5)	(6)	(7)	(8)	(9)	(10)	(11)	(12)	(13)	(14)	(15)	(16)
374	NGC5608	0.01	108	54	−85	15.12	0.05	14.88	0.04	0.24	0.06	15.11	0.05	14.87	0.04
375	UGC9240	0.01	132	132	0	14.80	0.05	14.55	0.03	0.25	0.06	14.82	0.05	14.55	0.03
376	UKS1424-460	0.13	...	...	...	...	...	...	...	...	...	...	...	...	...
377	ESO222-G010	0.27	...	...	...	...	...	...	...	...	...	...	...	...	...
378	UGC9405	0.01	126	44	−35	16.74	0.06	16.37	0.03	0.37	0.07	16.71	0.07	16.30	0.07
379	MRK475	0.01	30	22	80	17.39	0.05	17.16	0.03	0.23	0.06	17.38	0.05	17.14	0.03
380	ESO272-G025	0.16	...	...	...	...	...	...	...	...	...	...	...	...	...
381	UGC9497	0.01	72	14	63	16.33	0.06	16.21	0.04	0.12	0.07	16.32	0.06	16.20	0.04
382	NGC5832	0.03	162	96	45	14.56	0.05	14.28	0.03	0.28	0.06	14.55	0.05	14.26	0.03
383	ESO223-G009	0.26	...	...	...	...	...	...	...	...	...	...	...	...	...
384	UGC9660	0.02	72	36	83	15.82	0.05	15.48	0.03	0.34	0.06	15.82	0.05	15.47	0.03
385	ESO274-G001	0.25	...	...	...	...	...	...	...	...	...	...	...	...	...
386	NGC5949	0.02	162	74	−33	15.14	0.05	14.70	0.03	0.44	0.06	15.15	0.05	14.73	0.03
387	UGC9893	0.01	78	28	42	16.66	0.05	16.29	0.03	0.37	0.06	16.66	0.05	16.27	0.03
388	UGC9992	0.04	114	71	−20	16.30	0.07	16.00	0.03	0.30	0.08	16.31	0.09	15.98	0.03
389	LEDA100404	0.05	...	...	...	...	...	...	...	...	...	...	...	...	...
390	ESO137-G018	0.25	...	...	...	...	...	...	...	...	...	...	...	...	...
391	ESO179-IG013	0.27	...	...	...	...	...	...	...	...	...	...	...	...	...
392	UGC10669	0.03	42	42	0	18.33	0.15	17.73	0.07	0.60	0.16	18.28	0.16	17.58	0.07
393	UGC10736	0.03	210	61	−25	15.94	0.09	15.57	0.03	0.37	0.10	15.95	0.09	15.57	0.03
394	IC4662	0.07	162	92	−75	12.43	0.05	12.35	0.03	0.08	0.06	12.44	0.05	12.35	0.03
395	NGC6503	0.03	528	178	−57	13.15	0.05	12.71	0.03	0.44	0.06	13.18	0.05	12.79	0.03
396	ESO140-G019	0.08	...	...	...	...	...	...	...	...	...	...	...	...	...
397	IC4710	0.09	...	...	...	...	...	...	...	...	...	...	...	...	...
398	NGC6689	0.07	...	...	...	...	...	...	...	...	...	...	...	...	...
399	ESO104-G022	0.08	...	...	...	...	...	...	...	...	...	...	...	...	...
400	NGC6744	0.04	1002	646	15	11.14	0.07	10.69	0.03	0.45	0.08	11.12	0.07	10.71	0.04
401	ESO104-G044	0.04	72	61	−18	17.28	0.06	16.64	0.04	0.64	0.07	17.26	0.07	16.58	0.04
402	NGC6789	0.07	60	46	−35	16.22	0.05	15.65	0.03	0.57	0.06	16.21	0.05	15.61	0.03
403	ESO594-G004	0.12	132	96	−85	14.89	0.12	14.65	0.03	0.24	0.12	14.89	0.12	14.61	0.03
404	IC4870	0.11	72	40	−44	14.63	0.13	14.43	0.04	0.20	0.14	14.58	0.13	14.41	0.04
405	NGC6822	0.23	918	800	0	10.08	0.05	9.62	0.07	0.46	0.09	10.05	0.06	9.54	0.07
406	IC4951	0.04	204	36	−4	15.22	0.05	14.94	0.04	0.28	0.06	15.22	0.05	14.94	0.04
407	UGC11583	0.31	...	...	...	...	...	...	...	...	...	...	...	...	...
408	LEDA166192	0.28	...	...	...	...	...	...	...	...	...	...	...	...	...
409	LEDA166193	0.45	...	...	...	...	...	...	...	...	...	...	...	...	...
410	NGC6946	0.34	504	429	52	10.29	0.34	9.70	0.10	0.59	0.36	10.30	0.34	9.70	0.11
411	KKR55	0.70	...	...	...	...	...	...	...	...	...	...	...	...	...
412	DDO210	0.05	96	48	−80	16.59	0.05	16.23	0.04	0.36	0.07	16.54	0.05	16.10	0.11
413	KKR56	0.73	...	...	...	...	...	...	...	...	...	...	...	...	...
414	CEPHEUS1	0.92	...	...	...	...	...	...	...	...	...	...	...	...	...
415	IC5052	0.05	348	47	−37	13.92	0.05	13.37	0.03	0.55	0.06	13.93	0.05	13.38	0.03
416	KKR59	0.88	...	...	...	...	...	...	...	...	...	...	...	...	...
417	KKR60	1.03	...	...	...	...	...	...	...	...	...	...	...	...	...
418	NGC7064	0.01	282	45	−89	14.15	0.05	13.89	0.03	0.26	0.06	14.15	0.05	13.89	0.03
419	NGC7090	0.02	552	97	−53	14.06	0.06	13.50	0.06	0.56	0.09	14.10	0.06	13.53	0.06
420	IC5152	0.03	228	140	−80	12.33	0.05	11.99	0.03	0.34	0.06	12.33	0.05	11.98	0.03
421	UGC11891	0.35	...	...	...	...	...	...	...	...	...	...	...	...	...
422	ESO238-G005	0.01	216	97	5	16.44	0.05	16.23	0.04	0.21	0.07	16.44	0.05	16.23	0.04
423	IC5256	0.03	78	36	19	16.72	0.05	16.32	0.03	0.40	0.06	16.72	0.05	16.32	0.03
424	NGC7640	0.11	...	...	...	...	...	...	...	...	...	...	...	...	...
425	UGC12588	0.15	...	...	...	...	...	...	...	...	...	...	...	...	...
426	UGCA438	0.01	84	67	0	15.31	0.05	15.26	0.03	0.05	0.06	15.31	0.05	15.25	0.03
427	ESO347-G017	0.02	204	44	−86	15.61	0.05	15.31	0.03	0.30	0.06	15.61	0.05	15.32	0.03
428	UGC12613	0.07	216	117	−60	15.71	0.06	14.94	0.06	0.77	0.08	15.73	0.06	14.93	0.06
429	UGC12632	0.14	156	128	20	14.66	0.07	14.20	0.11	0.46	0.13	14.56	0.07	14.09	0.12
430	IC5332	0.02	462	367	17	12.55	0.05	12.35	0.03	0.20	0.06	12.48	0.07	12.27	0.06
431	NGC7713	0.02	...	...	...	...	...	...	...	...	...	...	...	...	...
432	UGC12713	0.06	72	43	65	16.43	0.06	16.13	0.04	0.30	0.07	16.43	0.06	16.12	0.04
433	UGCA442	0.02	258	37	48	14.83	0.05	14.67	0.04	0.16	0.06	14.83	0.05	14.67	0.04

Table 2
(Continued)

No.	Galaxy Name	$E(B-V)$	a	b	P.A.	FUV_{ap}		NUV_{ap}		$(FUV-NUV)_{ap}$		FUV_{asym}		NUV_{asym}	
			(″)	(″)	(deg)	(mag)		(mag)		(mag)		(mag)		(mag)	
(1)	(2)	(3)	(4)	(5)	(6)	(7)	(8)	(9)	(10)	(11)	(12)	(13)	(14)	(15)	(16)
434	ESO348-G009	0.01	162	68	83	16.27	0.05	16.05	0.04	0.22	0.06	16.25	0.05	16.01	0.04
435	ESO149-G003	0.01	162	30	−32	15.66	0.05	15.59	0.03	0.07	0.06	15.66	0.05	15.59	0.03
436	NGC7793	0.02	618	418	−82	11.12	0.05	10.97	0.03	0.15	0.06	11.13	0.05	10.97	0.03
1	ESO410-G005	0.01	108	83	54	18.26	0.09	17.20	0.04	1.06	0.10	18.29	0.11	17.20	0.05
2	SCULPTOR-DE1	0.01	102	79	−10	(23.60)	...	18.45	0.20	...	...	...	...	17.82	0.92
3	ESO294-G010	0.01	72	46	6	18.12	0.07	17.57	0.04	0.55	0.08	18.02	0.12	17.43	0.04
4	ESO540-G030	0.02	108	81	−70	19.10	0.11	18.08	0.10	1.02	0.15	19.28	0.15	18.30	0.28
5	ESO540-G032	0.02	30	18	0	19.58	0.08	19.07	0.05	0.51	0.09	19.53	0.10	18.66	0.07
6	UGC521	0.06	60	40	50	16.03	0.05	16.05	0.03	−0.02	0.06	16.02	0.05	16.04	0.03
7	NGC0404	0.06	396	396	0	14.94	0.26	13.69	0.17	1.25	0.32	14.94	0.43	13.68	0.54
8	IC2049	0.02	60	54	3	16.46	0.05	16.11	0.04	0.35	0.06	16.45	0.05	16.10	0.04
9	UGCA133	0.04	...	...	...	(23.07)	...	(23.07)	...	...	...	...	...	...	...
10	F8D1	0.10	100	100	0	24.37	2.74	17.12	0.13	...	...	...	...	...	...
11	FM2000_1	0.08	54	48	0	(23.95)	...	19.88	0.07	...	...	...	...	19.68	0.10
12	LEDA166101	0.14	102	76	20	(22.24)	...	18.00	0.10	...	...	...	...	18.10	0.99
13	ARPSLOOP	0.09	78	69	0	18.49	0.09	17.97	0.05	0.52	0.10	17.31	0.73	17.76	0.75
14	KKH057	0.02	24	20	10	(23.24)	...	20.87	0.14	...	...	...	...	20.31	0.23
15	AM1001-270	0.08	114	86	−20	17.11	0.35	16.44	0.14	0.67	0.38	16.44	0.50	16.07	0.17
16	BK05N	0.06	42	32	−45	(23.18)	...	20.31	0.12	...	...	...	...	19.69	0.41
17	UGC05442	0.05	84	44	23	(23.42)	...	18.39	0.05	...	...	...	...	17.80	0.09
18	IKN	0.06	...	...	...	(22.90)	...	(23.06)	...	...	...	...	...	...	...
19	HS98_117	0.12	...	...	...	(20.82)	...	(20.98)	...	...	...	...	...	...	...
20	DDO078	0.02	...	...	...	(22.01)	...	(22.05)	...	...	...	...	...	...	...
21	BK06N	0.01	...	...	...	(23.39)	...	(23.30)	...	...	...	...	...	...	...
22	UGC6782	0.03	144	144	0	16.85	0.16	16.48	0.09	0.37	0.18	16.87	0.16	16.48	0.09
23	ESO321-G014	0.09	102	44	20	16.41	0.14	16.12	0.04	0.29	0.14	16.42	0.15	16.08	0.05
24	UGC7321	0.03	246	18	82	16.10	0.05	15.46	0.03	0.64	0.06	16.09	0.05	15.44	0.03
25	KKH086	0.03	72	51	0	19.27	0.12	18.54	0.11	0.73	0.17	19.46	0.16	18.58	0.13
26	KKR25	0.01	66	36	20	(23.45)	...	19.11	0.06	...	...	...	...	18.91	0.11
27	KKH098	0.12	54	29	−5	17.20	0.06	17.00	0.04	0.20	0.07	17.19	0.07	16.94	0.05

(This table is also available in a machine-readable form in the online journal.)

growth curve in each *GALEX* UV band is computed. A linear fit to the cumulative magnitude versus the cumulative-magnitude gradient is performed, and the y-intercept of the fit is adopted as the asymptotic magnitude. The uncertainty in the fit is also included in the reported errors. This procedure is relatively standard at optical wavelengths (see, e.g., Cairós et al. 2001) and has been shown to be accurate for the determination of total magnitudes in *GALEX* UV imaging of nearby galaxies (Gil de Paz et al. 2007).

Aperture fluxes are measured within the outermost elliptical annulus where both FUV and NUV surface photometry can be performed. We define this annulus as the one beyond which either the flux error becomes larger than 0.8 mag or where the intensity falls below that of the sky background in both FUV and NUV bands. These matched aperture fluxes are appropriate for computing the integrated color.

Finally, fluxes are also measured in the apertures used for the Local Volume Legacy *Spitzer* imaging in Dale et al. (2009) to provide a complete set of matched UV-to-IR aperture photometry as mentioned above.

The results of our photometry, on the AB magnitude scale, are presented in Table 2 as follows.

Column 1: index number, repeated from Table 1.

Column 2: galaxy name, repeated from Table 1.

Column 3: $E(B-V)$ based on the maps of Schlegel et al. (1998).

Columns 4–6: semimajor axis, semiminor axis, and position angle of the outermost elliptical annulus where *both* FUV and NUV surface photometry can be performed. We define this as the distance beyond which the annular flux error becomes larger than 0.8 mag, or where the intensity falls below that of the sky background in both FUV and NUV bands, whichever occurs first. The position angle is measured east of north as usual.

Columns 7–10: FUV and NUV magnitude and error, measured in the common elliptical aperture described by the preceding columns. Corrections for Milky Way (MW) foreground extinction have been applied using the $E(B-V)$ values listed here, and the Cardelli et al. (1989) extinction law with $R_V = 3.1$. That is, $A_{FUV} = 7.9\,E(B-V)$ and $A_{FUV} = 8.0\,E(B-V)$. For non-detections, 3σ point source upper limits are listed, enclosed in parenthesis. The quoted errors include the photometric uncertainty within the aperture and the error in the zero point (0.05 and 0.03 m_{AB} in the FUV and NUV, respectively; Morrissey et al. 2007).

Columns 11 and 12: FUV − NUV color and error, corrected for MW extinction as described previously.

Columns 13–16: FUV and NUV asymptotic magnitude and error, measured from a growth curve which is computed using fixed central coordinates, ellipticity, and position angle as described above, and corrected for MW extinction. Here, the quoted errors include the photometric uncertainty, the error

Table 3
GALEX Photometry in *Spitzer* Local Volume Legacy Apertures

No.	Galaxy Name	*a* ($''$)	*b* ($''$)	P.A. (deg)	$FUV_{LocalVolumeLegacy}$ (mag)		$NUV_{LocalVolumeLegacy}$ (mag)	
(1)	(2)	(3)	(4)	(5)	(6)	(7)	(8)	(9)
2	WLM	336	170	0	12.52	0.05	12.40	0.03
5	NGC24	150	108	225	14.08	0.05	13.81	0.03
6	NGC45	288	228	336	12.58	0.05	12.39	0.03
7	NGC55	1126	357	106	10.16	0.05	9.86	0.03
8	NGC59	128	90	302	16.06	0.06	15.31	0.03
14	IC1574	101	62	0	16.56	0.05	16.08	0.03
15	NGC247	738	290	352	11.38	0.05	11.16	0.03
16	NGC253	1025	404	50	11.15	0.05	10.62	0.03
17	UGCA15	75	39	28	16.78	0.05	16.60	0.04
18	SMC	...	...	...	...	...	...	...
19	NGC300	754	564	114	10.23	0.05	10.10	0.03
21	UGC668	341	274	60	11.70	0.05	11.67	0.03
22	UGC685	90	74	122	16.02	0.06	15.61	0.04
23	UGC695	64	54	0	16.64	0.05	16.27	0.03
24	UGC891	97	59	42	16.30	0.05	16.07	0.03
25	UGC1056	62	58	0	16.63	0.05	16.26	0.03
26	UGC1104	83	52	0	15.60	0.05	15.41	0.03
27	NGC598	2226	1381	12	8.00	0.05	7.72	0.03
28	NGC625	250	128	90	13.72	0.05	13.36	0.03
29	NGC628	440	404	90	11.68	0.05	11.40	0.03
30	UGC1176	101	84	25	15.79	0.06	15.62	0.05
32	ESO245-G005	179	126	318	13.66	0.05	13.62	0.03
33	UGC1249	234	102	331	13.45	0.05	13.28	0.03
34	NGC672	278	180	67	13.18	0.05	12.83	0.03
36	ESO245-G007	144	120	0	16.25	0.10	15.52	0.04
37	NGC784	240	96	3	13.91	0.05	13.51	0.03
39	NGC855	95	86	68	15.88	0.11	15.22	0.04
50	ESO115-G021	200	56	221	14.65	0.05	14.39	0.03
55	ESO154-G023	243	124	39	13.78	0.05	13.52	0.04
59	NGC1291	420	402	0	14.22	0.11	13.38	0.05
60	NGC1313	448	347	338	10.62	0.07	10.45	0.04
61	NGC1311	150	70	36	14.83	0.05	14.42	0.03
64	UGC2716	87	62	90	15.91	0.06	15.43	0.05
65	IC1959	126	57	330	14.37	0.05	14.25	0.03
69	NGC1487	215	130	70	13.44	0.05	13.25	0.03
72	NGC1510	63	61	0	15.09	0.05	14.87	0.03
73	NGC1512	501	464	83	13.44	0.05	13.21	0.05
74	NGC1522	76	50	37	15.17	0.05	15.03	0.03
76	ESO483-G013	102	74	322	15.77	0.05	15.42	0.03
83	ESO158-G003	100	86	0	15.47	0.05	15.21	0.03
85	ESO119-G016	110	58	26	16.03	0.06	15.76	0.03
86	NGC1705	84	60	220	13.36	0.05	13.42	0.03
88	NGC1744	330	158	349	13.07	0.05	12.90	0.03
89	NGC1796	128	102	99	14.91	0.05	14.40	0.03
90	ESO486-G021	58	50	90	15.30	0.05	15.08	0.03
91	MCG-05-13-004	...	...	...	...	...	...	...
92	NGC1800	114	82	107	14.60	0.05	14.43	0.03
96	UGCA106	162	122	14	14.06	0.05	13.94	0.05
98	LMC	...	...	...	...	...	...	...
112	KKH37	52	40	90	18.29	0.08	17.74	0.04
119	NGC2366	308	158	31	12.47	0.05	12.39	0.03
123	NGC2403	756	465	304	10.33	0.05	10.13	0.03
128	NGC2500	137	117	75	13.48	0.05	13.34	0.03
129	NGC2537	106	100	0	13.89	0.05	13.69	0.03
130	UGC4278	160	40	351	14.44	0.05	14.21	0.03
131	UGC4305	278	232	60	12.35	0.05	12.25	0.03
132	NGC2552	156	102	54	14.27	0.05	14.09	0.03
133	M81dwA	39	39	90	17.35	0.05	17.36	0.03
135	UGC4426	103	72	10	16.76	0.06	16.53	0.03
136	UGC4459	67	56	120	15.32	0.05	15.38	0.03
138	UGC4483	47	29	0	15.75	0.05	15.80	0.03
139	NGC2683	411	210	41	14.09	0.05	13.45	0.09
140	UGC4704	152	54	296	15.83	0.07	15.60	0.03

Table 3
(Continued)

No.	Galaxy Name	a	b	P.A.	$FUV_{LocalVolumeLegacy}$ (mag)		$NUV_{LocalVolumeLegacy}$ (mag)	
		($''$)	($''$)	(deg)				
(1)	(2)	(3)	(4)	(5)	(6)	(7)	(8)	(9)
142	UGC4787	106	54	5	15.99	0.05	15.57	0.04
150	UGC4998	94	81	71	17.98	0.18	17.15	0.04
152	NGC2903	412	230	17	12.31	0.05	11.76	0.03
153	UGC5076	82	70	90	...	...	...	...
154	CGCG035-007	63	48	63	17.13	0.06	16.72	0.03
157	UGC5139	132	110	63	14.74	0.06	14.71	0.03
158	IC559	68	62	63	16.44	0.05	16.06	0.03
160	NGC2976	228	156	322	13.07	0.08	12.73	0.03
162	UGC5272	98	48	112	14.96	0.05	14.88	0.03
163	UGC5288	82	70	331	15.73	0.05	15.52	0.03
165	BK3N	20	20	90	18.84	0.06	18.78	0.04
166	NGC3031	814	562	154	10.77	0.05	10.47	0.03
167	NGC3034	349	290	65	12.56	0.09	11.47	0.03
168	UGC5340	87	50	10	15.16	0.05	15.18	0.03
169	KDG61	107	60	49	21.53	1.54	18.44	0.12
170	UGC5336	124	90	220	15.04	0.06	14.90	0.05
173	UGC5364	156	96	67	14.62	0.05	14.35	0.03
174	UGC5373	166	134	90	13.72	0.05	13.52	0.04
175	UGCA193	142	34	14	16.27	0.05	15.94	0.04
176	NGC3109	798	174	91	11.37	0.12	11.11	0.07
177	NGC3077	244	218	64	...	...	...	...
181	UGC5428	98	84	90	17.93	0.08	...	...
183	UGC5423	54	35	140	16.60	0.05	16.43	0.03
187	UGC5456	80	60	322	14.95	0.05	14.62	0.03
190	SextansA	204	158	35	12.58	0.05	12.55	0.03
192	NGC3239	158	136	63	12.81	0.05	12.59	0.03
193	UGC5672	144	52	340	17.14	0.05	16.48	0.03
194	UGC5666	432	243	59	12.15	0.06	12.10	0.04
195	UGC5692	153	106	0	16.39	0.06	15.65	0.03
196	NGC3274	174	71	110	14.26	0.05	14.05	0.03
199	NGC3299	132	104	0	16.26	0.08	15.64	0.06
200	UGC5764	75	42	44	16.25	0.05	16.16	0.03
201	UGC5797	70	69	0	16.85	0.05	16.42	0.03
203	UGC5829	142	126	20	14.08	0.05	14.00	0.03
204	NGC3344	257	224	330	12.44	0.05	12.11	0.03
205	NGC3351	293	228	10	13.27	0.05	12.73	0.03
207	NGC3368	256	174	346	14.04	0.06	13.41	0.03
208	UGC5889	101	95	0	16.30	0.06	15.88	0.05
210	UGC5923	48	30	353	17.24	0.05	16.71	0.03
211	UGC5918	70	56	65	16.82	0.13	16.56	0.04
214	NGC3432	238	94	38	13.26	0.05	12.84	0.03
215	KDG73	63	50	345	18.83	0.12	18.41	0.18
217	NGC3486	248	194	83	12.50	0.05	12.35	0.03
219	NGC3510	155	68	345	14.61	0.05	14.33	0.03
222	NGC3521	384	247	343	13.05	0.06	12.28	0.04
225	NGC3593	186	106	86	16.77	0.25	15.23	0.07
229	NGC3623	332	166	352	14.95	0.07	13.91	0.07
230	NGC3627	373	244	347	12.65	0.05	11.98	0.03
231	NGC3628	520	310	102	14.23	0.09	13.18	0.03
235	UGC6457	75	56	19	16.34	0.06	15.97	0.03
237	UGC6541	62	44	316	15.38	0.05	15.20	0.03
238	NGC3738	110	88	343	13.76	0.05	13.45	0.03
239	NGC3741	100	54	10	15.17	0.05	15.03	0.03
241	UGC6817	135	72	65	14.92	0.05	14.75	0.03
242	UGC6900	102	72	107	17.40	0.06	16.88	0.05
244	NGC4020	111	68	18	15.20	0.05	14.83	0.03
246	NGC4068	128	89	22	14.30	0.05	14.08	0.03
247	NGC4080	76	66	312	16.08	0.05	15.68	0.03
248	NGC4096	278	122	18	14.09	0.05	13.60	0.03
250	NGC4144	218	94	103	13.95	0.05	13.57	0.03
251	NGC4163	106	82	4	15.35	0.05	14.96	0.03
252	NGC4190	105	82	45	14.77	0.05	14.32	0.03
253	UGC7242	78	42	0	16.07	0.05	15.55	0.04

Table 3
(Continued)

No.	Galaxy Name	a (″)	b (″)	P.A. (deg)	$FUV_{LocalVolumeLegacy}$ (mag)		$NUV_{LocalVolumeLegacy}$ (mag)	
(1)	(2)	(3)	(4)	(5)	(6)	(7)	(8)	(9)
254	UGCA276	80	72	301	16.07	0.05	18.70	0.07
256	UGC7267	94	49	45	16.29	0.05	15.94	0.03
258	NGC4214	312	284	0	11.50	0.05	11.28	0.03
259	CGCG269-049	47	34	319	16.63	0.05	16.39	0.03
261	NGC4236	620	184	342	11.81	0.05	11.63	0.03
262	NGC4244	591	121	47	12.67	0.05	12.20	0.03
263	NGC4242	205	156	28	13.88	0.05	13.54	0.03
264	NGC4248	126	85	107	16.82	0.05	15.83	0.04
266	NGC4258	621	266	332	11.85	0.05	11.43	0.03
268	ISZ399	66	51	314	...	...	...	...
269	NGC4288	95	82	139	14.62	0.05	14.41	0.03
270	UGC7408	110	96	90	16.11	0.05	15.50	0.03
271	UGC7490	113	110	0	...	...	...	...
273	NGC4395	504	395	328	11.64	0.05	11.52	0.03
274	UGCA281	44	36	81	15.18	0.05	15.18	0.03
275	UGC7559	120	66	307	15.15	0.05	15.06	0.03
276	UGC7577	135	90	301	14.84	0.05	14.54	0.03
279	NGC4449	236	177	57	10.86	0.05	10.81	0.03
280	UGC7599	60	36	306	16.13	0.05	16.03	0.03
281	UGC7605	70	43	17	15.82	0.05	15.67	0.03
282	NGC4455	100	45	198	14.46	0.05	14.19	0.03
283	UGC7608	105	104	0	14.83	0.05	14.77	0.03
284	NGC4460	169	74	37	15.52	0.06	14.77	0.03
286	UGC7639	116	70	334	16.13	0.05	15.71	0.03
288	NGC4485	90	67	343	13.61	0.05	13.39	0.03
289	NGC4490	209	116	121	12.03	0.05	11.55	0.03
291	UGC7690	98	76	36	14.68	0.05	14.31	0.03
292	UGC7699	135	52	32	14.74	0.05	14.45	0.03
293	UGC7698	140	94	9	14.88	0.05	14.71	0.03
294	UGC7719	79	43	347	15.99	0.05	15.79	0.03
296	UGC7774	100	28	100	16.34	0.05	15.77	0.03
298	UGCA292	58	38	0	16.46	0.06	16.36	0.04
299	M104	278	116	90	12.98	0.05	12.57	0.03
300	NGC4605	249	165	303	14.67	0.06	13.55	0.04
301	NGC4618	168	134	22	12.83	0.05	12.56	0.03
302	NGC4625	150	107	280	14.63	0.05	14.32	0.03
303	NGC4631	476	270	80	11.29	0.05	11.07	0.03
304	UGC7866	98	86	357	14.68	0.05	14.61	0.03
305	NGC4656	360	128	220	11.58	0.05	11.58	0.03
306	UGC7916	76	50	170	15.86	0.05	15.79	0.03
309	UGC7950	72	62	0	15.23	0.05	15.02	0.03
310	UGC7949	82	50	24	16.06	0.05	15.96	0.03
311	NGC4707	104	88	20	15.09	0.05	14.95	0.03
312	NGC4736	516	412	100	11.76	0.05	11.39	0.03
313	UGC8024	100	63	213	14.94	0.05	14.97	0.03
315	NGC4826	362	224	113	13.51	0.08	12.55	0.03
316	UGC8091	62	46	32	15.23	0.06	15.18	0.03
318	UGCA319	65	45	24	16.58	0.06	16.09	0.03
319	UGCA320	246	82	114	13.93	0.08	13.71	0.04
321	UGC8188	190	163	90	13.38	0.05	13.19	0.03
322	UGC8201	134	75	90	14.53	0.05	14.20	0.03
323	MCG-03-34-002	65	40	320	16.09	0.05	15.73	0.03
325	UGC8245	96	50	70	16.47	0.05	15.99	0.03
326	NGC5023	205	64	26	14.65	0.05	14.25	0.03
327	CGCG217-018	57	44	35	16.58	0.05	16.12	0.03
329	UGC8313	96	57	30	16.31	0.05	15.99	0.03
330	UGC8320	146	99	341	14.55	0.05	14.21	0.04
331	UGC8331	118	58	323	15.95	0.05	15.73	0.04
332	NGC5055	549	356	80	12.35	0.05	11.81	0.03
333	NGC5068	306	296	90	11.94	0.09	11.55	0.04
336	IC4247	64	39	333	15.97	0.05	15.55	0.03
338	NGC5204	169	106	351	12.95	0.05	12.72	0.03

Table 3
(Continued)

No.	Galaxy Name	a ($''$)	b ($''$)	P.A. (deg)	$FUV_{LocalVolumeLegacy}$ (mag)		$NUV_{LocalVolumeLegacy}$ (mag)	
(1)	(2)	(3)	(4)	(5)	(6)	(7)	(8)	(9)
339	NGC5194	850	565	15	11.01	0.05	10.53	0.03
340	NGC5195	102	96	0	15.72	0.06	14.65	0.03
341	UGC8508	80	60	305	...	...	...	...
344	NGC5229	140	51	347	15.70	0.07	15.35	0.03
345	NGC5238	108	83	0	15.19	0.05	14.98	0.03
347	[KK98]208	180	75	57	< 23.75		< 23.90	
348	NGC5236	550	528	0	10.07	0.05	9.59	0.03
349	ESO444-G084	63	44	310	16.05	0.05	15.82	0.03
350	UGC8638	90	66	73	15.76	0.05	15.57	0.03
351	UGC8651	97	70	59	15.63	0.05	15.52	0.03
352	NGC5253	160	122	44	12.29	0.05	11.94	0.03
354	NGC5264	134	113	66	14.69	0.06	14.28	0.06
359	UGC8760	108	56	29	15.84	0.05	15.61	0.03
360	UGC8837	182	74	17	...	...	...	...
361	UGC8833	60	58	0	16.64	0.05	16.42	0.04
363	NGC5457	900	723	37	9.98	0.05	9.83	0.03
365	NGC5474	206	186	90	12.94	0.05	12.84	0.03
366	NGC5477	84	62	64	14.89	0.05	14.90	0.03
367	KKR03	34	24	0	18.43	0.06	18.22	0.03
370	UGC9128	64	44	36	16.30	0.07	15.90	0.04
372	NGC5585	196	133	38	13.14	0.05	12.81	0.03
375	UGC9240	111	91	90	14.82	0.05	14.57	0.03
378	UGC9405	100	68	333	16.70	0.07	16.31	0.03
379	MRK475	36	36	196	17.37	0.05	17.13	0.03
382	NGC5832	146	90	49	14.58	0.05	14.29	0.03
386	NGC5949	110	68	324	15.15	0.05	14.72	0.03
388	UGC9992	78	54	340	16.33	0.06	16.04	0.03
395	NGC6503	320	116	119	13.22	0.05	12.78	0.03
406	IC4951	112	46	355	15.08	0.05	14.95	0.03
412	DDO210	80	38	103	16.65	0.05	16.35	0.04
415	IC5052	225	84	323	13.90	0.05	13.36	0.03
418	NGC7064	125	40	90	14.17	0.05	13.90	0.03
419	NGC7090	270	80	308	14.10	0.05	13.53	0.04
420	IC5152	156	137	90	12.44	0.05	12.02	0.03
423	IC5256	62	38	22	16.72	0.05	16.32	0.03
426	UGCA438	94	82	0	15.30	0.05	15.24	0.03
427	ESO347-G017	106	64	90	15.59	0.05	15.31	0.03
428	UGC12613	230	134	113	15.68	0.06	14.90	0.06
430	IC5332	322	286	0	12.58	0.05	12.37	0.03
431	NGC7713	185	114	345	...	...	...	...
433	UGCA442	122	58	43	14.86	0.05	14.70	0.03
435	ESO149-G003	124	50	332	15.63	0.05	15.57	0.03
436	NGC7793	378	250	90	11.15	0.05	10.98	0.03
1	ESO410-G005	61	45	308	18.32	0.08	17.20	0.04
2	Sculptor-dE1	80	52	0	(23.60)	...	18.92	0.17
3	ESO294-G010	82	51	0	18.08	0.08	17.54	0.04
4	ESO540-G030	84	74	0	19.19	0.10	18.13	0.08
5	ESO540-G032	50	46	0	19.53	0.10	18.66	0.06
6	UGC00521	54	54	90	16.02	0.05	16.04	0.03
7	NGC404	105	105	90	16.18	0.10	14.45	0.04
8	IC2049	60	53	0	16.46	0.05	16.12	0.03
9	UGCA133	108	76	0	(23.07)	...	(23.07)	...
10	F8D1	127	127	90	18.11	2.30	17.27	0.43
11	[FM2000]1	44	44	90	(23.95)	...	19.98	0.06
12	LEDA166101	110	76	33	(22.24)	...	17.98	0.10
13	Arp'sLoop	68	68	90	18.63	0.09	18.14	0.05
14	KKH057	36	26	45	(23.24)	...	20.75	0.18
15	AM1001-270	84	48	319	17.46	0.21	16.81	0.09
16	BK05N	104	51	330	(23.18)	...	20.26	1.20
17	UGC05442	98	62	34	(23.42)	...	18.16	0.05
18	IKN	90	78	180	(22.90)	...	(23.06)	...
19	[HS98]117	106	64	0	(20.82)	...	(20.98)	...
20	DDO078	70	70	90	(22.01)	...	(22.05)	...

Table 3
(Continued)

No.	Galaxy Name	a ($''$)	b ($''$)	P.A. (deg)	$\mathrm{FUV_{LocalVolumeLegacy}}$ (mag)		$\mathrm{NUV_{LocalVolumeLegacy}}$ (mag)	
(1)	(2)	(3)	(4)	(5)	(6)	(7)	(8)	(9)
21	BK06N	116	54	304	(23.39)	...	(23.30)	...
22	UGC06782	68	57	115	17.14	0.06	16.75	0.04
23	ESO321-G014	86	52	22	16.44	0.14	16.14	0.04
24	UGC07321	185	39	81	16.05	0.05	15.40	0.03
25	KKH086	66	42	0	19.30	0.09	18.58	0.06
26	KKR25	47	44	0	(23.45)	...	19.09	0.06
27	KKH098	63	40	5	17.18	0.06	16.94	0.04

(This table is also available in a machine-readable form in the online journal.)

in the zero point, as well as the uncertainty due to the error-weighted fit of the growth curve.

In Table 3, we list only those galaxies in the Local Volume Legacy sample, providing the following.

Column 1: index number, as in Table 1.

Column 2: galaxy name, as in Table 1.

Columns 3–5: semimajor axis, semiminor axis, and position angle of the elliptical annulus used by Dale et al. (2009) to extract photometry from *Spitzer* IRAC and MIPS imaging, reproduced from Table 1 of Dale et al. (2009).

Columns 6–9: FUV and NUV magnitude and error, measured in the common elliptical aperture described by the preceding columns. Corrections for MW foreground extinction have been applied using the $E(B-V)$ values listed here, and the Cardelli et al. (1989) extinction law with $R_V = 3.1$. That is, $A_{\mathrm{FUV}} = 7.9\,E(B-V)$ and $A_{\mathrm{FUV}} = 8.0\,E(B-V)$. For non-detections, 3σ point source upper limits are listed, enclosed in parenthesis. The quoted errors include the photometric uncertainty within the aperture and the error in the zero point (0.05 and 0.03 m_{AB} in the FUV and NUV, respectively; Morrissey et al. 2007).

3. RESULTS AND DISCUSSION

3.1. *Basic Sample Properties*

The *GALEX* observations presented here significantly improve the depth to which complete, statistical sampling of Local Volume star-forming (aka, "blue sequence") galaxies is achieved. This is illustrated in Figure 2, which shows the number distributions of FUV and NUV absolute magnitudes. The filled histograms represent *GALEX*'s resultant coverage of the primary 11HUGS target volume ($|b| < 30°$, $d < 11$ Mpc) prior to our observations, and the solid line shows the distributions when our observations are included. While the more limited sample with prior coverage begins to become incomplete for $\gtrsim -15$ mag, our sample continues to increase until about -13 mag. 11HUGS mitigates the previous $\sim$4-fold underrepresentation of Local Volume galaxies at low luminosities.

Luminosity functions based on surveys that have well-determined selection functions and cover much larger volumes than 11HUGS also provide an interesting point of comparison for our M_{FUV} and M_{NUV} number distributions. Such luminosity functions are subject to typical biases toward the most luminous, massive, high-surface brightness systems, and therefore are generally well sampled at the bright end, but are not robustly constrained in the dwarf galaxy regime. In Figure 2, we overplot UV luminosity functions,[18] as computed by Schiminovich et al. (2007), for disk galaxies in the SDSS DR4 spectroscopic sample (Adelman-McCarthy et al. 2006) that have also been observed in the *GALEX* Medium Imaging Survey (Martin et al. 2005). The curves give their best fitting Schechter function fits, with the dashed segments representing extrapolations past the last data point shown. To force approximate agreement between the number distributions and the Schiminovich et al. (2007) luminosity functions at $\sim L^*$, the latter has been multiplied by two times the $|b| > 30$, $d < 11$ Mpc 11HUGS target volume. The factor of two implies that the portion of the Local Volume probed by 11HUGS is over-dense compared with cosmological volumes, as discussed in Karachentsev et al. (2004) and Lee et al. (2009a). Qualitatively, there is good agreement between the relative shapes of both M_{FUV} and M_{NUV} luminosity functions and the 11HUGS number distributions prior to the sharp falloff of galaxies fainter than ~ -13 mag. This provides some assurance that the 11HUGS sampling of bright galaxies, while sparse due to the small target volume, is not heavily biased relative to the global distribution of UV luminosities. The extrapolated faint-end slopes of the luminosity functions appear to also be reasonable in comparison with our local data set. In M_{FUV}, the 11HUGS data set appears to prefer a slightly steeper rise at the faint end ($\alpha \sim 1.06$; gray), though this is well within the uncertainties of the value of $\alpha = 1.02 \pm 0.05$ reported by Schiminovich et al. (2007). If the standard SFR conversion recipe of Kennicutt (1998b) is applied to the FUV luminosities, the SFRs probed by the sample span roughly six orders of magnitude, from $\sim 10\,M_\odot\,\mathrm{yr}^{-1}$ to $\sim 10^{-6}\,M_\odot\,\mathrm{yr}^{-1}$.

The dominance of low-luminosity star-forming galaxies in the sample is also illustrated by distributions in the FUV $-$ NUV color (corrected for MW reddening, but not for dust attenuation internal to the galaxies themselves). In Figure 3, we show a histogram of the UV color and also plot it as a function of EW(Hα), M_{FUV}, and M_B. The points are coded to indicate different morphological types, and the histogram is shaded in a corresponding manner. The sample is concentrated in a fairly narrow range of UV color: the median is 0.29 mag, and 79% of the galaxies have $0 <$ FUV $-$ NUV < 0.5. Such blue colors are primarily a result of the recent star formation activity in such systems (e.g., van Zee 2001; Hunter & Elmegreen 2004; Lee et al. 2007), while low metallicities (e.g., Skillman et al. 1989; van Zee et al. 1997; Lee et al. 2004) and low dust attenuation (e.g., Lee et al. 2009b) also play a role.

[18] The luminosity functions were rescaled to reflect $H_0 = 75$ km s^{-1} Mpc^{-1} as is assumed here to calculate distances for objects without standard candle/ruler estimates.

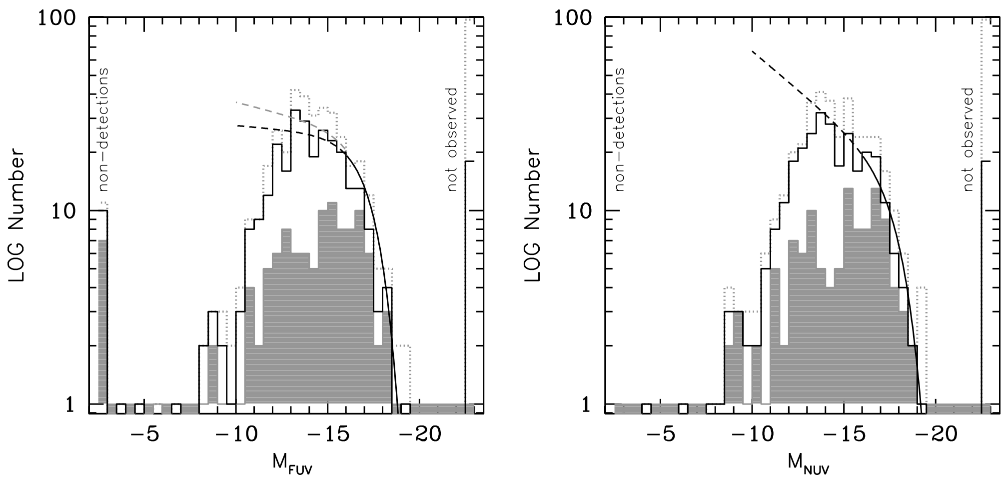

Figure 2. Number distributions in NUV and FUV absolute magnitude for all galaxies with *GALEX* data in the overall parent (Paper I) sample (dotted gray histogram), and the subset of the sample which is most complete: spiral and irregular galaxies ($T > 0$) which avoid the plane of the MW $|b| > 30°$ (black histogram). Corrections for foreground MW extinction, but not extinction internal to the galaxies, have been applied. The gray area shows the *GALEX* coverage of the $|b| > 30°$, $T > 0$ galaxies prior to observations by 11HUGS. Non-detections are plotted at the far left of the figure, while the number of galaxies that have not been observed by *GALEX* are shown at the far right. For comparison, we overplot Schechter fits to *GALEX* luminosity functions computed by Schiminovich et al. (2007) for disk-dominated galaxies in the Sloan Digital Sky Survey (SDSS) spectroscopic sample (solid curve; the dashed portion is an extrapolation from the last data point shown). These luminosity functions have been multiplied by twice the $|b| > 30$, $d < 11$ Mpc 11HUGS survey volume to provide approximate agreement with the observed number distributions (see Section 3.1 for the discussion). Our *GALEX* program significantly improves the depth to which complete, statistical sampling of Local Volume star-forming galaxies is achieved.

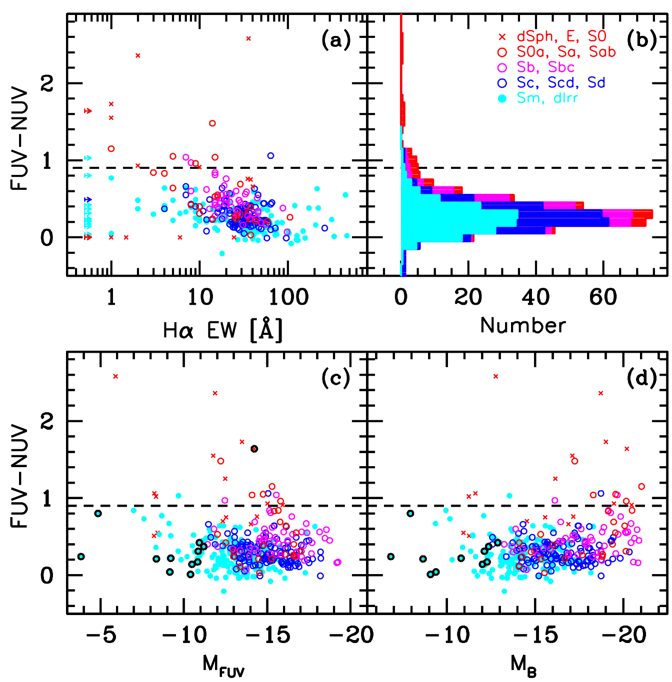

Figure 3. Distributions of the integrated FUV − NUV color. Corrections for MW reddening, but not dust attenuation internal to the galaxies, have been applied. Different symbols and colors are used to distinguish between morphological type as indicated in panel (b). Dashed lines are drawn at FUV − NUV = 0.9, which Gil de Paz et al. (2007) have determined to provide good separation between early-type elliptical and lenticular "red sequence" galaxies, and late-type spiral and irregular "blue sequence" galaxies. Galaxies which were undetected in Hα narrowband imaging, but have one-orbit-depth *GALEX* FUV imaging are circled in black, and largely exhibit blue UV colors characteristic of star-forming galaxies. Blue star-forming dwarf galaxies dominate the sample by construction.

(A color version of this figure is available in the online journal.)

Late-type spiral and irregular "blue sequence" galaxies can be roughly separated from early-type "red sequence" galaxies using a division at FUV − NUV = 0.9 (plotted as a dashed line in Figure 3) as described in Gil de Paz et al. (2007). Again, by design our sample does not contain many early-type galaxies, and there are few galaxies with FUV – NUV > 0.9. For the star-forming galaxies with FUV – NUV < 0.9, the UV color does not show strong trends with either $M_{\rm FUV}$ or M_B, except perhaps for slightly redder values at M_B brighter than −19, at which the sample is predominantly composed of earlier type spirals. There is also a weak trend toward redder colors at lower equivalent width. This trend is expected, since EW(Hα) traces the current SFR relative to the past lifetime average, which provides a measure of the recent star formation history.

3.2. GALEX Non-detections

Late-type galaxies in the Local Volume that do not have measurable UV emission appear to very rare, at least among the $B < 15.5$ population where our observations are concentrated (see Figure 1). Only 22 of the 390 galaxies in our sample which were observed by *GALEX* were not detected in the FUV. About half of these ($N = 12$) are galaxies classified as faint dwarf spheroidals/ellipticals and would not be expected to have UV emission from the recent star formation.[19] Another eight are classified as late-type dwarfs, but only have shallow imaging ($\lesssim$200 s) available; in these cases a detection is also not expected given the galaxies' low *B*-band luminosities and/or low Hα-based SFRs.[20] The remaining two, UGC5428 and UGCA276, do have deep *GALEX* imaging ($t \sim 1700$ s) and are cases for which further follow-up may be valuable as described further below. Both have extremely low luminosities with $M_B \sim -12$ and are nearby ($D \sim 3$ Mpc). The *GALEX* imaging of these galaxies is sensitive enough to detect a single early-type B star ($\sim$15 $M_\odot$).

UGC5428 is a member of the M81 group and has been classified as a "transition" dwarf—a system whose properties are

[19] Sculptor-dE1, UGCA133, FM2000-1, LEDA166101, KKH057, BK05N, UGC5442, IKN, DDO78, BK06N, [KK98]208, and KKR25.

[20] IC2782, LSBCD565-06, LSBCD634-03, UGCA86, KKH34, UGCA92, HS[98]117, and LEDA166115.

intermediate between those of late- and early-type galaxies (e.g., Mateo 1998; Grebel et al. 2003). Although it is seen to be dominated by an old stellar population based upon ANGST *HST* imaging (D. R. Weisz et al. 2011, in preparation), and H I gas has not been observed to a limit of $\sim 10^6\ M_\odot$ (Karachentsev & Kaisin 2007), a few faint, compact Hα knots have been tentatively identified in narrowband imaging (Karachentsev & Kaisin 2007; Paper I). *HST* stellar color–magnitude diagrams have been used to reconstruct the star formation history, indicating that the average SFR over the past Gyr is $\sim 8 \times 10^{-4}\ M_\odot\ \mathrm{yr}^{-1}$, but with error bars consistent with no star formation (D. R. Weisz et al. 2011, in preparation). The narrowband excess sources may therefore be background galaxies. Follow-up spectroscopy is required to confirm the nature of these detections. No significant FUV emission is measurable in apertures spanning the extent of the galaxy, but photometry with a smaller aperture limited to the region where the narrowband excess sources are found, yields an FUV flux that is consistent with that expected from the Hα emission within large uncertainties ($m_{\mathrm{FUV}} = 24.5 \pm 3.3$). The faint, extended diffuse emission observed in the NUV likely arises from older main-sequence turn-off stars.

UGCA276 belongs to a prominent association of dwarf galaxies around NGC 4214 at 2.9 Mpc (Tully et al. 2006). Morphologically, it has been classified as a dwarf irregular. There is a published H I flux for the system, though the detection is uncertain (de Vaucouleurs et al. 1991; Karachentsev et al. 2004). However, there is no observable Hα emission (Paper I). The NUV emission in this system is also faint, extended, and diffuse, so it is not likely to arise from very recent star formation. *HST* resolved stellar population imaging from ANGST also shows that UGCA276 is dominated by an old stellar population and has had little recent activity. Similar to UGC5428, the reconstructed star formation history over the past Gyr is $\sim 4 \times 10^{-4}\ M_\odot\ \mathrm{yr}^{-1}$, but with error bars consistent with zero (D. R. Weisz et al. 2011, in preparation). If the detection of H I is found to be robust, this would make the system extremely peculiar as UGCA276 would be the only galaxy in our sample with detectable H I gas but no evidence of recent star formation. Further detailed study of both objects would be useful to establish the basis of their current evolutionary status and to understand the possible impact of their group environments.

In the NUV, only 10 galaxies were not detected and are a subset of the FUV non-detections. Half are dwarf irregulars which only have shallow exposures ($\lesssim$200 s),[21] and the other half are dwarf spheroidals.[22]

The nearly ubiquitous presence of UV emission in local spirals and irregulars is not surprising given that they are star-forming systems, and moreover, because Hα has already been detected in the vast majority of late-type galaxies surveyed (e.g., Meurer et al. 2006; James et al. 2008; Paper I). This finding reinforces the idea that the intermittent cessation of activity is uncommon, as we rarely observe such systems in an "off" mode, at least for the $B < 15.5$ population probed (Lee et al. 2009a). The result is particularly relevant for dwarf galaxies, which generally appear to have fluctuating or bursty star formation histories (e.g., Weisz et al. 2008; Tolstoy et al. 2009, and references therein), because it implies that the fluctuations do not go to zero for durations comparable to the lifetimes of UV emitting stars (∼100 Myr). For the higher luminosity galaxies in the sample ($M_B \lesssim -14$), star formation over galaxy-wide scales further appears to be virtually continuous—the 100% Hα detection rate for this subset of our sample (Paper I; Lee et al. 2009a) constrains gaps in activity to be less than the lifetimes of ionizing stars ($\lesssim$10 Myr).

It is not clear whether this picture continues to be true for star-forming dwarfs with lower luminosities. In Lee et al. (2009a), it was noted that all of the late-type galaxies which were undetected in the Paper I Hα survey had very low luminosities, with $-7.6 \leqslant M_B \leqslant -13.6$. Thus, it is possible that off-modes may be a general feature of the star formation histories of this extreme population. However, it is not straightforward to interpret the lack of Hα as an absence of star formation. Such systems have lifetime-averaged SFRs on the order of 10^{-3}–$10^{-4}\ M_\odot\ \mathrm{yr}^{-1}$, *so Poisson fluctuations in the sampling of the IMF may lead to the absence of O-stars, even when continuous star formation is in fact occurring*. The FUV should be more immune to this Poisson noise, and as we discuss below, sufficiently deep *GALEX* observations of Hα non-detections show them to generally have normal levels of recent star formation activity relative to the broader population of dwarf irregular galaxies. We may therefore speculate that extremely low-luminosity dwarfs also do not commonly undergo intermittent periods of complete inactivity which last for $\gtrsim$100 Myr. This is only a speculation because our sample is incomplete in this luminosity regime. Obtaining Hα and FUV observations of a large complete sample of extremely low-luminosity galaxies, or better yet, of a complete sample of galaxies with low H I masses ($M_{\mathrm{H\,I}} \leqslant 10^8\ M_\odot$), is required to examine whether the rarity of UV non-detections (or equivalently the rarity of temporarily halted star formation) persists.

3.3. A Re-examination of Star Formation Properties in the FUV

In light of the finding that *GALEX* FUV observations may be a more robust probe of star formation in low-density environments than typical Hα narrowband imaging (see the introduction), it is instructive to use our dwarf galaxy dominated sample to re-examine commonly studied star formation properties which have been largely based on Hα measurements over the past three decades. Here, we illustrate how our view of evolutionary status of dwarf galaxies may change by recalculating two coarse measures of the global star formation efficiency: the SFR per unit H I mass ($M_{\mathrm{H\,I}}$) and the SFR per unit stellar mass (M_*). These quantities provide the basis for computing timescales of future and past star formation and are related to the "gas consumption timescale" and the "stellar birthrate," respectively (e.g., Kennicutt 1983; Hunter & Gallagher 1985; Kennicutt et al. 1994; van Zee et al. 1997; van Zee 2001; Skillman et al. 2003; Brinchmann et al. 2004; Lee et al. 2004, 2009a; Karachentsev & Kaisin 2007; James et al. 2008; Côté et al. 2009; Bothwell et al. 2009). In this context, it is also particularly interesting to examine the UV properties of late-type galaxies that were not detected in earlier Hα imaging and thus appeared to be devoid of star formation.

3.3.1. Global Star Formation Efficiencies

In Figure 4, the SFR is plotted against $M_{\mathrm{H\,I}}$ in the left panel, and SFR/$M_{\mathrm{H\,I}}$ is shown as a function of M_B in the right. There are two sets of points: the gray set gives the value of the ordinate using Hα-based SFRs, while the colored set shows those based upon the FUV. Only galaxies that have both FUV and Hα measurements are shown. The SFRs are computed as in Lee

[21] HS98_117, UGCA86, UGCA92, KKH34, and LSBCD634-03.

[22] UGCA133, IKN, DDO078, BK06N, and [KK98]208.

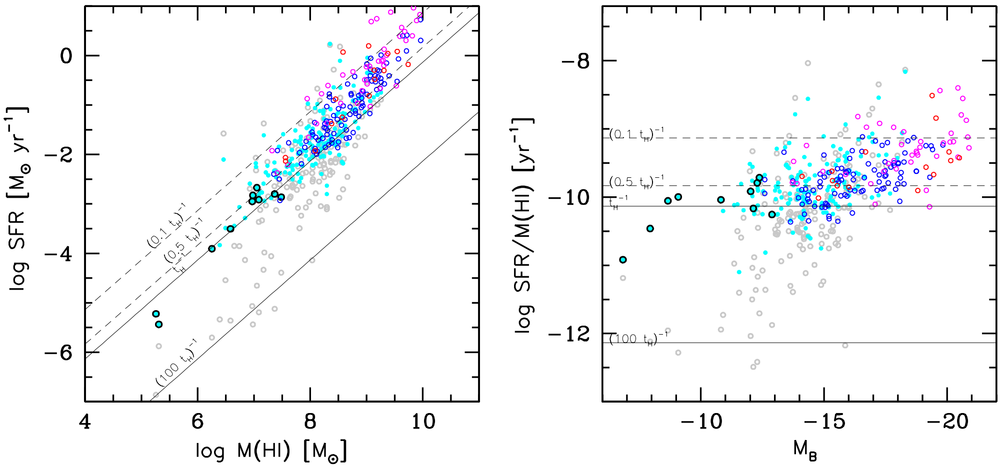

Figure 4. Comparison between star formation efficiencies, as measured by the SFR per unit H I mass, when the FUV emission (colored symbols) is used as the star formation tracer, instead of Hα (gray symbols). Different symbols and colors are used to distinguish between morphological types as in Figure 3. Only galaxies that have both FUV and Hα measurements are shown. Best-effort attenuation corrections are applied before computing the SFR as in Lee et al. (2009b).

(A color version of this figure is available in the online journal.)

et al. (2009b), where best-effort corrections have been applied for internal dust attenuation.[23]

The H I masses are computed from single-dish 21 cm line fluxes compiled from the literature as described in Lee et al. (2009a), where the measurements are primarily drawn from Springob et al. (2005); the H I Parkes All Sky Survey (HIPASS) catalog as published in Meyer et al. (2004); and the homogenized H I compilation of Paturel et al. (2003) as made available through the Hyperleda database. The lines in Figure 4 indicate values of constant SFR/$M_{\rm H\,I}$, in units of the age of the universe ($t_{\rm H}$ = 13.7 Gyr).

The difference between the global star formation efficiencies inferred from the two SFR tracers is immediately apparent. The Hα-based values yield significantly lower efficiencies for the late-type dwarf galaxies with $M_B \gtrsim -15$ and $M_{\rm H\,I} \lesssim 10^{8.5}$ relative to the more luminous and more massive spirals. This behavior is consistent with the results of many previous authors who have reported gas depletion timescales ($\propto M_{\rm H\,I}$/SFR) in excess of several Hubble times for samples of dwarf irregular galaxies (e.g., van Zee 2001; Skillman et al. 2003; Karachentsev & Kaisin 2007; Knapen & James 2009; Bothwell et al. 2009). In contrast, the FUV-based values generally do not fall below $t_{\rm H}^{-1}$. Most spiral and irregular galaxies in our Local Volume sample have SFR(UV)/H I values on the order of $t_{\rm H}^{-1}$, with 75% between $t_{\rm H}^{-1}$ and $0.1t_{\rm H}^{-1}$. Analogous plots for the SFR per unit stellar mass are shown in Figure 5, where the stellar masses are computed using M_B and mass-to-light ratios based on the $B-V$ color, as in Bothwell et al. (2009). Similar differences between the Hα- and UV-based values are evident. Therefore, dwarf irregular galaxies may not be as drastically inefficient at forming stars as previously determined.

[23] Briefly, the Hα attenuation is measured from the Balmer decrement, for galaxies with available integrated optical spectroscopy. The FUV attenuation is measured from the total infrared-to-UV flux ratio, for galaxies with available *Spitzer* IR imaging. Otherwise, empirical scaling relations are used to estimate the attenuation from M_B. There is some current debate on whether the discrepancies between the UV and Hα SFRs may be an artifact of uncertain attenuation corrections (e.g., Boselli et al. 2009; Meurer 2010). However, it is important to note that in the present sample of dwarf galaxies, there is a trend of decreasing Hα-to-FUV flux prior to any attenuation corrections. Thus, the conclusions reported both here and in Lee et al. (2009b) should be robust to the effects of dust.

Of course, a proper analysis of star formation efficiencies requires accounting for a number of other factors that we have not considered here, for example, the molecular gas mass and the mass returned to the interstellar medium through stellar evolutionary processes (e.g., Kennicutt et al. 1994; Bigiel et al. 2008). However, this exercise is not meant to be a detailed examination of efficiencies, as would be required, for example, in a study of the Schmidt Law (Schmidt 1959; Kennicutt 1998a). Rather, the purpose is to provide a cautionary illustration of the significant differences that can arise in our understanding of the star formation properties of galaxies in the low-density regime, when the FUV is used to trace the SFR instead of Hα. It is important to carefully re-evaluate previous conclusions regarding the evolutionary state of such galaxies that have been based on Hα measurements.

In this context of re-examining previous Hα-based results, we also note that another similar analysis of star formation efficiencies (discussed in terms of the gas depletion and stellar mass buildup times) was recently presented by Pflamm-Altenburg et al. (2009), but under the premise that the true SFR can be recovered from Hα measurements given their non-universal model of the stellar IMF. Briefly, in the "integrated galactic stellar initial mass function" (IGIMF; Kroupa & Weidner 2003; Weidner & Kroupa 2005, 2006), it is assumed that (1) all stars form in clusters; (2) the maximum mass of a star formed in a cluster is a deterministic function of the cluster mass, and this maximum mass is lower than would be expected from random sampling of a universal IMF; and (3) the most massive cluster that is formed in a galaxy is dependent on its SFR. Thus, according to the IGIMF model, the stellar mass distribution of galaxies with low SFRs will be deficient in massive stars (and more deficient than would be expected from simple Poisson sampling), leading to a nonlinear relationship between the SFR and the Hα luminosity. The results given by Figures 4 and 5 are qualitatively consistent with those of Pflamm-Altenburg et al. (2009), in that the majority of galaxies have efficiencies greater than $t_{\rm H}^{-1}$ when the UV flux is used to measure the star formation activity. *However, in our analysis, no change in the assumptions about the form of IMF was required to arrive at this conclusion*. Instead, we make the more conservative assumption that the FUV luminosity provides a more robust measure of the recent SFR than Hα in the low-density regime because it (1) primarily originates from a

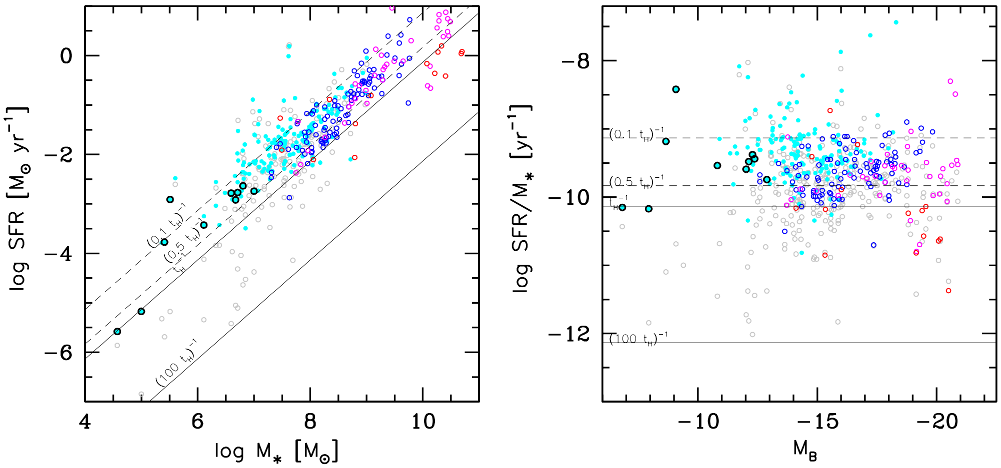

Figure 5. Same as Figure 4, but for the SFR per unit stellar mass.
(A color version of this figure is available in the online journal.)

more abundant population of B-stars and thus is not as prone to stochastic effects and (2) is emitted directly from the stellar photospheres and so does not suffer from possible uncertainties in photoionization of gas in low-density media. We do not yet draw a firm conclusion on the underlying cause of the Hα/UV systematic, as this requires further investigation as discussed in Lee et al. (2009b), and references therein, and in Eldridge (2010).

Finally, it should be noted that the optical limit of the current sample may select against star-forming dwarf galaxies with low UV-based efficiencies ($<t_{\rm H}^{-1}$). The $B = 15.5$ limit corresponds to log(SFR) $= -2.6$, for a typical FUV-B color of 2.5 (Gil de Paz et al. 2007) at a distance of 8.5 Mpc, which encloses approximately half the volume of our survey. Therefore, the apparent bound of the UV-based efficiencies shown in Figures 4 and 5 to values greater than $t_{\rm H}^{-1}$ should be tested using a sample with a fainter optical limit or more ideally with an H I-selected sample complete to masses of about $10^7\ M_\odot$.

3.3.2. UV Properties of Hα Non-detections

As discussed in Paper I and Lee et al. (2009a), late-type galaxies that are completely devoid of star formation as traced by Hα emission are rare. In those papers, it was reported that Hα is not detected in only 22 of the 410 Local Volume galaxies that had been observed. Among these, 3 were classified as early-type galaxies, and 19 as dwarf irregulars. All of the 19 late-type Hα non-detections have extremely low B-band luminosities ($M_B \gtrsim -13.6$) and most also have some indication of the presence of H I gas. Therefore, we concluded that the lack of Hα emission might not necessarily indicate a lack of current star formation, but rather, may merely reflect the low probability of forming massive ionizing stars. This plausibility of this scenario can be tested with the current *GALEX* data set. Ongoing star formation that does not result in the production of ionizing stars and hence does not manifest itself via Hα emission should still be detectable with one-orbit-depth *GALEX* imaging. This is because B-stars down to $\sim 3\ M_\odot$ significantly contribute to the FUV flux and are formed at much higher frequency than the more massive ionizing stars.

Of the 19 late-type Hα non-detections, 12 have observations which are at least one-orbit deep.[24] False-color images of these galaxies are shown in Figure 6. All have measurable FUV emission except for UGCA276, which was discussed in the preceding section. These 11 Hα undetected, UV-bright dwarf irregular galaxies are plotted in the color–magnitude diagrams in Figure 7 as the circled points. In contrast to Figure 3, only Sc and later-type spirals are now shown, and galaxies without Hα observations have been removed to focus the comparison. All 11 galaxies have blue UV colors typical of star-forming galaxies except for the two Local Group galaxies LGS3 and LeoT, which are the lowest-luminosity galaxies in the sample. The color of LeoT has too large of an error for the value to be meaningful, while LGS3's position off of the blue sequence may be an indication that star formation has not occurred in the past ~100 Myr. However, with a lifetime-averaged SFR of $\sim 5 \times 10^{-5}\ M_\odot$ yr^{-1}, even the UV emission of these systems is susceptible to Poisson noise in the formation of B-stars.[25]

It happens that observations of the resolved stellar populations of both LGS-3 (Miller et al. 2001) and Leo T (de Jong et al. 2008) do indicate the presence of recent star formation (within the last few hundred Myr). These studies of LGS-3 and Leo T, together with the relatively blue UV colors of the remaining nine Hα non-detections, and the generally clumpy morphology of their FUV emission, provide evidence that the UV emission arises from stars that are a few hundred Myr old or younger, rather than from evolved stars as found in nearby elliptical galaxies (i.e., the "UV upturn;" O'Connell 1999, and references therein). If the observed FUV emission is translated into an Hα surface brightness (assuming the standard conversion of Kennicutt 1998b holds, and that the Hα and UV emission extend over the same regions of the disk), the expected values for all of the galaxies except LGS3 and LeoT are between 2×10^{-17} and 1×10^{-16} erg cm^{-2} s^{-1} arcsec^{-2} (emission measures

[24] UGCA15, LeoT, LSBCD564-08, ESO349-G031, UGC7298, UGCA276, M81dwA, LGS3, KDG73, KKR03, LSBCF573-01, and BK3N.

[25] Following Section 4.6 of Lee et al. (2009b), we can estimate when Poisson fluctuations may lead to FUV non-detections, by computing the SFR at which the number of OB stars at any given time would be ~10, as there will be times when a galaxy with said SFR will have $10 - 3\sqrt{10}$ (i.e., zero) OB stars. Assuming a Salpeter IMF with mass range of 0.1–100 $M_\odot$, 95% of the FUV light is emitted by main-sequence stars between 3.3 and 100 $M_\odot$. Thus, if the IMF is integrated between 3.3 and 100 $M_\odot$, the mass of stars that must be formed in order to produce 10 OB stars is 400 $M_\odot$. To transform this into a SFR, the mass is divided by the median lifetime of stars that significantly contribute to the UV luminosity, which is 100 Myr. The limiting SFR is roughly $4 \times 10^{-4}\ M_\odot$ yr^{-1}. Monte Carlo simulations by Tremonti et al. (2007) confirm that Poisson fluctuations do not begin to significantly affect the FUV emission until SFRs of until at least $4 \times 10^{-4}\ M_\odot$ yr^{-1}.

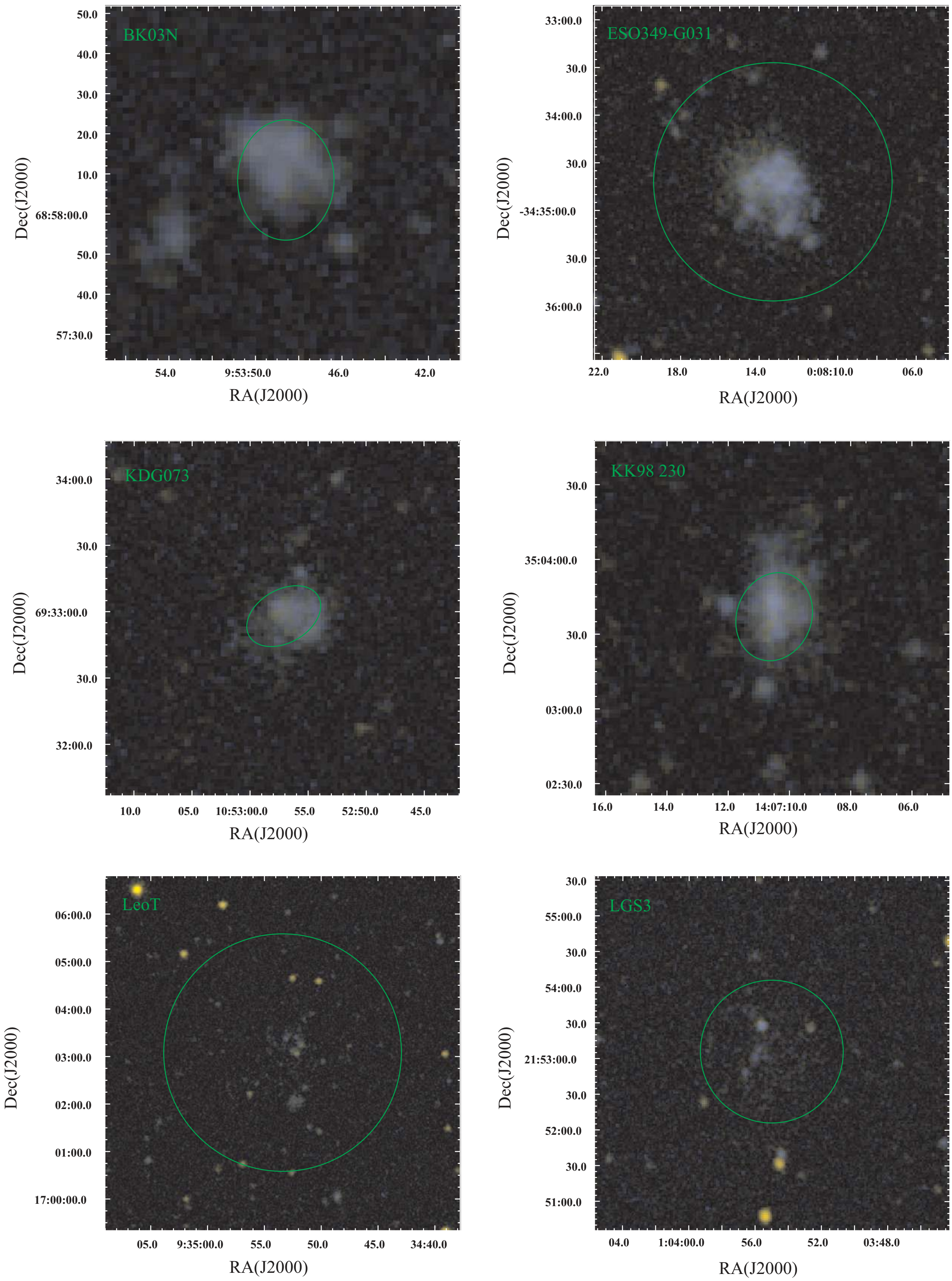

Figure 6. False-color images of late-type dwarf galaxies undetected in Hα narrowband imaging which have one-orbit-depth *GALEX* data ($\sim$1500 s). The NUV emission appears as yellow and the FUV emission as blue. The green ellipses mark the RC3 D_{25} ellipse. The FUV morphologies are generally clumpy suggesting that the UV emission arises from recent star formation.

(A color version of this figure is available in the online journal.)

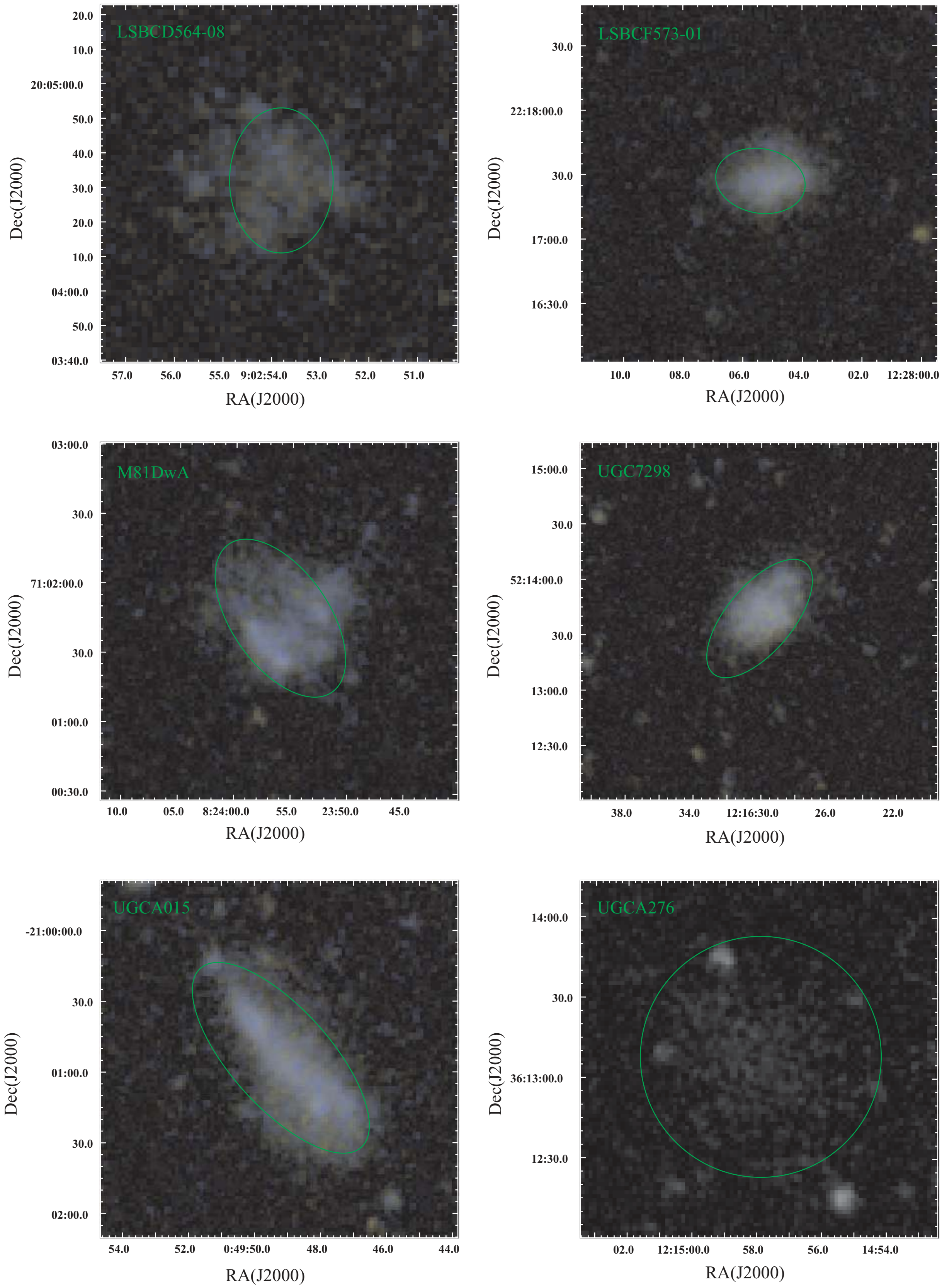

Figure 6. (Continued)

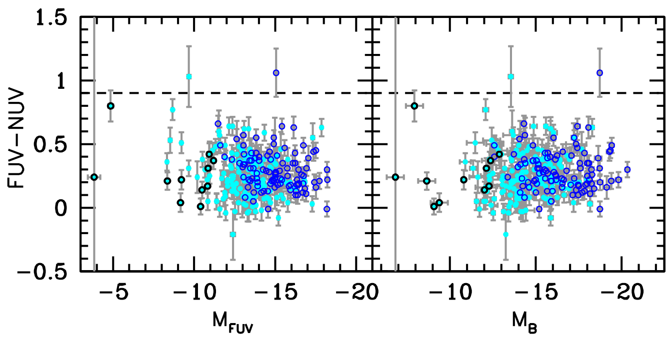

Figure 7. Same as the bottom panels of Figure 3, but with only Sc- and later-type galaxies shown. Only galaxies that have both FUV and Hα measurements are plotted. Errors are now also shown.

(A color version of this figure is available in the online journal.)

between ∼6 and 30 pc cm^{-6}). Therefore, the Hα non-detection of these galaxies should not be due to the limiting depth of the previous narrowband observations which probed to a 3σ surface brightness of $\sim 1 \times 10^{-17}$ erg cm^{-2} s^{-1} arcsec^{-2}.

Given that the FUV emission likely arises from young stellar populations, the question then becomes whether the absence of H II regions is due to observing the galaxies during a particular time in their star formation histories when the most massive, ionizing stars have just died (i.e., star formation in the galaxy has recently halted), or whether it is merely the result of statistical fluctuations in the formation of massive stars in extremely low-mass systems (i.e., star formation is proceeding but massive stars have not been produced). Though it is difficult to unambiguously differentiate between these two scenarios with the current data set alone, we note that the Hα-undetected, UV-bright dwarf irregular galaxies all have $M_{\rm FUV} > -11.2$ (Figure 7). The corresponding SFR is 0.0018 or $10^{-2.74}\ M_\odot$ yr^{-1}, which coincides with the SFR limit below which Poisson fluctuations in the formation of high-mass ionizing stars begin to affect the Hα output, as computed in Lee et al. (2009b). Thus, the UV data are at least not inconsistent with the possibility that the non-detection of Hα is due to stochasticity in the sampling of the massive end of the stellar IMF in systems with ongoing but ultra-low star formation activities. Again, a large, complete sample of these lowest-luminosity dwarf irregulars would be needed to probe this issue further. A new generation of recently developed stellar population synthesis models that incorporate a random sampling of a standard IMF (e.g., Eldridge 2010; Fumagalli et al. 2010; Popescu & Hanson 2010) can be used to test whether the incidence of Hα-undetected, UV-bright galaxies and the distribution of the Hα-to-FUV flux ratio is consistent with the expectations of stochasticity, given a particular star formation history.

Another clue on the nature of star formation in Hα-undetected, UV-bright dwarf irregular galaxies is provided by examining their UV-based star formation properties relative to those of the overall population of late-type galaxies. In Figures 4 and 5, where the SFR per unit H I mass and stellar mass are plotted, the Hα non-detections are again circled in black. It is notable that most have global star formation efficiencies that are consistent with, and not highly deviant from, the distribution defined by the overall population. Aside from their extremely low luminosities, these galaxies appear to be relatively normal, at least by these global measures of the star formation activity. This picture is quite different from one based upon Hα observations alone. In fact, the non-detection of Hα in relatively gas-rich dwarf galaxies can potentially be used to identify "transition-type" systems, and this classification criterion was examined by Skillman et al. (2003). Transition-type systems are galaxies which have observed properties intermediate between dwarf spheroidals and dwarf irregulars, and thus, may be in a phase of transformation between the two galaxy classes (e.g., Mateo 1998; Grebel et al. 2003; Côté et al. 2009). In this context, the absence of Hα may be interpreted as an absence of the recent star formation, indicating that the galaxies are possibly evolving into red and dead spheroidals, or experiencing a temporary interruption of star formation due to effects within the group environment. However, galaxies classified as transition types also have very low luminosities. *The analysis and discussion presented here clearly demonstrate that the non-detection of Hα in such extreme dwarfs is a highly insufficient criterion for identifying systems that are truly in a transformational state*. An observation made by Skillman et al. (2003), that such transition types appear to be quite similar to dwarf irregulars (for example, in their spatial distribution within the group environment and in their gas properties), was suggestive of this conclusion. An absence of detectable FUV emission in gas-rich dwarfs would be a more compelling criterion, since the FUV flux is robust to stochastic fluctuations until much lower SFRs than Hα.[25] Alternately, an Hα non-detection accompanied by a red UV color (FUV − NUV $\gtrsim$ 0.6) in such systems would also provide a better indication of halted star formation than the non-detection of Hα alone.

4. SUMMARY

The primary purpose of this paper is to provide *GALEX* NUV- and FUV-integrated photometry for a statistically robust sample of star-forming galaxies within the 11 Mpc Local Volume. Our *GALEX* programs have leveraged upon previously available observations to mitigate the previous ∼4-fold underrepresentation of low-luminosity, nearby dwarfs with SFRs lower than $\sim 0.4\ M_\odot$ yr^{-1} ($M_{\rm FUV} \gtrsim -14.5$) in the *GALEX* archive. The resultant survey provides most complete UV imaging data set for Local Volume galaxies currently available. Together with the precursor Hα survey and the Local Volume Legacy infrared observations with *Spitzer* (as described in Kennicutt et al. 2008 and Dale et al. 2009, respectively), the *GALEX* observations reported here furnish a core data set for studying star formation and dust in the Galactic neighborhood.

We find that UV emission is present in nearly all of the late-type galaxies observed in our sample. This expected result supports the idea that the intermittent cessation of star formation is uncommon as we rarely observe such galaxies in an "off" mode (Lee et al. 2009a), at least for the $B < 15.5$ population which is the main focus of our survey.

In the context of the recent work suggesting that FUV observations offer a more robust probe of star formation in low-density environments compared with previous Hα narrowband imaging, we use the data set to re-examine two measures of the global star formation efficiency, the SFR per unit H I gas mass and the SFR per unit stellar mass. We find that dwarf galaxies may not be as drastically inefficient in converting gas into stars as suggested by prior Hα studies, with the vast majority of galaxies in our sample having star formation efficiencies greater than $t_{\rm H}^{-1}$.

We also examine the properties of late-type dwarf galaxies that previously appeared to be devoid of star formation because they were not detected in earlier Hα narrowband observations. We find that such galaxies have UV SFRs that fall below the limit where the Hα output is expected to begin to suffer from Poisson fluctuations in the formation of massive stars. We note that the Hα-undetected, UV-bright systems appear to be relatively normal with respect to the overall population of star-forming galaxies in their UV-based star formation efficiencies and UV colors. Thus, the UV data are at least not inconsistent with the possibility that the absence of Hα is simply due to stochasticity in the sampling of the massive end of the stellar IMF, in otherwise normal star-forming systems with ongoing but ultra-low star formation activities.

At a number of points in the discussion, we remark that obtaining FUV and Hα observations for a deeper sample of dwarf galaxies, or more ideally, an H I-selected sample probing masses down to 10^7 $M_\odot$, is needed to test some of our conclusions. Such new observations are required to examine whether the rarity of star formation that has been temporarily halted on ∼100 Myr timescales (i.e., the rarity of UV non-detections) persists in lower luminosity systems; test the apparent bound of star formation efficiencies to values greater than t_H^{-1}; and to further probe whether the non-detection of Hα in UV-bright, H I-rich dwarf galaxies can be fully explained by Poisson sampling of a universal IMF.

GALEX is a NASA Small Explorer, and we gratefully acknowledge NASA's support for construction, operation, and science analysis for the *GALEX* mission, developed in cooperation with the Centre National d'Etudes Spatiales of France and the Korean Ministry of Science and Technology. This research has made use of the NASA/IPAC Extragalactic Database (NED), which is operated by the Jet Propulsion Laboratory, California Institute of Technology, under contract with NASA, as well as the HyperLeda database (http://leda.univ-lyon1.fr). We thank the anonymous referee for useful feedback which helped to clarify some important points in our interpretation of the data. Special thanks are due to Chris Martin and the members of the *GALEX* team (http://www.galex.caltech.edu/about/team.html) for their dedicated support of the Guest Investigator Program, without which this work would not have been possible. A.G.d.P. is supported by the Spanish "Ramón y Cajal", Plan Nacional AYA2009-10368, Consolider-GTC and AstroMadrid (CAM S2009/ESP-1496) programs.

Facilities: Bok, CTIO:0.9m, GALEX, Spitzer, VATT

REFERENCES

Adelman-McCarthy, J. K., et al. 2006, ApJS, 162, 38
Bigiel, F., Leroy, A., Walter, F., Brinks, E., de Blok, W. J. G., Madore, B., & Thornley, M. D. 2008, AJ, 136, 2846
Blanton, M. R., Lupton, R. H., Schlegel, D. J., Strauss, M. A., Brinkmann, J., Fukugita, M., & Loveday, J. 2005, ApJ, 631, 208
Boselli, A., Boissier, S., Cortese, L., Buat, V., Hughes, T. M., & Gavazzi, G. 2009, ApJ, 706, 1527
Bothwell, M. S., Kennicutt, R. C., & Lee, J. C. 2009, MNRAS, 400, 154
Brinchmann, J., Charlot, S., White, S. D. M., Tremonti, C., Kauffmann, G., Heckman, T., & Brinkmann, J. 2004, MNRAS, 351, 1151
Cairós, L. M., Vílchez, J. M., González Pérez, J. N., Iglesias-Páramo, J., & Caon, N. 2001, ApJS, 133, 321
Cardelli, J. A., Clayton, G. C., & Mathis, J. S. 1989, ApJ, 345, 245
Côté, S., Draginda, A., Skillman, E. D., & Miller, B. W. 2009, AJ, 138, 1037
Dalcanton, J. J., et al. 2009, ApJS, 183, 67
Dale, D. A., et al. 2009, ApJ, 703, 517
de Jong, J. T. A., et al. 2008, ApJ, 680, 1112
de Vaucouleurs, G., de Vaucouleurs, A., Corwin, H. G., Buta, R. J., Paturel, G., & Fouque, P. 1991, Third Reference Catalog of Bright Galaxies, Vols. 1–3, XII (Berlin: Springer-Verlag)
Eldridge, J. J. 2010, arXiv:1008.1352
Fumagalli, M., da Silva, R., Krumholz, M., & Bigiel, F. 2010, arXiv:1009.0524
Gallagher, J. S., III, & Hunter, D. A. 1984, ARA&A, 22, 37
Gil de Paz, A., & Madore, B. F. 2005, ApJS, 156, 345
Gil de Paz, A., Madore, B. F., & Pevunova, O. 2003, ApJS, 147, 29
Gil de Paz, A., et al. 2005, ApJ, 627, L29
Gil de Paz, A., et al. 2007, ApJS, 173, 185
Goddard, Q. E., Kennicutt, R. C., & Ryan-Weber, E. V. 2010, MNRAS, 405, 2791
Grebel, E. K., Gallagher, J. S., III, & Harbeck, D. 2003, AJ, 125, 1926
Hodge, P. W. 1974, PASP, 86, 845
Hunter, D. A., & Elmegreen, B. G. 2004, AJ, 128, 2170
Hunter, D. A., Elmegreen, B. G., & Ludka, B. C. 2010, AJ, 139, 447
Hunter, D. A., & Gallagher, J. S., III. 1985, ApJS, 58, 533
James, P. A., Prescott, M., & Baldry, I. K. 2008, A&A, 484, 703
Karachentsev, I. D., & Kaisin, S. S. 2007, AJ, 133, 1883
Karachentsev, I. D., Karachentseva, V. E., Huchtmeier, W. K., & Makarov, D. I. 2004, AJ, 127, 2031
Karachentsev, I. D., & Makarov, D. A. 1996, AJ, 111, 794
Kennicutt, R. C., Jr. 1983, ApJ, 272, 54
Kennicutt, R. C., Jr. 1989, ApJ, 344, 685
Kennicutt, R. C., Jr. 1998a, ApJ, 498, 541
Kennicutt, R. C., Jr. 1998b, ARA&A, 36, 189
Kennicutt, R. C., Jr., Lee, J. C., Funes, S. J., José, G., Sakai, S., & Akiyama, S. 2008, ApJS, 178, 247 (Paper I)
Kennicutt, R. C., Jr., Tamblyn, P., & Congdon, C. E. 1994, ApJ, 435, 22
Knapen, J. H., & James, P. A. 2009, ApJ, 698, 1437
Kroupa, P., & Weidner, C. 2003, ApJ, 598, 1076
Lee, J. C., Kennicutt, R. C., Funes, S. J., José, G., Sakai, S., & Akiyama, S. 2007, ApJ, 671, L113
Lee, J. C., Kennicutt, R. C., José, G., Funes, S. J., Sakai, S., & Akiyama, S. 2009a, ApJ, 692, 1305
Lee, J. C., Salzer, J. J., & Melbourne, J. 2004, ApJ, 616, 752
Lee, J. C., et al. 2009b, ApJ, 706, 599
Martin, D. C., et al. 2005, ApJ, 619, L1
Mateo, M. L. 1998, ARA&A, 36, 435
Melena, N. W., Elmegreen, B. G., Hunter, D. A., & Zernow, L. 2009, AJ, 138, 1203
Meurer, G. R. 2010, arXiv:1008.3946
Meurer, G. C., et al. 2006, ApJS, 165, 307
Meurer, G. R., et al. 2009, ApJ, 695, 765
Meyer, M. J., et al. 2004, MNRAS, 350, 1195
Miller, B. W., Dolphin, A. E., Lee, M. G., Kim, S. C., & Hodge, P. 2001, ApJ, 562, 713
Morrissey, P. 2006, Proc. SPIE, 6266, 26
Morrissey, P., et al. 2005, ApJ, 619, L7
Morrissey, P., et al. 2007, ApJS, 173, 682
O'Connell, R. W. 1999, ARA&A, 37, 603
Paturel, G., Theureau, G., Bottinelli, L., Gouguenheim, L., Coudreau-Durand, N., Hallet, N., & Petit, C. 2003, A&A, 412, 57
Pflamm-Altenburg, J., & Kroupa, P. 2009, ApJ, 706, 516
Pflamm-Altenburg, J., Weidner, C., & Krapa, P. 2009, MNRAS, 395, 394
Popescu, B., & Hanson, M. M. 2010, ApJ, 724, 296
Schiminovich, D., et al. 2007, ApJS, 173, 315
Schlegel, D. J., Finkbeiner, D. P., & Davis, M. 1998, ApJ, 500, 525
Schmidt, M. 1959, ApJ, 129, 243
Skillman, E. D., Côté, S., & Miller, B. W. 2003, AJ, 125, 593
Skillman, E. D., Kennicutt, R. C., & Hodge, P. W. 1989, ApJ, 347, 875
Springob, C. M., Haynes, M. P., Giovanelli, R., & Kent, B. R. 2005, ApJS, 160, 149
Thilker, D. A., et al. 2005, ApJ, 619, L79
Thilker, D. A., et al. 2007, ApJS, 173, 538
Tolstoy, E., Hill, V., & Tosi, M. 2009, ARA&A, 47, 371
Tremonti, C. A., Lee, J. C., van Zee, L., Kennicutt, R. C., Gil de Paz, A., Sakai, S., Funes, J., & Akiyama, S. 2007, BAAS, 38, 894
Tully, R. B. 1988, AJ, 96, 73
Tully, R. B., et al. 2006, AJ, 132, 729
van Zee, L. 2001, AJ, 121, 2003
van Zee, L., Haynes, M. P., & Salzer, J. J. 1997, AJ, 114, 2479
Weidner, C., & Kroupa, P. 2005, ApJ, 625, 754
Weidner, C., & Kroupa, P. 2006, MNRAS, 365, 1333
Weisz, D. R., Skillman, E. D., Cannon, J. M., Dolphin, A. E., Kennicutt, R. C., Jr., Lee, J., & Walter, F. 2008, ApJ, 689, 160
Zaritsky, D., & Christlein, D. 2007, AJ, 134, 135